D-Serine facilitates aggressive migration and stemness of recurrent glioblastoma cells by interacting with host endothelial cells

by
Ryan Mota

A Thesis submitted to the Faculty of Graduate and Postdoctoral Studies of
The University of Manitoba
in partial fulfilment of the requirements of the degree of

MASTER OF SCIENCE

Department of Pharmacology and Therapeutics
Rady Faculty of Health Sciences
University of Manitoba
Winnipeg, MB

Abstract

Glioblastoma (GBM) is the most aggressive primary brain tumor in adults, with recurrence driven by therapy-resistant, stem-like tumor cell populations and maladaptive interactions with the tumor microenvironment. Despite aggressive multimodal treatment, recurrent GBM (rGBM) remains consistently lethal. While glutamatergic signaling has been implicated in GBM through excitotoxic effects on neural cells, its role in tumor/endothelial communication is not fully understood. Here, we identify a previously unrecognized tumor/vascular signaling axis in which rGBM-derived D-serine, along with glutamate, activates endothelial NMDA receptors (eNMDARs) to promote tumor aggressiveness. Using patient-derived rGBM models, endothelial co-culture systems, and intracranial xenografts, we show that rGBM cells upregulate serine racemase (SRR) and secrete D-serine into the tumor microenvironment. Endothelial interaction reprograms rGBM transcriptional states toward angiogenic, inflammatory, and pro-survival states while suppressing differentiation-associated pathways. Functional assays demonstrate that extracellular D-serine is required for endothelial-mediated enhancement of rGBM migration, invasion, and self-renewal, as enzymatic depletion of D-serine reverses these phenotypes and reduces expression of mesenchymal and stemness markers. Pharmacologic inhibition or genetic deletion of SRR impairs tumor growth, reduces vascular density, and prolongs survival *in vivo*. Spatial transcriptomic analysis further reveals that loss of SRR disrupts angiogenic, hypoxic, migratory, and proliferative gene programs within tumor regions. Importantly, endothelial-specific deletion of the NMDAR subunit GluN1, which binds D-serine, attenuates rGBM/endothelial crosstalk. These findings define SRR-driven D-serine signaling as a key driver of the rGBM vascular niche and identify endothelial glutamatergic signaling as a therapeutic vulnerability. Targeting this signaling axis pathway offers a novel strategy to disrupt tumor/vascular crosstalk in recurrent glioblastoma.

Acknowledgments

This work would not have been possible without the guidance and support of many individuals who contributed to both my scientific development and personal growth throughout my masters program.

First and foremost, I would like to thank my supervisors, Drs. Chris Anderson and Tanveer Sharif for their mentorship, patience, and unwavering support. Their scientific insight, critical thinking, and encouragement shaped not only this thesis but also my approach to research. I am deeply grateful for the freedom to explore ideas, the guidance through challenges, and the research standards they instilled in me.

I would also like to thank my thesis committee, Drs. Sachin Katyal and Galen Wright for their thoughtful feedback, challenging questions, and constructive advice over the years. Their perspectives helped refine this work and pushed me to think more broadly about its significance.

I am grateful to my lab members, past and present, for creating a collaborative and supportive environment. Thank you for the countless discussions at the bench, for troubleshooting experiments, and for sharing both successes and frustrations.

To my friends, thank you for your constant encouragement, humour, and understanding. Your support outside the lab provided balance and perspective. I am deeply appreciative of the times we have had during my program.

Finally, I owe my deepest thanks to my family. Your unconditional love, belief in me, and continued support made this journey possible. Even after I moved to a different province, your encouragement never wavered, and your willingness to support me from afar meant more than I can express. Thank you for always encouraging me to pursue my goals and for standing by me every step of the way.

Contribution of Authors

Ryan Mota: Experiment design, data analysis and interpretation, cell culture and treatments, viability assays, release assays, protein extraction, immunoblotting, RNA extraction, cytokine arrays, tumorsphere formation, migration assays, invasion assays, animal studies, immunohistochemistry, preparation of samples for spatial transcriptomic analysis, thesis writing and figure preparation.

Ping Lu: Experiment design, data analysis and interpretation, cell culture and treatments, protein extraction, immunoblotting, cytokine arrays, tumorsphere formation, migration assays, animal studies, CRISPR editing.

Lisa Liang: Protein extraction, immunoblotting, tumorsphere formation, data analysis and interpretation.

Alejandra Maria Cuesta: Protein extraction, immunoblotting, data analysis and interpretation.

Emma Martell: Project conceptualization, experiment design, data analysis and interpretation, tumorsphere formation, animal studies, bioinformatics analysis.

Helgi Kuzmychova: spatial transcriptomic analysis.

Agnes Fresnoza: Performed tumor xenograft surgeries for animal studies.

Sheila K. Singh: Provided all human patient-derived recurrent GBM cells.

Table of Contents

List to Tables

List of Figures

List of Abbreviations

2-HG - D-2-hydroxyglutarate

AMPAR - α-amino-3-hydroxy-5-methyl-4-isoxazolepropionic acid Receptor

AP5 - 2-amino-5-phosphonopentanoic acid

BBB – Blood Brain Barrier

CNS – Central Nervous System

DAAO – D-Amino Acid Oxidase

DCKA - 5,7-Dichlorokynurenic acid

DEPC - Diethyl Pyrocarbonate

ECM – Extracellular Matrix

EGF - Epidermal Growth Factor

EGFR – Epidermal Growth Factor Receptor

EMT - Epithelial-to-Mesenchymal Transition

eNMDAR – Endothelial N-methyl-D-aspartate Receptors

GBM – Glioblastoma

GLUT - Glucose Transporter

gRNA – Guide Ribonucleic Acid

GSC – Glioma Stem cell

hCMEC – Human Cerebral Microvascular Endothelial Cells

HIF – Hypoxia-inducible factors

IDH - Isocitrate dehydrogenase

IL-6 - Interleukin-6

L-NIO - N^5-(1-Iminoethyl)-L-ornithine, dihydrochloride

LDHA - Lactate Dehydrogenase A

MDSCs - Myeloid-Derived Suppressor Cells

MGMT - O6-methylguanine-DNA methyltransferase

MMP - Matrix Metalloproteinases

NMDAR - N-methyl-D-aspartate Receptors

NO- Nitric Oxide

PMS - Phenazine methosulfate

rGBM – Recurrent Glioblastoma

SAM - S-adenosylmethionine

SRR – Serine Racemase

TAMs – Tumor-associated Macrophage

TME – Tumor Microenvironment

TMZ – Temozolomide

VEGF - Vascular Endothelial Growth Factor

Chapter 1: Introduction

1.1 Clinical significance of Glioblastoma Multiforme

Glioblastoma (GBM) is a grade IV astrocytoma which represents about 50% of central nervous system (CNS) malignant gliomas and 80% of all malignant primary brain tumors[1,2]. GBM is one of the most aggressive brain tumors, leading to a median survival of only 15 months. With only 6.8% of patients who undergo treatment reach the 5-year timeline. In patients who withhold treatment, survival drops drastically to around 3 months. Diagnosis is usually due to an onset of symptoms, subsequently confirmed by MRI or biopsy. Symptoms include headaches, nausea, seizures, balance issues, and cognitive decline; however, they vary depending on tumor location and size.

GBM can arise at any age, but is most common in adults over 65 years of age[3], over 70% of patients diagnosed with GBM are in this elderly category. These patients have a worse prognosis compared to similarly treated younger patients[4]. An increase in age is a negative prognostic factor in the survival of the disease. GBM may still have a significant effect in other age categories, such as children and young adults, where tumor development is less frequent. Sex differences also play a role in the disease onset and prognosis; malignant brain tumors are more likely to arise in males regardless of other factors such as age or geographical location[6]. Clinically, the incidence of GBM occurs in a 1.6:1 ratio of males to females[7].

Along with increased risk of GBM onset, males also have a worse prognosis in comparison to females. Males respond worse to treatment and have a reduced survival[8,9]. However, the molecular mechanism behind these differences is not fully understood; there is research focusing on sex-specific gene expression and immune response to uncover the exact factors contributing to this difference[10].

Following GBM diagnosis, a multimodal treatment regimen including surgical resection, chemotherapy and radiation therapy is the current standard of care known as the STUPP protocol[11]. Temozolomide (TMZ) is the most common chemotherapy agent used in GBM treatment and is administered in concurrent and adjuvant phases. Despite aggressive, multi-pronged therapies, there remains a very poor prognosis, leading to a high recurrence rate. About 90% of patients who undergo treatment will develop a recurrent tumor within the first 2 years of diagnosis[12]. Unfortunately, recurrent tumors are usually more challenging to treat as they have developed resistance to the standard of care treatment and adapted to the surrounding brain tissue microenvironment. The main drivers of the high recurrence rate are glioma stem cells (GSCs)[13], which acquire resistance to treatment through multiple genetic mutations. These cells create both intra- and intertumoral heterogeneity, which also aids in the resistance to therapy. Tumor cell populations display extensive diversity both within a single tumor mass (intra-tumoral heterogeneity) and between tumors from different patients or from the same patient at different time points (inter-tumoral heterogeneity). At the intra-tumoral level, no single therapy can effectively target all malignant cell populations simultaneously, enabling residual disease to persist. At the inter-tumoral level, therapeutic responses are highly variable and difficult to generalize, complicating clinical trial design and drug development. In recurrent GBM, these challenges are worsened by treatment-driven clonal selection, increased aggressiveness, and heightened resistance mechanisms, including enhanced DNA repair capacity and stem-like phenotypes. The aggressive GBMs invade nearby brain tissue evading surgical and pharmacological treatments, leading to severe impediments for the patient. Currently, GBM is an incurable disease affecting 4 in 100,000 Canadians. Between 1995 and 2015, there was a 26.4% increase in GBM incidence, which was more than double the increase seen in the USA over the

same period[14]. Research must continue to unravel the mechanisms of GBM and accurately determine prospective molecular markers that sustain tumorigenesis and recurrence.

Due to the differences in treatment susceptibility between initial and recurrent tumors, their respective treatment courses differ slightly. Primary GBM tumors usually undergo the STUPP protocol as mentioned above, along with some newly approved immunotherapy treatments to reduce the tumor burden if necessary. However, recurrent GBM (rGBM) tumors have altered their pathology to the extent that it is difficult to determine if the patient's quality of life will improve with repeat surgery or reirradiation[15]. Currently, there is no standard of care treatment for rGBM, which causes physicians further question which treatment decision is best for the patient. Many patients will look to experimental treatments if available or undergo palliative care. Primary and rGBM can share similar symptomology, depending on the location and size of the tumor. Most times rGBM will mirror the initial symptoms but may worsen at a quicker rate, correlating to the more pronounced aggressiveness of these recurrent tumors. Further, past treatment of the primary tumor could lead to a faster onset of symptoms such as radionecrosis, surgical scarring, or chemotherapy toxicity[16,17].

1.2 Clinical and molecular differences of primary GBM to rGBM

The propensities of GBM to evolve under therapeutic pressure represents a critical challenge to achieving long-term control. The intratumoral heterogeneity of GBM, driven by genetic, epigenetic, and phenotypic diversity, allows the tumor to adapt rapidly to external stressors. For instance, subclonal populations within the tumor may possess pre-existing resistance mechanisms, enabling them to survive initial treatment and repopulate the tumor. These therapy-resistant clones

often exhibit increased expression of stemness-related genes, enhanced migratory potential, and altered metabolic pathways[18].

GBM begins with a complex arrangement of genetic mutations that allow cells to evade apoptosis and cell cycle regulation. These mutations drive tumor progression and permit the recurrence of resistant GBM tumors. Epidermal growth factor receptor (EGFR) is a common mutation that occurs in about 60% of GBM tumors, the mutations frequently lead to an amplification of this receptor[19]. Under normal physiological conditions, EGFRs are responsible for regulating tissue development and homeostasis; they can also function as modulators for migration, differentiation, and signal transduction[20,21]. However, in tumor cells there is a common in-frame deletion of the EGFR coding region of the extracellular domain, leading to a constitutively active receptor[22]. The over-activation of the EGFR gene expression causes an amplified receptor response, which can enhance downstream signaling pathways. The genetic mutation causing the formation of a constitutively active receptor is known as EGFRvIII and is known to support GBM cell survival and progression[22]. Both the tumor cells and the microenvironment surrounding the tumor can secrete ligands to enhance the effect of these mutations commonly found in GBM cells causing a more aggressive cancer with a poor prognosis.

Isocitrate dehydrogenase (IDH) mutations within the tumor represent a molecular biomarker in GBM, shaping prognosis and therapeutic response, with implications that extend across both primary and recurrent disease. IDH plays a role in the citric acid cycle, catalyzing the conversion of isocitrate to α-ketoglutarate, allowing for energy production. Once an IDH mutation occurs, like in 70% of secondary GBM tumors, the mutant protein gains a function[23]. IDH mutant proteins can convert isocitrate into a metabolite, D-2-hydroxyglutarate (2-HG). The production of 2-HG

reduces the α-ketoglutarate levels within the cancerous cell but also affects the downstream metabolic energy production. The mutation also produces less NADPH within the citric acid cycle, leading to an imbalance of redox homeostasis, causing an increase in oxidative stress. IDH mutant gliomas are usually linked to a better prognosis in secondary tumors that have arisen from primary lower-grade gliomas. A majority of GBM tumors will be IDH wildtype; another factor in why GBM displays such an aggressive phenotype with a poor prognosis[24].

Genetic mutations within tumor suppressor genes significantly contribute to the increase in proliferation and evasion of apoptosis by the cancerous cells. Two commonly altered tumor suppressors in GBM are *PTEN* and *p53*, which can undergo a loss-of-function mutation. Both can demonstrate a cooperative relationship to regulate control of cell fate in the proliferative cycle. Over 80% of patient GBM tumors have *p53* mutations, while approximately 40% of GBM tumors will harbour a *PTEN* mutation[25,26]. This mutation leads to a decrease in cell cycle arrest and apoptosis, while increasing DNA repair in these cancerous cells.

Beyond the core tumor suppressor alterations in *PTEN* and *TP53*, GBM is further stratified into molecular subtypes defined by distinct transcriptional and signalling programs that shape tumor behaviour. The proneural subtype is commonly associated with *PDGFRA* alteration and IDH1 mutation, together with expression of lineage-related markers such as SOX, DCX, and DLL3, consistent with a more developmentally restricted, oligodendrocyte progenitor-like state. In contrast, the mesenchymal subtype is enriched for abnormalities in *NF1, TP53*, and *PTEN*, and is characterised by increased NF-κB pathway activity and expression of markers including CD44, VEGF, and MERTK, which collectively support inflammatory signalling, invasion, angiogenesis, and therapeutic resistance. The classical subtype is defined primarily by EGFR amplification, frequent gain of chromosome 7 with concurrent loss of chromosome 10, and relative scarcity of

TP53 mutations, while markers such as NES, NOTCH3, and JAG1 reflect enhanced stem-like signalling and sustained proliferative potential. Finally, the neural subtype has been associated with expression of neuronal differentiation markers including GABRA1, NEFL, and SLC12A5, suggesting a transcriptional program resembling mature neural tissue, although this category has also been debated as potentially reflecting, in part, contamination from non-neoplastic brain cells[27]. Collectively, these subtype-specific gene signatures illustrate that GBM is biologically heterogeneous disease in which distinct genetic and transcriptional networks converge to influence tumor initiation, cellular plasticity, invasiveness, and response to treatment[28]. GBM tumors can exhibit a variety of these genetic alterations; therefore, it remains a challenge to define how primary and rGBM will function in growth and aggressiveness on a case-by-case basis (Figure. 1).

Alongside genetic mutations, the role of epigenetic reprogramming in GBM displays key mechanisms that allow for tumor adaptation and recurrence. A challenge in managing GBM is the ability of tumor cells to evolve under therapeutic pressure. Standard-of-care treatments, including TMZ and radiotherapy, can induce selective pressures that remodel tumor molecular landscape. One of the best-characterized examples is the loss of O6-methylguanine-DNA methyltransferase (MGMT) promoter methylation, which often occurs following TMZ exposure. While initial MGMT methylation is associated with increased sensitivity to TMZ which is seen in 30-60% of GBM patients[29], the demethylation and subsequent re-expression of MGMT enable recurrent tumors to repair TMZ-induced DNA lesions, thereby conferring resistance efficiently. In addition to MGMT, other therapy-induced epigenetic changes, including altered DNA methylation patterns, histone modifications, and chromatin remodelling, contribute to the occurrence of treatment-

resistant clones. These adaptations reduce the efficacy of subsequent lines of therapy, making recurrent GBM such a challenge to treat.

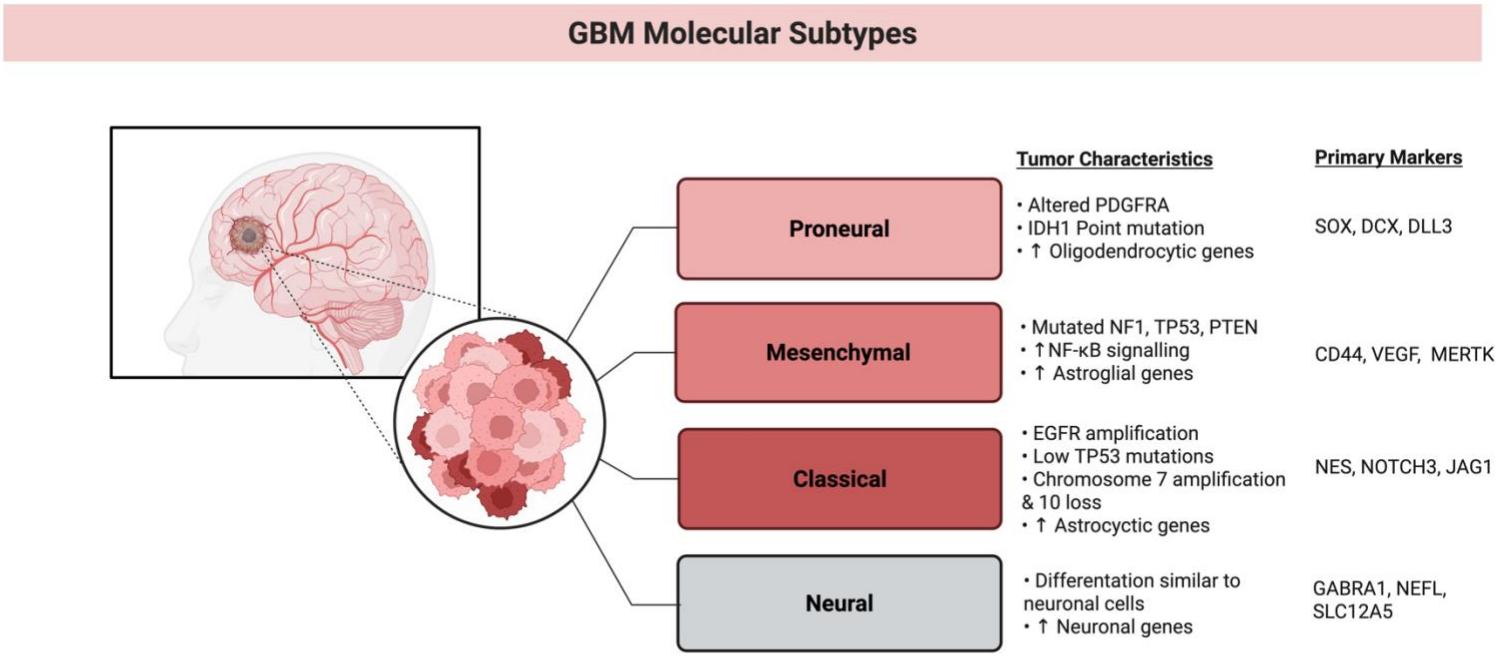

Figure 1. Molecular subtypes of GBM and their defining features, including characteristic genetic alterations, lineage-associated transcriptional programs, and representative primary markers for the proneural, mesenchymal, classical, and neural subtypes.

1.3 The tumor microenvironment and gliomas

The tumor microenvironment (TME) in gliomas is a complex and dynamic system that influences tumor progression, therapeutic resistance, and immune evasion. Unlike peripheral tumors, the glioma TME is modulated by the unique characteristics of the CNS, including the immune-privileged environment and the blood-brain barrier (BBB). Within this microenvironment, tumor cells interact with an array of cellular and acellular components, creating a permissive niche that supports tumor growth and sustains its malignant potential[30]. Glioma cells exhibit substantial intra- and inter-tumoral heterogeneity due to genetic and epigenetic variations, as well as adaptive

responses to microenvironmental conditions. This heterogeneity supports their ability to invade surrounding brain tissue, evade immune surveillance, and adapt to therapeutic interventions[31,32]. These cells secrete various cytokines, growth factors, and enzymes that remodel the extracellular matrix (ECM), enhance angiogenesis, and recruit other cell types into the TME. One of the most prominent features of gliomas is their ability to promote angiogenesis, primarily driven by vascular endothelial growth factor (VEGF) and other pro-angiogenic factors secreted by tumor cells[33]. These factors stimulate the formation of abnormal vasculature, which not only supplies nutrients and oxygen but also contributes to the disruption of the BBB, further facilitating tumor progression and immune cell infiltration.

Immune cells play a dual role within the glioma TME, either supporting anti-tumor immunity or promoting tumor growth through immunosuppressive mechanisms. Tumor-associated macrophages and microglia (TAMs), which often constitute up to 30% of the tumor mass, are frequently polarized toward an M2-like phenotype under the influence of glioma-derived signals[34]. These M2-polarized TAMs promote tumor growth by enhancing angiogenesis, suppressing cytotoxic T-cell activity, and facilitating ECM remodeling. Similarly, other immune cell populations, such as myeloid-derived suppressor cells (MDSCs) and regulatory T cells, contribute to the immunosuppressive landscape, effectively preventing the immune system from mounting an effective anti-tumor response[35]. Glioma cells also exploit the immune-privileged nature of the CNS, leveraging local immune regulatory mechanisms to escape immune detection. Collectively, these cellular interactions within the TME create a highly immunosuppressive and tumor-supportive environment that poses significant challenges to current therapeutic strategies.

The acellular components of the glioma TME further contribute to its complexity. The ECM, which provides structural support to the tumor, is actively remodelled by tumor and stromal cells through the secretion of matrix metalloproteinases (MMPs) and other proteolytic enzymes[36]. This remodeling facilitates tumor invasion into surrounding brain tissue and alters the biochemical composition of the microenvironment, influencing the tumor cell behaviour. The hypoxic and acidic conditions commonly observed in gliomas, a result of rapid tumor growth and inadequate vascularization, further enhance tumor aggressiveness by promoting the selection of more invasive and therapy-resistant cell populations. Hypoxia-inducible factors (HIFs) play a central role in mediating these adaptations, driving the expression of genes involved in angiogenesis, metabolism, and invasion. Together, the cellular and acellular components of the glioma TME form a highly interactive and adaptive system that supports tumor growth, promotes immune evasion, and drives resistance to current treatment modalities.

1.4 Metabolic rewiring in glioblastoma

Metabolic reprogramming constitutes a defining hallmark of GBM, enabling tumor cells to adapt bioenergetic and biosynthetic pathways to dynamic microenvironmental constraints. GBM exhibits the Warburg phenotype, favouring aerobic glycolysis despite sufficient oxygen availability, thereby generating metabolic intermediates for nucleotide, lipid, and amino acid biosynthesis[37]. At the same time, lactate accumulation acidifies the extracellular environment to promote angiogenesis, invasion, and immune evasion. HIF-1α/2α coordinate this glycolytic shift through transcriptional upregulation of glucose transporters (GLUT1/3) and key glycolytic enzymes (e.g., HK2, Lactate Dehydrogenase A [LDHA])[38]. GBM cells will also engage oxidative phosphorylation when oxygen and substrates are accessible, with glutaminolysis and fatty acid oxidation replenishing tricarboxylic acid (TCA) cycle intermediates and sustaining NADPH-

dependent redox homeostasis[39]. This metabolic plasticity confers resistance to therapy by enabling GBM cells to actively buffer oxidative stress generated by radiotherapy and chemotherapy. Ionizing radiation induces cytotoxicity largely through the production of reactive oxygen species (ROS), while temozolomide similarly increases oxidative and metabolic stress[40,41]. GBM cells counter these effects by reprogramming carbon metabolism toward NADPH-generating pathways, particularly the pentose phosphate pathway, thereby sustaining glutathione- and thioredoxin-dependent antioxidant systems[42]. Activation of NRF2-dependent transcription further reinforces redox homeostasis and has been directly linked to resistance to temozolomide and radiation in GBM[43,44].

This redox adaptability occurs within a broader framework of metabolic flexibility in which GBM cells dynamically shift between glycolytic, mitochondrial, and glutamine-dependent programs in response to environmental and therapeutic stress[45]. Such flexibility helps explain the limited clinical success of metabolism-targeted therapies, as inhibition of individual pathways is frequently offset by compensatory metabolic rerouting[45].

Moreover, stromal interactions and aberrant vasculature increase metabolic heterogeneity which supply alternative substrates and strengthens tumor microenvironmental niches. This metabolic adaptability not only sustains cellular energetics but also promotes invasive and migratory phenotypes, as lactate-induced acidosis, hypoxia-driven HIF signaling, and glutamine metabolism converge to remodel the ECM, enhance epithelial-to-mesenchymal transition (EMT) like processes, and activate pro-migratory signaling pathways[46].

1.5 Cancer stem cells

GSCs constitute a small but functionally dominant subpopulation of GBM tumor, capable of self-renewal, multilineage differentiation, and tumor initiation. Their proposed origins trace back to neural stem cells or glial progenitors that have experienced oncogenic transformation through

cumulative genetic and epigenetic modifications. GSCs occupy the top of a cellular hierarchy, driving tumorigenesis while giving rise to more differentiated, short-lived progeny that comprise most of the tumor bulk. This hierarchical model explains the persistence of GSCs despite aggressive therapy, positioning them as the central driver of tumor initiation, progression, and recurrence.

Molecularly, GSCs express neural stem cell–associated markers including CD133, Nestin, Sox2, OLIG2, and integrin α6, which are frequently used for experimental isolation and characterization of these cells. These markers play functional roles in maintaining stemness, proliferation, and therapeutic resistance. GSCs demonstrate distinct plasticity, interconverting between stem-like and differentiated states in response to therapeutic or microenvironmental stress. This phenotypic flexibility is regulated by transcriptional programs (e.g., Notch, Wnt/β-catenin, Hedgehog) and metabolic rewiring, allowing GSCs to survive fluctuating oxygen and nutrient conditions while maintaining tumor-propagating potential[47].

Further, the TME plays a role in sustaining GSC phenotypes; within perivascular niches, endothelial cells provide instructive cues through VEGF, nitric oxide, and Notch ligands such as DLL4, reinforcing self-renewal and therapy resistance. Hypoxic regions further support GSC maintenance via HIF-mediated induction of stemness genes and metabolic adaptation. Beyond stromal cues, GSCs actively remodel their niche by secreting angiogenic factors, matrix metalloproteinases, and immunomodulatory cytokines, thereby promoting angiogenesis, ECM remodelling, and immune evasion. The reciprocal communication between GSCs and immune cells, particularly tumor-associated macrophages and microglia, increases immunosuppressive signaling, further protecting GSCs from anti-tumor immunity.

GSCs are also strongly implicated in therapeutic resistance. Their enhanced DNA repair capacity, elevated expression of ABC transporters, and robust antioxidant defences confer resilience against radiation and TMZ chemotherapy[48,40]. Furthermore, MGMT promoter unmethylation and activation of checkpoint kinases enhance their ability to withstand DNA damage[49]. This resistance enables GSCs to persist after therapy, reconstituting the tumor and driving recurrence with more aggressive phenotypes. Clinically, the persistence of GSCs represents a major obstacle to therapeutic success. GSC targeting strategies being researched include inhibition of stemness signaling pathways (Notch, Hedgehog, Wnt), metabolic vulnerabilities (e.g., glutamine addiction, fatty acid oxidation), Immunotherapeutic approaches, and disruption of supportive niches such as the vascular microenvironment[50].

1.6 Mechanism of GBM tumor invasion and migration

GBM is extremely invasive, with GSCs infiltrating surrounding brain tissue and disrupting standard brain architecture. Primary GBM tumors most commonly arise *de novo* within the supratentorial cerebral hemispheres, particularly in the frontal and temporal lobes and adjacent subcortical white matter. By contrast, recurrent GBM usually reforms locally at or near the original tumor site, with most recurrences developing within approximately 2 to 3 cm of the resection cavity, although less commonly they can present as more distant or infratentorial lesions[51]. The secretion of ECM-degrading enzymes, adhesion molecule alterations, and the utilization of existing anatomical structures, such as white matter tracts or blood vessels, facilitate this infiltration. The diffuse infiltration of GBM cells into adjacent tissue leads to challenges for surgical resection, as complete removal of the tumor is often impossible without damaging critical

brain structures. This invasive behaviour, driven primarily by the molecular alterations within GBM cells and their dynamic interactions with the tumor microenvironment, generates highly invasive tumors that evade conventional therapies.

MMPs, particularly MMP-2 and MMP-9, play a critical role in facilitating tumor invasion by degrading ECM components[52]. GSCs secrete high levels of these enzymes, which break down structural barriers and create pathways for cell migration. MMPs also release ECM-bound growth factors, such as VEGF and epidermal growth factor (EGF), which further enhance GSC motility and invasiveness[36]. The expression of MMPs is tightly regulated by HIFs and other signaling pathways active in the TME, linking matrix degradation to the hypoxic conditions of GBM.

Beyond enzymatic degradation of the ECM, GBM cells utilize cell adhesion and cytoskeleton molecules/receptors to facilitate invasion into surrounding brain tissue. Proteins such as N-cadherin, vimentin, and CD44 are upregulated during EMT-like processes, increasing GBM cell motility and promoting infiltration into peritumoral regions[53]. These changes weaken cell–cell junctions within the tumor while concurrently strengthening interactions with the ECM and vascular structures, allowing GBM cells to migrate more efficiently. The upregulation of adhesion or cytoskeleton molecules correlated with the tumors invasiveness and also with a poorer prognosis in patients[54].GSCs exhibit a unique ability to invade surrounding brain tissue by migrating along pre-existing blood vessels, a process known as perivascular invasion[55]. This method of invasion is facilitated by adhesive interactions between GSCs and endothelial cells through mechanisms previously discussed. The perivascular niche provides an optimal microenvironment for GSC survival, presents access to oxygen, nutrients, and signaling molecules. By migrating along blood vessels, GSCs bypass the ECM and evade hypoxic conditions in the tumor core, enabling diffuse

infiltration. Chemokine signaling also plays a crucial role in establishing GSC invasion and migration. GSCs express chemokine receptors, such as CXCR4, which respond to ligands like CXCL12 secreted by stromal cells and endothelial cells[56]. This interaction activates downstream signaling pathways that promote cytoskeletal remodelling, adhesion, and directional migration, leading GSCs to the perivascular niche. Additionally, autocrine signaling loops involving chemokines and growth factors enhance GSC motility and invasiveness, further driving tumor distribution.

1.7 Therapeutic challenges and resistance in GBM treatment

Although GBM is known to disrupt the BBB, particularly in regions of active angiogenesis, this disruption is heterogeneous. As a result, drug penetration remains suboptimal. Furthermore, the abnormal vasculature within GBM contributes to uneven drug distribution and the development of hypoxic and nutrient-deprived regions, which promote therapeutic resistance. This limited access to the tumor causes a need for novel strategies to overcome the BBB to treat primary and recurrent GBM.

The infiltrative nature of GBM, characterized by its ability to extend along white matter tracts and invade the surrounding brain parenchyma, often prohibits complete resection. Even with advanced imaging techniques such as intraoperative fluorescence-guided surgery using 5-aminolevulinic acid (5-ALA)[57], residual tumor cells remain, serving as a source for recurrence. Further, radiotherapy, typically delivered in fractionated doses over multiple treatment periods, induces DNA damage primarily through the generation of double-strand breaks. While effective in targeting rapidly dividing tumor cells, GBM's heterogeneity and the presence of radioresistant subpopulations limit its efficacy. Additionally, hypoxic regions within the tumor core act as

protective niches, reducing the effectiveness of radiotherapy by decreasing oxidative stress levels required for DNA damage[58].

TMZ induces cytotoxicity primarily through methylation of the O6 position of guanine residues, generating DNA lesions that trigger replication stress and cell death. In practice, however, the clinical benefit of TMZ is highly variable and frequently challenged by intrinsic and acquired resistance mechanisms. Expression of MGMT is a major determinant of therapeutic response, with MGMT-proficient tumors exhibiting limited sensitivity to treatment. Even among patients with MGMT promoter methylation, long-lasting responses are uncommon, reflecting the ability of GBM cells to engage alternative DNA damage response pathways and adaptive survival programs under therapeutic pressure. As a result, TMZ primarily delays progression rather than producing sustained tumor control.

GBM is inherently resistant to therapy, a feature driven by a multitude of molecular and microenvironmental mechanisms. One of the primary drivers of resistance is the tumor DNA repair machinery. GSCs, in particular, display heightened activation of DNA repair pathways, including homologous recombination HR and non-homologous end joining NHEJ[59]. The overexpression of repair proteins such as RAD51, ATM, and ATR presents a survival advantage to tumor cells following chemoradiotherapy administration. Furthermore, GBM cells often accumulate mutations in tumor suppressor genes such as TP53, which exacerbate genomic instability and enable adaptive responses to DNA damage.

1.8 Emerging therapeutic targets and future directions

The failure of current multimodal treatments in GBM can be attributed to a combination of biological and clinical factors. These limitations of current treatments have led to a surge of

research focusing on novel approaches that address the tumor's inherent complexity and adaptability. GSCs represent a key therapeutic target due to their fundamental role in GBM progression, recurrence, and resistance to therapy. Approaches to eliminate GSCs include targeting their surface markers, such as CD133 and integrin α6, and disrupting key signaling pathways that maintain their stemness and survival. Inhibitors of the Notch, Wnt, and Hedgehog pathways, which are critical for GSC self-renewal, have shown promise in preclinical studies[60]. Additionally, differentiation therapy, which aims to induce GSCs to transition into less tumorigenic and more therapy-sensitive cell types, represents a novel approach to reducing the GSC population[61,62].

Targeting angiogenesis has long been a central strategy in glioblastoma therapy, motivated by the highly vascular and permeable nature of these tumors. Anti–VEGF agents such as bevacizumab were developed to normalize aberrant tumor vasculature, reduce edema, and improve the delivery of cytotoxic therapies. Although bevacizumab reduces contrast enhancement and peritumoral edema, large randomized clinical trials failed to demonstrate an improvement in overall survival in newly diagnosed or recurrent GBM[63–65]. Moreover, accumulating clinical and preclinical evidence indicates that VEGF blockade can promote adaptive responses characterized by increased tumor cell invasion, diffuse infiltration, and mesenchymal transition, ultimately contributing to treatment failure[66,67] . These findings suggest that anti-angiogenic therapy alters the mode of tumor progression, enabling GBM cells to escape angiogenic need through altered invasion and microenvironmental remodeling. Combination approaches targeting VEGF alongside pathways such as PI3K/AKT/mTOR, MET, EGFR, or FGFR have therefore been explored to overcome resistance however, clinical benefit has remained limited[68]. Collectively, these outcomes highlight that angiogenesis in GBM is regulated by interactions between tumor cells, endothelial cells, and the surrounding microenvironment. A deeper understanding of the cellular crosstalk that drives

invasion and therapy-induced adaptation is therefore essential for identifying vulnerabilities that cannot be bypassed through vascular or metabolic programs.

Immunotherapy agents are emerging as a novel treatment for brain tumors, leveraging how patients' immune system can be activated to fight off malignant cells. Chimeric antigen receptor (CAR)-T cells targeting GBM-specific antigens, such as EGFRvIII and IL13Rα2, have shown encouraging results in early-phase clinical trials[69]. Similarly, dendritic cell vaccines and peptide-based vaccines targeting tumor antigens, aim to stimulate an anti-tumor immune responses[70]. Moreover, immune checkpoint inhibitors, targeting PD-1/PD-L1 and CTLA-4, seek to restore T-cell activity within the immunosuppressive GBM microenvironment alongside standard of care treatment[71]. While these approaches face challenges, such as limited immune cell infiltration and antigen heterogeneity, they hold considerable capacity for improving GBM survival outcomes.

Advances in genomic and epigenomic profiling have paved the way for precision medicine in patients diagnosed with GBM. By detecting patient-specific mutations, such as those in IDH1, TP53, and PTEN, clinicians can modify therapies to target the unique molecular weaknesses of individual tumors. Epigenetic profiling, including the assessment of MGMT promoter methylation, provides prognostic information and guides the use of alkylating agents like TMZ. Emerging technologies, such as single-cell sequencing, further enable the characterization of intratumoral heterogeneity, facilitating the development of highly personalized treatment regimens. CRISPR-Cas9 genome-editing technology offers a novel approach to GBM treatment by allowing precise targeting of oncogenes, drug resistance mechanisms, and immune evasion pathways. Preclinical studies have demonstrated the potential of CRISPR to disrupt key drivers of GBM growth, such as EGFR amplification and PTEN loss, among others[72]. Nanoparticle-based

drug delivery systems represent another strategy to overcome the challenges of the BBB and improve drug distribution within the tumor[73]. These systems can be engineered to carry chemotherapeutic agents, RNA-based therapeutics, or imaging agents straight to the site of the tumor. These new technologies bypass the BBB with the drug intact, offering a platform for both treatment and diagnosis of hard-to-reach tumors like brain malignancies. Finally, the modulation of neurotransmitter pathways, such as those involving glutamate and D-serine, provides a novel avenue for targeting GBM. By disrupting the pro-tumorigenic effects of these signaling molecules, researchers aim to inhibit tumor growth and invasion while mitigating the neurological deficits associated with GBM tumor location.

1.9 Role of Neurotransmitters in GBM Progression and interaction with microenvironment

Glutamate, a major excitatory neurotransmitter in the CNS, plays a role in GBM progression. GBM cells secrete excessive amounts of glutamate through the system Xc− antiporter, which exchanges intracellular glutamate for extracellular cystine. This dysregulated glutamate release creates a hyperexcitable microenvironment that promotes tumor proliferation and invasion[74]. Glutamate acts on ionotropic receptors, such as N-methyl-D-aspartate receptors (NMDARs) and α-amino-3-hydroxy-5-methyl-4-isoxazolepropionic acid (AMPA) receptors, to activate intracellular signaling pathways involved in cell survival, migration, neurotransmission, synaptic plasticity, and higher-order cognitive functions in the CNS[75]. At the molecular level, functional neuronal NMDARs form heterotetrameric units, typically comprising two GluN1 subunits and a combination of GluN2 (A–D) and/or GluN3 subunits. Their activation requires the co-binding of glutamate and a co-agonist; either glycine or D-serine, alongside postsynaptic depolarization to mitigate the voltage-dependent magnesium block. Once activated, NMDARs permit calcium influx in addition to sodium and potassium conductance.

Although once considered largely neuron-restricted, research now supports NMDAR expression and function across multiple non-neuronal cell types. Glial populations provide some of the evidence, as astrocytes regulate the availability of the NMDAR co-agonist D-serine and can dynamically tune D-serine levels as a function of behavioural state and neuromodulatory inputs[76]. In parallel, oligodendrocyte lineage cells express NMDARs and receive glutamatergic input, with evidence that NMDAR signaling contributes to oligodendrocyte precursor cell differentiation and myelination-related programs in vivo[77]. Beyond the CNS, NMDAR subunits and functional responses have been reported in immune cells. Human T lymphocytes express NMDAR subunits and exhibit signaling cascades during receptor activation, supporting the concept that glutamatergic signaling can shape cellular behaviour outside synapses[78]. These findings collectively argue that NMDARs participate in intercellular communication across tissues, often operating in microenvironmental contexts where ligand availability and receptor coupling differ from synaptic transmission.

Among non-neuronal NMDARs, endothelial NMDARs (eNMDARs) have gained attention because endothelial cells occupy an anatomical and functional interface where metabolic cues, inflammatory mediators, and paracrine signals play a role. Work in brain endothelium suggests that eNMDARs can regulate permeability-related processes and cytoskeletal or vesicular trafficking pathways, shaping BBB transport properties[79,80]. Mechanistic evidence indicates that endothelial NMDAR signaling can influence permeability through pathways that are not strictly dependent on canonical ion flux, highlighting that eNMDARs may engage nonionotropic or metabotropic signaling modes in vascular cells[80]. Consistent with these observations, NMDAR activation has been shown to increase BBB permeability and engage signaling pathways such as Rho/ROCK in primary human brain microvascular endothelial cell models[81]. More recent work

has further reinforced the view that NMDAR activation can induce structural and transport changes at the BBB, including modulation of endocytic/transcytosis machinery, and that these responses can show regional heterogeneity across the brain vasculature [82].

The presence of NMDAR-related programs in endothelial biology is also relevant in cancer, where vascular cells are reprogrammed by tumor-derived signals to support angiogenesis, barrier disruption, immune evasion, and therapy resistance. Tumor microenvironments can contain elevated extracellular glutamate and altered serine/D-serine metabolism. Conditions that may activate eNMDARs and cause vascular behaviour to support tumor growth. In colorectal cancer, for instance, endothelial expression of an NMDAR subunit (GRIN2D) has been proposed as a tumor endothelial marker linked to angiogenic function, supporting the idea that NMDAR biology can be co-opted within tumor vasculature[83]. While the extent to which such mechanisms generalize across tumor types remains unknown, these findings call for deeper investigation of how endothelial glutamatergic signaling integrates metabolic ligands and microenvironmental cues to shape vascular phenotypes in disease. The field still lacks a clear map of subunit composition across vascular beds, the relative contribution of glutamate versus co-agonists (including D-serine) under physiological and pathological conditions, and the downstream signaling outcomes that distinguishes protective from pathological outcomes. A more precise understanding of eNMDAR regulation and function may therefore reveal new ways to disrupt maladaptive neurovascular and tumor–vascular crosstalk.

Within the brain tumor context, these principles of glutamatergic signaling overlap with well-established mechanisms of excitotoxicity, which have been implicated in glioblastoma progression and microenvironmental remodeling. Excitotoxicity, driven by excessive glutamate release,

contributes to GBM progression by inducing the death of non-cancerous neurons and astrocytes in the tumor vicinity. This process is mediated by overactivation of AMPA and NMDARs, leading to calcium overload and subsequent neuronal apoptosis. The loss of healthy neurons creates physical space for tumor expansion and releases bioactive molecules that further promote GBM cell survival and invasion[84]. Cancerous cells can exploit this mechanism by upregulating genes upstream of NMDAR activation. Many studies have shown the increase in glutamate release, but only a few have linked D-serine to cancer progression. Enzymes such as Serine Racemase (SRR) can be upregulated in cancerous cells, leading to an increase in the D-serine pool[85,86]. SRR is a pyridoxal-5'-phosphate (PLP)-dependent enzyme that catalyzes the racemization of L-serine to D-serine, as well as the α,β-elimination of water from both L- and D-serine to form pyruvate and ammonia. SRR is localized predominantly in astrocytes, neurons, and microglia within the healthy CNS. Regulation of the D-serine pool and SRR activity is critical because it has been shown that they modulate NMDAR-dependent synaptic plasticity, including long-term potentiation and long-term depression[87]. Dysregulation of SRR activity and D-serine availability has been implicated in multiple neurological and psychiatric conditions, such as Alzheimer's and schizophrenia. SRR has also been shown to be involved in other solid cancers, whose activity contributes to an anti-apoptotic effect leading to a poorer prognosis[85]. Activation of NMDARs through glutamate and D-serine triggers calcium influx and the subsequent activation of downstream signaling pathways, including PI3K/AKT and MAPK, which promote tumor growth, survival, and resistance to apoptosis.

Further, GBM cells establish complex paracrine interactions with neurons, leveraging neuronal activity to support tumor growth. Neurons release neurotransmitters and growth factors, such as

brain-derived neurotrophic factor, in response to tumor-induced synaptic activity[88]. These factors, enhance GBM cell proliferation and migration through the activation of receptor tyrosine kinases and other signaling pathways. Conversely, GBM cells secrete glutamate and other excitatory molecules to stimulate neuronal activity, creating a feedback loop that amplifies tumor-neuron interactions.

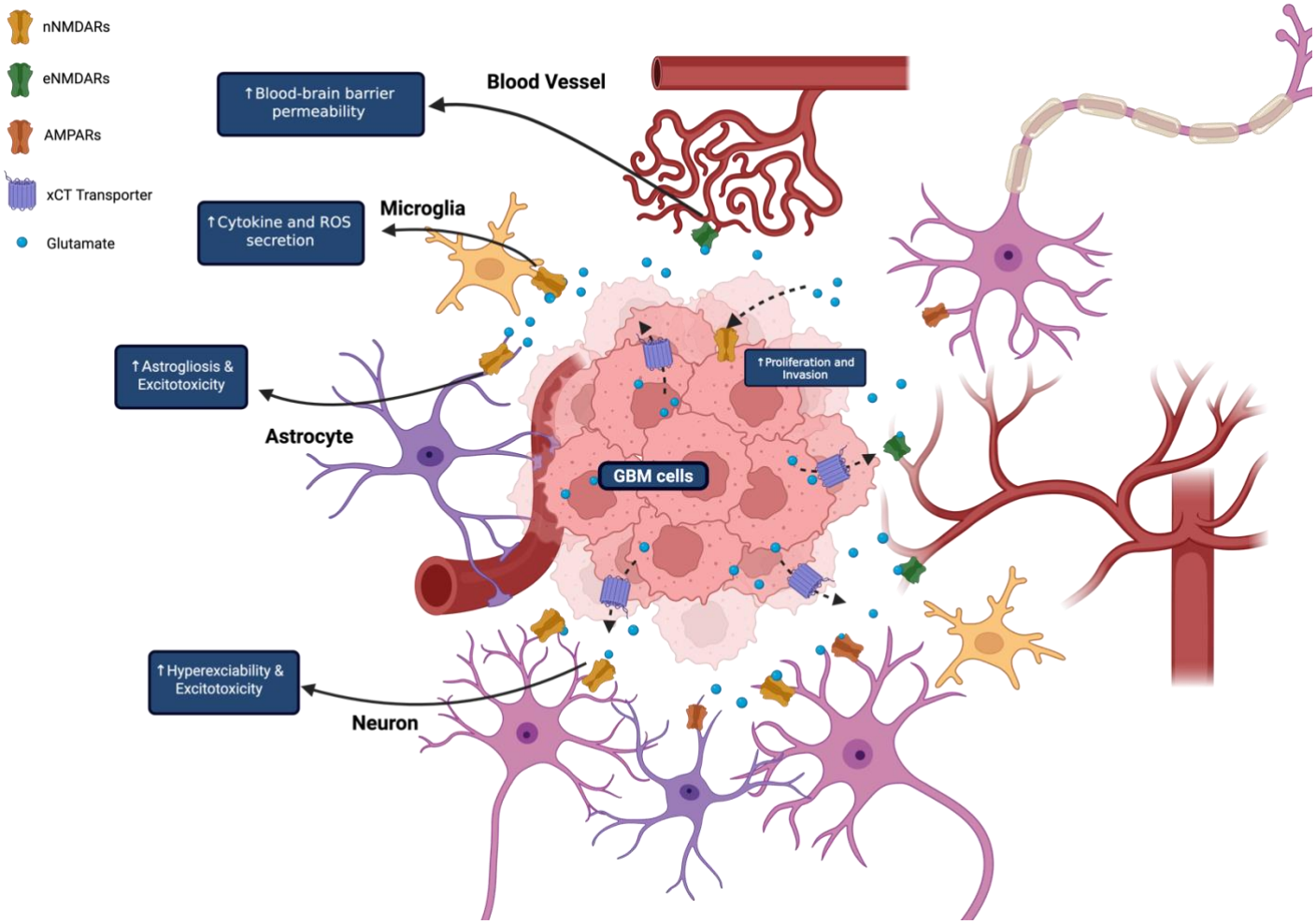

Figure 2. Glioblastoma crosstalk with neural, glial, immune, and vascular cell populations through NMDA- and AMPA-receptor-associated signalling pathways. Tumor-derived glutamate and related receptor activity within GBM cells and the surrounding microenvironment contribute to proliferation and invasion, while also promoting astroglial and neuronal excitotoxicity, microglial cytokine and reactive oxygen species release, and increased blood-brain barrier permeability.

1.10 GBM interaction with Brain ECs and the role of ECs in GBM progression

Glioblastoma growth is tightly coupled to the vasculature, blood vessels act as a source of oxygen, nutrients, and a signaling partner that shapes tumor cell behaviour. Early histological and functional studies showed that stem-like glioma cells are preferentially localized to perivascular regions and that proximity to endothelial cells is associated with enhanced tumor-initiating capacity[89]. These observations led to the concept of a vascular niche in GBM, in which endothelial cells actively support stem-associated cascades. Subsequent work confirmed that endothelial cells can directly influence self-renewal, survival, and resistance phenotypes in glioma stem-like cells[89,90].

This niche develops within a vascular system that is structurally and functionally abnormal. GBM vessels are disorganized, dilated, and highly permeable, resulting in heterogeneous perfusion and chronic hypoxia while sustaining tumor expansion[91]. These abnormalities arise from sustained pro-angiogenic signaling and inflammatory cues. VEGF plays a dominant role in this process by promoting endothelial proliferation, migration, and permeability, and its expression is particularly enriched in stem-like glioma populations[91]. Glioma stem-like cells secrete VEGF along with chemokines such as stromal-derived factor 1 (SDF-1/CXCL12), which recruit and activate endothelial cells and contribute to vascular expansion under tumor conditions[92]. The resulting vasculature creates spatial gradients that favor selection of invasive and therapy-resistant cell states.

Endothelial cells, in turn, exert direct control over glioma stem-like cell behaviour. Contact-dependent signaling has emerged as a critical component of this interaction. Endothelial cells express Notch ligands that bind Notch receptors on adjacent tumor cells, activating transcriptional programs associated with self-renewal and stemness[90]. Diffusible mediators further strengthen this effect, endothelial-derived nitric oxide activates Notch signaling in neighboring glioma stem-like

cells through a cGMP-dependent mechanism, accelerating tumor initiation and growth in vivo[93]. In parallel, glioblastoma-associated endothelial cells act as a source of inflammatory cytokines, with Interleukin-6 (IL-6) emerging as a prominent factor within perivascular regions. Spatial and functional analyses have identified tumor-associated endothelial cells as a major source of IL-6 in the GBM microenvironment, where endothelial IL-6 shapes local niche biology and promotes tumor-supportive immune programming[94]. Genetic reduction of endothelial IL-6 in vivo shifts the immunosuppressive landscape and constrains tumor progression, emphasizing that IL-6 release can be endothelial-driven in GBM[95]. Given the established role of IL-6/STAT3 signaling in supporting glioma stem-like cell growth and survival, endothelial IL-6 provides a plausible mechanism by which the vasculature can reinforce stem-like phenotypes through paracrine cytokine signaling in addition to Notch and NO pathways[96]. GBM vascularization is further complicated by endothelial-independent mechanisms. Vasculogenic mimicry, in which tumor cells form vessel-like structures without endothelial lining, has been observed in human GBM specimens and provides an alternative route for perfusion in poorly vascularized regions[97]. In parallel, glioma stem-like cells exhibit a capacity for lineage plasticity, differentiating into vascular-associated cell types under specific microenvironmental conditions. Several studies have reported endothelial-like differentiation of glioma stem cells, contributing directly to tumor vasculature and limiting the efficacy of therapies that target endothelial angiogenesis alone[98,99]. Beyond endothelial transdifferentiation, glioma stem-like cells can generate pericyte-like cells that integrate into the vessel wall and regulate vascular stability, further embedding tumor cells within the vascular niche[100].

Hypoxia intensifies these interactions. Poor perfusion and high metabolic demand create regions of sustained low oxygen tension, activating hypoxia-inducible transcriptional programs in tumor

cells. One consequence is increased release of extracellular vesicles. Hypoxic glioma cells produce exosomes enriched in angiogenic proteins and regulatory RNAs that reprogram endothelial cells toward a pro-angiogenic, tumor-supportive phenotype[101]. This mode of communication allows hypoxic tumor regions to influence distant endothelial compartments and contributes to the persistence of vascular abnormalities even when angiogenic signaling is therapeutically suppressed.

To conclude, these observations indicate that the vascular niche in GBM is maintained through multiple signaling mechanisms that extend beyond classical angiogenic pathways. While Notch ligands, nitric oxide, and hypoxia-driven vesicle exchange contribute to endothelial–tumor crosstalk, they do not fully account for how metabolic states within tumor cells are identified and translated into endothelial responses. The persistence of vascular support following anti-angiogenic therapy suggests that additional modes of communication operate within the perivascular space, particularly those capable of coupling tumor metabolism to endothelial signaling. In this context, glutamatergic signaling represents a compelling but underexplored mechanism. Endothelial cells express functional NMDA receptors, positioning them to respond to locally available ligands. Tumor-associated alterations in serine metabolism and D-serine production therefore raise the possibility that metabolic cues directly activate endothelial NMDA receptor signaling to reinforce a tumor-permissive vascular niche. Defining how this pathway integrates with established endothelial programs may reveal a distinct layer of vascular regulation that contributes to GBM progression and recurrence.

Chapter 2: Hypothesis/Rationale

Specific Aim: Determine if D-Serine facilitates aggressive migration and stemness of recurrent glioblastoma cells by interacting with host endothelial cells.

Rationale: GBM cells invade deep brain structures along endothelial-guided paravasculature pathways that support stemness and malignant properties. This allows access to nutrient-rich environments, causing infiltration and expansion of recurrent tumors. Elucidating the mechanism by which GBM and endothelial cells communicate to permit widespread distribution of recurrent tumors is critically important. One pathway that could link GBM and ECs is glutamate release by GBM. GBM cells release large amounts of glutamate, which leads to enhanced tumor malignancy by poorly understood mechanisms, likely involving NMDARs in the brain. Work from our group identified a robust role for NMDA receptors expressed specifically by brain eNMDARs in transducing signals initiated by parenchymal cells in the brain. This raises the possibility that eNMDARs respond to tumor-derived glutamate and co-agonists to yield a pro-tumor environment. The ECs secretome contributing to synergistic paracrine signaling aiding angiogenesis, migration, stemness, and proliferation of recurrent GBM. Some of our work has shown that the presence of eNMDARs in GBM models increases malignant properties and glutamate release *in vitro*. It is not clear, however, if NMDAR co-agonists play a role. D-serine, a co-agonist of NMDARs is released from GBM cells, potentially acting as a co-agonist of EC-mediated recurrent tumorigenesis. The potential co-requirement of glutamate and D-Serine at eNMDARs is the foundation of the following experiments assessing how D-serine affects the phenotype of recurrent GBM through EC-mediated signals.

Hypothesis: GBM cells release NMDAR co-agonists glutamate and D-serine, leading to the enhancement of endothelium-dependent rGBM migration, stemness and invasiveness.

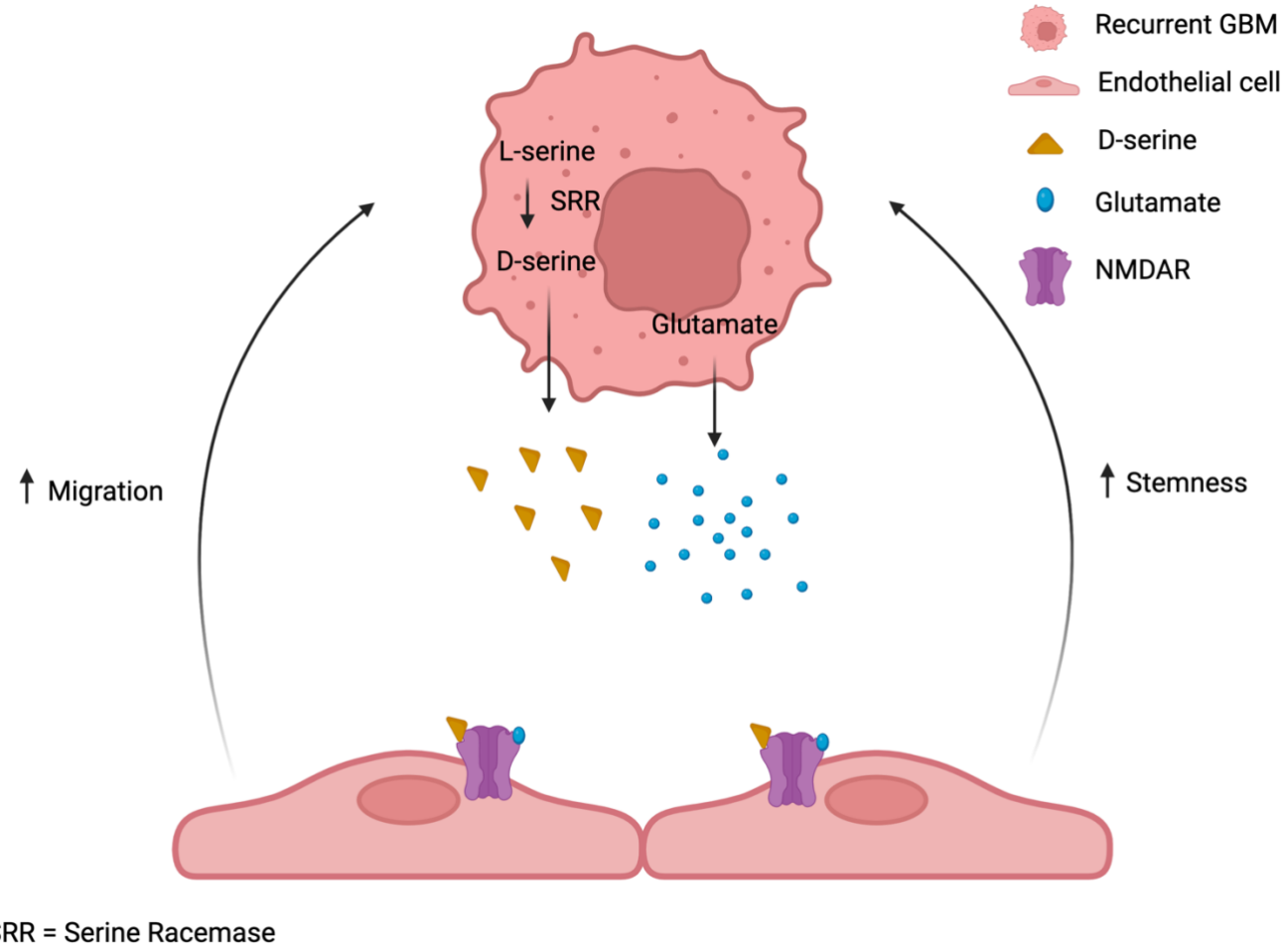

Figure 3. Endothelial NMDA receptor activation by tumor-derived glutamate and D-serine sustains aggressive phenotypes in recurrent glioblastoma. Altered serine metabolism and release of glutamate and D-serine from recurrent GBM cells promote endothelial NMDAR signalling, which is associated with increased stemness and migratory behaviour.

Chapter 3: Experimental methods and materials

Cell Culture

Dr. Sheila Singh kindly provided the patient-derived GBM tumor cells BT241 and BT972 (Centre for Discovery in Cancer Research, McMaster University; MTA no. MTO20-120) (Table. 1). Patient-derived GBM cells were maintained in serum-free DMEM/F12 media (Gibco, Cat #11320033) with 20 ng/mL of EGF (STEMcell, Cat #78006), 10 ng/mL of bFGF (STEMcell, Cat #78003), 1× NeuroCult SM1 Supplement (STEMcell, Cat #05711), 1× N2 Supplement (STEMcell, Cat #07152), 2 µg/mL Heparin (STEMcell, Cat #07980), and 1× antibiotic-Antimycotic (Sigma-Aldrich, Cat #A5955).

Table 1. Clinical data of patient-derived GBM models.

Sample	Age/Sex	Diagnosis	Subtype	Survival (months)	PTEN Variant(s)	TP53 Expression	TP53 variant(s)	IDH Status
BT 241	69/F	Recurrent GBM	Mesenchymal	23	VL317-318X	40.14	R208K, P72R	WT
BT 972	53/M	Recurrent GBM	Mesenchymal	41	H123Y	68.33	P190L, G244D	WT

Human cerebral microvascular endothelial cells (hCMEC/D3) were purchased from Cedarlane (Cat #CLU512). They were maintained in Endothelial Cell Growth Basal Medium-2 **(**EBM2, Lonza Bioscience, Cat #00190860) media with 5% FBS (Gibco, Cat #A3160702), 1.4 uM hydrocortisone (Sigma-Aldrich, Cat #H0135), 5 ug/ml acid ascorbic (Sigma-Aldrich, Cat #A4544), 1× chemically defined lipid concentrate (Gibco, Cat #11905031), 10 mM HEPES (Sigma-Aldrich, Cat #H0887), 1 ng/ml bFGF (STEMcell, Cat #78003), and 1× antibiotic-Antimycotic (Sigma-Aldrich, Cat #A5955).

CRISPR editing

Two lentiviral CRISPR/Cas9 plasmids were designed to target distinct SRR gene regions to knock out SR expression. Plasmid SR KO 1 (V1) was constructed using the pLentiCRISPR V2 backbone (Genscript) and carried a guide RNA (gRNA) sequence of 5'-GTATACAATTGACGCTCCGT-3'. Plasmid SR KO 2 (V3), based on the pLentiCRISPR V2 backbone (Genscript), included a gRNA sequence 5'-CATCATGGTACATCCCAA-3'. Both plasmids were designed to target critical regions within the SR coding sequence, maximizing the likelihood of complete gene disruption by introducing frameshift mutations. Lentiviral particles were produced by the University of Manitoba Lentivirus Core Service Platform using standard packaging protocols. The resulting lentiviral preparations were titrated and utilized for transducing the target cells to achieve stable and efficient CRISPR/Cas9 system delivery. Cells (20,000/well) were seeded in a 24-well plate, and then 2 µL of lentivirus was introduced to the cells. Puromycin (2 ng/µL) selection was performed 3 days after transduction and single-cell colonies were isolated and expanded. Following transduction and selection of stable clones, the efficiency of SRR knockout was evaluated through Western blot analysis. Membranes were incubated with an anti-SRR antibody (Abcam, Cat #ab200833) at a dilution of 1:1000, followed by incubation with an HRP-conjugated secondary antibody (Santa Cruz, goat anti-rabbit IgG, Cat #sc-2004). The blot was developed using enhanced chemiluminescence, and band intensity was quantified to confirm the reduction or absence of SRR expression. The same protocol was used to knock out GluN1 KO cells with the following products; LentiArray CRISPR Negative Control Lentivirus (Thermo Fisher, Cat #A32062), LentiArray Cas9 lentivirus (Thermo Fisher, Cat #A32064), and LentiArray CRISPR GluN1 lentivirus (ThermoFisher, #A32042). Knockout was confirmed with western blot using GluN1 antibody (Millipore, Cat #Ab9864R, 1:1000).

Chemicals used

The chemicals used inhibited D-serine levels or NMDA activation, such as Phenazine methosulfate (PMS, Sigma-Aldrich, Cat #P9625), D-amino acid oxidase (DAAO, Sigma-Aldrich, Cat #A5222), 5,7-Dichlorokynurenic acid (DCKA, Tocris, Cat #0286/10) AP5 (Sigma-Aldrich, Cat #A8054), MK801 (Tocris, Cat #0924/10), MCPG (Tocris, Cat #0336/10). Other chemicals used altered indirect pathways from our D-serine hypothesis like L-NIO (Tocris, Cat #0546/10), Anti- Il6 (R&D systems, Cat #MAB206-100), and Human IL-6 Recombinant Protein (ThermoFisher, Cat #PHC0064).

Molecularly characterized patient sample analysis

This study collected GBM and non-GBM data from multiple online databases. RNA sequencing data along with survival data was collected from TCGA TARGET GTEx, Rembrandt, TCGA GBM-LGG, and CGGA datasets. These datasets were used to screen human tissue samples for SRR mRNA levels in cancerous, non-cancerous, and different grades of glioma tumors. The analysis includes SRR transcripts for each sample characterized by non-tumor tissue, tumor tissue, glioma grades I-IV, and primary vs recurrent gliomas.

NanoString nCounter analysis

RNA was extracted from cells using the BioRad Aurum™ Total RNA Mini Kit per manufacturer's protocol. 300 ng of total RNA of each sample were hybridized to barcoded oligo CodeSets curated nCounter® Tumor Signaling 360 Panel to profile 780 genes. Samples were hybridized overnight for at least 16 hours in a thermal cycler at 67°C with a heated lid at 72°C. The resulting RNA hybridized to barcode tags were subsequently detected and counted using an nCounter Prep Station and Digital Analyzer (NanoString Technologies) the following day. Raw counts were background subtracted then normalized using the geometric mean of the samples analyzed using NanoString nSolver. The RNA quality was assessed using both Nanodrop and Qubit Fluorometer. The 260/280

ratios of all samples are confirmed to be within 1.9-2.1 as measured by Nanodrop spectrophotometry. The Quibit RNA IQ Assay was used to assess RNA quality and fragmentation. The assay uses two dyes to measure the ratio of large (intact) to small (degraded) RNA, and scores are given on a 1-10 scale, with 1 being highly degraded and 10 being completely intact. All samples are confirmed to have an RNA IQ Score >7. Equal concentrations of RNA were loaded for each sample. All genes were used in the enrichment analysis (including housekeeping genes). Prior to gene-ontology enrichment analysis, differentially expressed genes were identified using DESeq2 analysis in R, which corrects false discovery rates using the Benjamini and Hochberg (BH) method.

Cytokine profile analysis

Cytokine profiles were analyzed in the culture media of patient-derived GBM and hCMEC cells. Ten thousand hCMEC cells were plated 2 days before the GBM cells to allow for adhesion, then 2×10^5 GBM cells were plated in the top chamber of a 0.4 μm transwell (Corning, Cat #07-200-165). Samples were incubated in a 37°C, 5% CO_2 incubator for 24 hours to condition the media. After 24 hours, the media was centrifuged at [1000xg] for 5 minutes to remove all cells; the media was then concentrated with centrifugal filters (Sigma-Aldrich, Cat #UFC910024) by spinning at 3220xg for 10 minutes. Samples were then diluted with 1× blocking buffer provided by the Human Cytokine Membrane Antibody Array (Abcam, Cat #ab133998). The manufacturer's protocol was then followed to analyze the cytokine expression differences of 80 human targets. The printed membranes were scanned under high-resolution chemiluminescence using the ChemiDoc MP imaging system (BioRad).

Colorimetric D-serine Release Assay

D-serine levels in the media were quantified using a chemiluminescent assay. Media samples were collected over various time points between 1-72 hours from a transwell system. Collected media

were heated at 95°C for 5 minutes to denature any enzymes that might interfere with the assay. Following this step, 10-30 µL of each sample was mixed with 100 µL of assay buffer containing 100 mM Tris·HCl (pH 8.8), 20 U/mL peroxidase (Sigma, #P6782), and 8 µL of luminol. Samples were incubated at room temperature. After, 10 µL of D-amino acid oxidase (DAAO; Sigma, #A5222, 75 U/mL) was added to each sample. The reaction proceeded, and chemiluminescence activity was recorded at room temperature using the Varioskan Lux Plate reader (ThermoFisher). Data were expressed and normalized to control conditions and analyzed to determine changes in D-serine levels by various conditions.

Protein Extraction and Western immunoblotting

Cells in co-culture were collected separately from each other by the transwell system. GBM cells were collected from the top chamber, and hCMEC cells were detached by gently using a cell scraper on the bottom chamber, and both were washed with cold 1× PBS at pH 7.4. Cells were then centrifuged at 500xg for 5 min at 4 °C. Pellets were resuspended in RIPA lysis buffer (25 mM Tris pH 7.6, 150 mM NaCl, 1% NP-40, 1% sodium deoxycholate, 1% SDS) containing 1% PIC and phosphatase inhibitors. Following the addition of lysis buffer, cells were incubated on ice for 1 hour. The cell lysates were centrifuged at max rpm for 15 min at 4 °C, and the supernatant from the samples was collected and stored at -20°C until used. Protein concentrations for the collected samples were quantified using the Pierce BCA protein assay kit (Thermo Fisher. Cat #23225). Equal amounts of protein were boiled in Laemmli sample buffer (BioRad) containing 5% β mercaptoethanol for 5 min and then resolved by SDS-PAGE. Protein was transferred onto PVDF membranes (Biorad, Cat #1620177) that have been activated. Total protein was determined with 2,2,2-Trichloroethanol activation using UV illumination and then scanned following the transfer to the membrane with the ChemiDoc MP imaging system (BioRad). Membranes were blocked in

5% non-fat milk in TBST (TBS, 0.05% Tween 20) for 1 hr, washed in TBST and incubated in the appropriate primary antibody overnight at 4 °C with gentle rocking. The primary antibodies were prepared at a 1:1000 dilution in 1% BSA in PBST. The following day, membranes were washed in TBST before incubating in appropriate horseradish peroxidase (HRP)-conjugated secondary antibodies (Santa Cruz, goat anti-rabbit IgG, Cat #sc-2004). Secondary antibodies were prepared at a 1:1000 dilution in 5% non-fat milk in PBS and added to the membranes for 2 hr at room temperature. Following secondary antibody incubation, membranes were washed, and proteins were detected using Clarity ECL Western substrate (Bio-Rad, Cat #170-5061) and visualized using the ChemiDoc MP imaging system (Bio-Rad) chemiluminescent setting. Semi-quantitative analysis of the protein densitometry signal was performed using Image lab software normalized to total protein or a housekeeping gene.

Transwell Migration Assay

The transwell assay was performed to evaluate the motility capacity of GBM cells. Prior to the assay, 2,000 hCMECs were seeded in the lower chamber of a transwell system (Corning, Cat #07-200-150). The cells were maintained in 600 µL of EBM-2 and incubated at 37°C in a humidified atmosphere containing 5% CO_2 for 48 hours to allow adherence and initial growth.

For the assay, GBM cells (2×10^5) were resuspended in 200 µL of serum-free DMEM/F12 medium and added to the upper chamber of a transwell insert with an 8.0-µm pore polycarbonate membrane (Corning, Cat #07-200-150). The transwell insert was placed over the lower chamber containing the hCMEC monolayer. The co-culture system was incubated at 37°C for 24 hours. Following incubation, non-migrated cells were removed by taking off the top transwell chamber. Migrated GBM cells on the lower surface of the whole well were visualized using an inverted fluorescence

microscope. Migrated cells were manually counted across the entire well at 10× magnification using an EVOS fluorescent microscope (Thermofisher). Representative images were used to depict migratory capabilities.

Tumorsphere formation Transwell Assay

The sphere formation assay was conducted to assess the stemness capacity of GBM cells in co-culture with hCMECs. hCMECs (2,000 cells) were seeded in the lower chambers of 24-well plates (Corning, Cat #07-200-147) 48 hours before the initiation of co-culture experiments. Cells were maintained in EBM-2 during the 48 hours.

For the sphere formation assay, GBM cells (2,000) were seeded into the transwell inserts (upper chambers) of the same 24-well plate system, which allowed physical separation but facilitated interaction through the membrane. The transwell inserts utilized had a pore size of 0.4 μm (Corning, Cat #07-200-147). The co-culture was maintained in DMEM/F12 medium for 4–6 days at 37°C and 5% CO_2 to allow for sufficient tumorsphere growth. Spheres were imaged using an EVOS fluorescent microscope (Thermofisher) at 4x magnification and stitched together to analyze all spheres in a well. Images were analyzed using ImageJ's "analyze particles" software, spheres > 50μm were subjected to quantification based on microscope resolution and magnification. Data collected was based on the output from the average size, number of spheres, and total area of the whole well.

3D Spheroid Invasion Assay

To evaluate the invasive properties of GBM cells, spheroids were generated and cultured in a co-culture system with hCMECs. GBM cells (10,000) were cultured in 6-well plates (Corning, Cat #3516) for six days to induce spheroid formation. The resulting spheroids, with diameters ranging between 100–200 μm, were used for subsequent experiments.

Matrigel (Corning, Cat#354234) was diluted with 450 μL of serum-free stem cell media (DMEM/F12) to prepare a supportive extracellular matrix. A 60μL aliquot of this Matrigel mixture was added to each well of a 96-well plate (Falcon, Cat #08-772-2C) and incubated at 37°C for 30–60 minutes to solidify. This Matrigel layer served as a bedding to prevent spheroid adhesion to the plastic surface and to support spheroid maintenance during the assay.

Approximately 8–10 spheroids per condition were embedded in 80μL of undiluted Matrigel and transferred into 96-well plates. Following a 30-minute incubation at 37°C in a 5% CO_2 incubator, hCMECs (1,000 cells) were seeded on top of the Matrigel-coated spheroids and overlaid with 100 μL of serum-free DMEM/F12 medium.

The co-culture system was monitored using an inverted EVOS fluorescence microscope (ThermoFisher) at 0, 1, 2, and 3 days post-initiation. Spheroid morphology and invasion characteristics were documented, and ImageJ software was used to quantify invasion metrics.

Cell viability assay

rGBM cells BT241 or BT972 were seeded (10,000 cells/well) in a 96-well plate containing 100μL of media with various concentrations of PMS. Cells were incubated for 24 hours in a 37°C, 5% CO_2 incubator. 10μL of Presto Blue reagent (Thermofisher, Cat #A13261) was added to each well and incubated in a 37°C, 5% CO_2 incubator for 30 minutes protected from light. Cell viability was then determined using fluorescence emission of 560nm and excitation of 590nm with the

Varioskan Lux Plate reader (ThermoFisher) and doing background subtraction. The correlation of the fluorescent reading is related to the GBM cell viability at each PMS concentration

Patient-derived xenograft animal studies

All experiments involving animals were approved by the University of Manitoba's Animal Care Committee (protocol #20-052). Non-obese diabetic (NOD) severe combined immunodeficient (SCID) mice were purchased from Central Animal Care Services (CACS) at the University of Manitoba. These animals were used for all experiments and housed in sterilized cages, and all supplies were autoclaved before being introduced to the animals. Animals were manipulated only under a biosafety cabinet to monitor the health and function of the animal along with cage changeover. Animals were kept in a temperature-regulated room with a 12-hour light cycle. For GBM xenografting, 10-12-week-old animals received 5uL of PBS containing $1x10^5$ patient-derived BT241 GBM cells. Animals were anesthetized using isoflurane gas and underwent stereotactic surgery, where cells were injected into the frontal lobe. To test our hypothesis, PMS or vehicle treatment (3 mg/kg body weight, intraperitoneal injection, daily) started 10 days after GBM injection and continued until the mice reached the humane endpoint.

Other experiments, including xenografting of either SRR KO GBM cells or scramble GBM cells, were conducted to determine the effects of D-serine on recurrent tumorigenesis. Animals were subjected to T2 MRI imaging using an MR Solutions cryogen-free FlexiScan 7T system (MR Solutions, Guildford, Surrey, UK) at 4- and 6-weeks post-injection. Animals were given Metacam (5mg/kg) alongside saline subcutaneously at a 10% reduction in body weight or physical signs of pain (fur ruffling, sunken eyes, decreased mobility). Animals were sacrificed at humane endpoints as defined by a 20% reduction from peak body weight or decline in movement or neurological function such as seizures.

Tissue Collection and Preparation

Animal subjects were anesthetized using isoflurane to induce surgical anesthesia. Once anesthetized, the animals underwent cardiac perfusion using 1× PBS (Thermofisher, Cat #10010023), followed by perfusion with 4% paraformaldehyde (Sigma-Aldrich, Cat #158127) to fix the tissue *in situ*. Following perfusion, the brains were carefully dissected and immediately immersed in 4% PFA for post-fixation.

Cryostat Sectioning

Collected tissue was placed in 20% sucrose (Sigma-Aldrich, Cat #S0389) dissolved in 1× PBS at 4°C until the brains sank to the down of the tube, then transferred to 30% sucrose for cryoprotection. Tissues were subsequently flash-frozen using flash freeze spray (Decon, Cat #22-281-496). Frozen brain tissue was embedded in an optimal cutting temperature (OCT) compound (Scigen, Cat #23-730-571) and sectioned at 10-25 μm thickness using a cryostat (Leica 1860). Free-floating sections were collected into 24-well plates containing 0.02% Sodium Azide (Sigma-Aldrich, Cat #SX029901) in 1× PBS or mounted on cleaned Superfrost Plus microscope slides (Fisher Scientific, Cat #1255015) and kept at 4°C or -80°C for subsequent staining procedures.

Immunohistochemistry and Immunofluorescence Staining

Free-floating sections were incubated in citrate buffer (pH 6.0) at 95°C for 15 minutes in a water bath (VWR, Cat #97025-114). Sections were washed three times with PBS (10 minutes per wash) to remove any residual fixative or retrieval buffer. Sections were allowed to cool to RT for 20-30 min before initiating blocking. Blocking was performed by incubating the sections in a blocking buffer composed of 5% serum (Thermofisher, Cat #16210064), 0.1% bovine serum albumin (BSA, Sigma-Aldrich, Cat #A4737), and 0.3% Triton X-100 (Sigma-Aldrich, Cat #X100) in PBS.

Free-floating sections were incubated in the blocking buffer for 1 hour at room temperature with gentle agitation on a rocker. After blocking, the primary antibody solution diluted in blocking buffer was added to the sections. The specific antibodies and dilutions used for the study included; anti-SOX2 (Abcam, Cat #ab97959, 1:1000), anti-Nestin (CST, Cat #733349S, 1:2000), anti-BMI-1 (Novus, Cat #NB100-87026, 1:500), anti-CD-44 (Novus, Cat #NBP1-31488, 1:300), anti-Vimentin (CST, Cat #5741S, 1:500), anti-N-Cadherin (Novus, Cat #NBP2-38856, 1:250), anti-Ki67 (CST, Cat #94495, 1:500). Sections were incubated in the primary antibody solution overnight at 4°C with gentle rocking.

After primary antibody incubation, sections were washed three times with PBS for 10 minutes each. Free-floating sections were then incubated in an anti-rabbit fluorophore-conjugated secondary antibody (1µg/mL, ThermoFisher, Cat #A-11037) or an anti-mouse fluorophore-conjugated secondary antibody (1 µg/mL, ThermoFisher, Cat #A-11032) diluted in blocking buffer. Incubation was carried out at room temperature for 2 hours protected from light. After secondary antibody incubation, sections were washed three times with PBS for 10 minutes each.

For mounting, sections were transferred to pre-cleaned Superfrost Plus microscope slides (Fisher Scientific, Cat #1255015) using a fine glass rod to minimize tissue damage. Excess liquid was gently removed using a lint-free tissue, and the sections were mounted with DAPI-containing mounting media (ThermoFisher, Cat #00-4959-52).

Slides were imaged using a confocal microscope (Zeiss, Axio Observer Z1) with excitation/emission filters compatible with Alexa 594 and DAPI. images were captured at 20×, 40×, and 63× magnifications to assess marker localization and intensity. Quantification of fluorescence intensity and colocalization was performed using CellProfiler software (version: 4.2.8). At least three fields of view per section and three sections per sample were analyzed to

ensure statistical robustness. Images presented were collected and analyzed at the Live Cell Imaging Facility at the University of Manitoba.

Digital spatial profiling on GBM xenograft tumor samples

Representative fixed frozen mouse brains with GBM xenografts were cut into 10µm slide sections and processed following the GeoMx™ DSP slide preparation user manual (MAN-10087-04). All solutions were prepared using deionized water treated with diethyl pyrocarbonate (DEPC) water (Thermo Fisher, Cat #AM9922), unless otherwise stated.

Briefly, slides were baked at 60°C for 30 minutes and dehydrated. Antigen retrieval was performed using 1× Tris-EDTA at a pH of 9.0 heated to 100°C in a steamer for 15 minutes. RNA targets were exposed by incubating slides in 1× PBS containing 1 µg/mL of Proteinase K (Thermo Fisher, Cat #AM2546) at 37°C for 15 minutes.

In situ hybridization was performed overnight in a humidified chamber at 37°C. Slides were covered in hybridization solution containing UV-photocleavable barcode-conjugated probes from the Nanostring Technologies GeoMx Human RNA Immune Pathways Panel (Bruker Spatial Biology, Cat #GMX-RNA-NCT-HIP-12), diluted in Buffer R, provided in the Nanostring Technologies GeoMx RNA Slide Prep Kit (Bruker Spatial Biology, Cat # GMX-PREP-RNA-FFPE-PCLN-12), according to manufacturer instructions.

The following day, slides were washed 2 x 25 minutes at 37°C in stringent wash solution, containing 1:1 100% deionized formamide (Thermo Fisher, Cat #AM9342) and 4× SSC Buffer (Prepared by a 1/5 dilution in DEPC water of 20× SSC, SigmaAldrich, Cat #S6639). Following stringent wash, slides were further washed 2 x 2 minutes at room temperature in 2× SSC Buffer (Prepared by a 1/10 dilution of 20× SSC in DEPC water).

Following washes, slides were blocked using Buffer W, provided in the Nanostring Technologies GeoMx RNA Slide Prep Kit, for 30 minutes at room temperature. Slides were stained with morphology marker primary antibodies for 1 hour in a humidified chamber at room temperature. Slides were covered with morphology marker primary antibody solution consisting of: 1:20 dilution of goat anti-CD31 (R&D Systems, Cat #AF3628), and 1:200 dilution of rabbit anti-LDHA (Cell Signaling Technology, Cat #3582S), diluted in Buffer W according to manufacturer's instructions. Following primary antibody incubation, slides were washed 3 x 5 minutes at room temperature in 2× SSC Buffer and incubated in fluorescent-conjugated secondary antibodies and DNA stain for 1 hour in a humidified chamber at room temperature. Slides were covered with secondary antibody solution and reagents consisting of 1:100 dilution of AlexaFluor 594-conjugated donkey anti-goat IgG (Jackson ImmunoResearch, Cat #705-585-147), 1:100 dilution of Cy5-conjugated donkey anti-rabbit IgG (Jackson ImmunoResearch, Cat #711-175-152) and 200 nM Syto13 (Thermo Fisher, Cat #S7575) DNA stain diluted in Buffer W according to manufacturer's instructions.

Following morphology marker staining, slides were washed 2 x 5 minutes at room temperature in 2× SSC Buffer before loading onto the NanoString Technologies GeoMx™ Digital Spatial Profiler microscope (Bruker Spatial Biology). Fluorescent images were scanned at 20x and regions of interest (ROIs) were selected. Oligos from RNA probes were cleaved and collected into 96-well plates. Oligos were dried down completely by incubating overnight at RT with a permeable plate seal, and then rehydrated and hybridized with NanoString Technology GeoMx HybCode barcodes (Bruker Spatial Biology, GMX-RNA-HYB-96), according to manufacturer's instructions. Samples were hybridized overnight for at least 16 hours in a thermal cycler at 67 °C with a heated lid at 72 °C.

The resulting oligos hybridized to barcode tags were detected and counted using the Nanostring Technologies nCounter Prep Station and Digital Analyzer (Bruker Spatial Biology) the following day. The digital counts of each antibody for each ROI were generated for data analyses and analyzed using the built-in Data Analysis Suite on the GeoMx instrument. All ROIs that passed the built-in quality control (QC) metrics were normalized by scaling to the negative control IgG probes, constituting a signal to noise ratio (SNR) to correct for background. Further built-in QC consisted of FOV registration, binding density, positive control normalization, minimum nuclei and surface area count. Counts were further scaled to five internal reference genes included in the panel, and the normalized gene counts from that were calculated and exported.

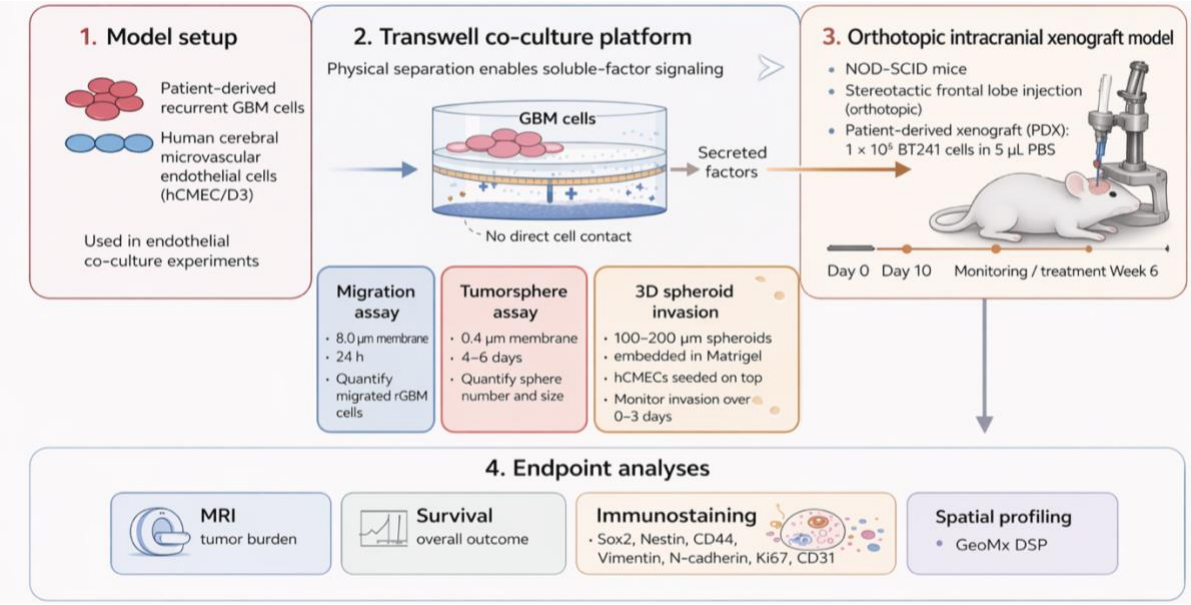

Figure 4. Methods overview

Statistics

GraphPad Prism version 10 was used for statistical analysis. Data are shown as means ± standard Deviation (SD) and are illustrated with error bars in graphs. To compare two groups on a single variable, unpaired two-tailed t-tests were used. To assess significant differences among more than two groups of normally distributed data, we used one-way or two-way ANOVA, followed by a

Tukey's multiple comparisons test, and when each mean was compared only to the control mean, Dunnett's multiple comparisons test was used. $p < 0.05$ was regarded as statistically significant unless otherwise noted.

Graphics and illustrations

Original graphics and schematics were generated using Microsoft PowerPoint, Adobe Illustrator, R, or with BioRender.com.

Chapter 4: Results

N-Counter based targeted transcriptional analysis of mono and co-cultured rGBM cells

Transcriptomic profiling was used to investigate the influence of endothelial cell interaction on rGBM cell signaling. rGBM cells cultured alone (monoculture) were compared to those co-cultured with endothelial cells. Heatmap analysis revealed a broad suppression of tumor-suppressive signaling molecules in the co-culture condition, indicating that endothelial interaction diminishes anti-tumor gene expression (Figure 4A). This pattern suggests that endothelial-derived signals may reprogram rGBM cells toward a more aggressive phenotype. Volcano plot analysis further supported this transcriptional shift by highlighting significantly upregulated genes in co-cultured rGBM cells, many of which are known to participate in inflammatory, pro-survival, and angiogenic signaling pathways (Figure 4B). This transcriptional shift likely contributes to a tumor-supportive microenvironment.

To gain insights into biological processes affected by endothelial interaction, gene ontology (GO) enrichment was conducted on the differentially expressed genes. Results revealed that activation of pathways linked to angiogenesis, extracellular matrix remodeling, and inflammatory responses, while homeostatic and differentiation-related pathways were suppressed (Figure 4C). These findings suggest that endothelial co-culture drives rGBM cells into a more malignant transcriptional state.

Altered rGBM cytokine profiles with endothelial cell interaction

Given the enrichment of inflammatory and angiogenic transcriptional programs in co-cultured rGBM cells, we next assessed whether these changes were reflected at the level of secreted cytokines. Cytokine profiling confirmed that co-cultured media contained higher levels of pro-

tumorigenic cytokines, such as IL-6, VEGF, and IL-8 (Figure 4D), which may act in both autocrine and paracrine fashions to further enhance tumor aggressiveness. This illustrates that co-culture first alters gene expression, which then produces proteins that are released into the TME. Together, these results demonstrate that endothelial cells directly influence the rGBM transcriptional landscape, enhancing features associated with progression and resistance.

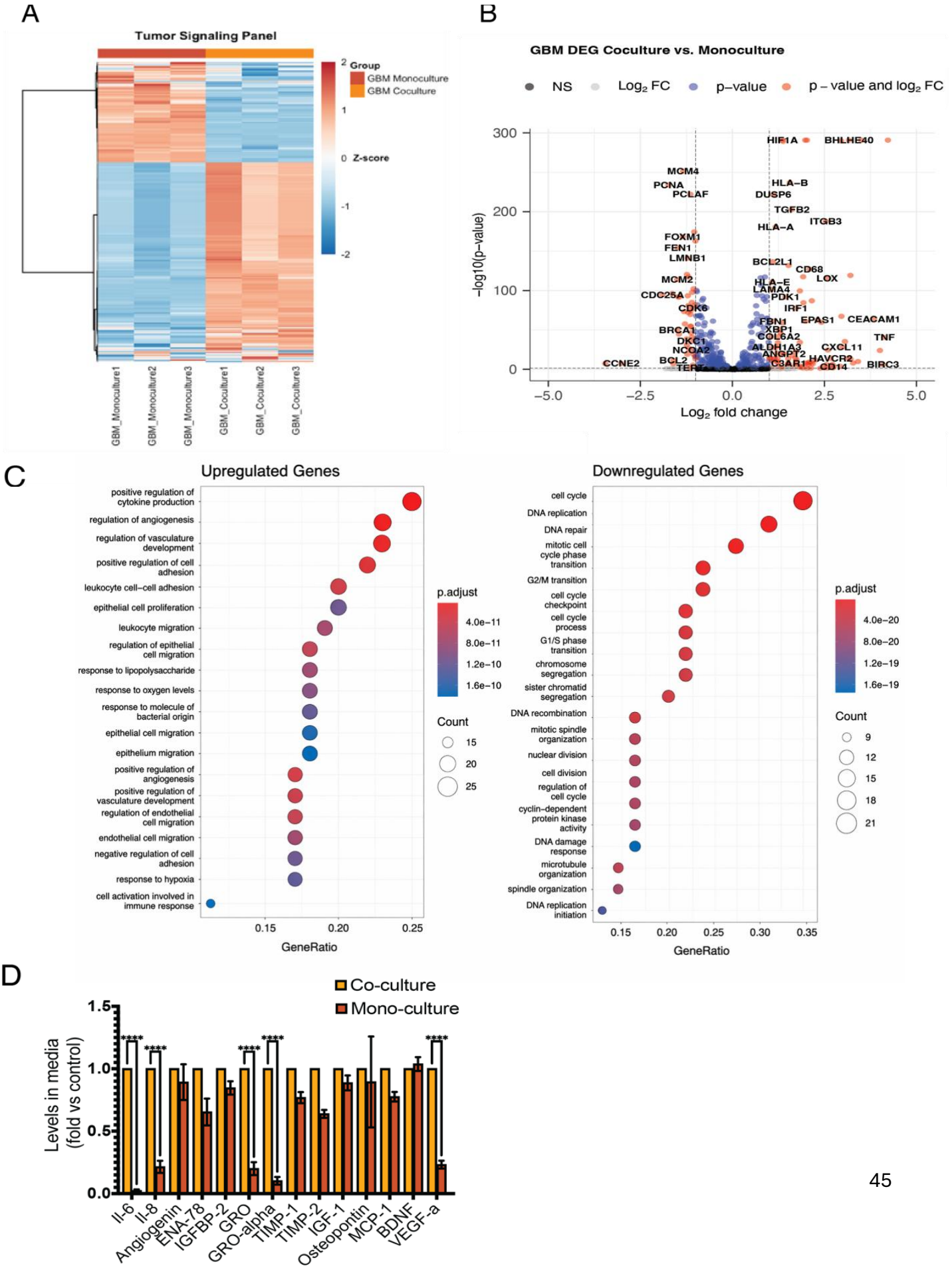
A
Tumor Signaling Panel
Group
GBM Monoculture
GBM Coculture
Z-score
GBM_Monoculture1
GBM_Monoculture2
GBM_Monoculture3
GBM_Coculture1
GBM_Coculture2
GBM_Coculture3
B
GBM DEG Coculture vs. Monoculture
NS
Log2 FC
p–value
p – value and log2 FC
–log10(p–value)
Log2 fold change
HIF1A
BHLHE40
MCM4
PCNA
PCLAF
HLA–B
DUSP6
TGFB2
ITGB3
HLA–A
FOXM1
FEN1
LMNB1
BCL2L1
CD68
LOX
MCM2
HLA–E
LAMA4
PDK1
CDC25A
IRF1
CDK6
FBN1
EPAS1
CEACAM1
XBP1
BRCA1
COL6A2
TNF
DKC1
ALDH1A3
CXCL11
NCOA2
ANGPT2
HAVCR2
BCL2
C3AR1
CD14
BIRC3
CCNE2
TERT
C
Upregulated Genes
positive regulation of cytokine production
regulation of angiogenesis
regulation of vasculature development
positive regulation of cell adhesion
leukocyte cell–cell adhesion
epithelial cell proliferation
leukocyte migration
regulation of epithelial cell migration
response to lipopolysaccharide
response to oxygen levels
response to molecule of bacterial origin
epithelial cell migration
epithelium migration
positive regulation of angiogenesis
positive regulation of vasculature development
regulation of endothelial cell migration
endothelial cell migration
negative regulation of cell adhesion
response to hypoxia
cell activation involved in immune response
GeneRatio
p.adjust
Count
Downregulated Genes
cell cycle
DNA replication
DNA repair
mitotic cell cycle phase transition
G2/M transition
cell cycle checkpoint
cell cycle process
G1/S phase transition
chromosome segregation
sister chromatid segregation
DNA recombination
mitotic spindle organization
nuclear division
cell division
regulation of cell cycle
cyclin–dependent protein kinase activity
DNA damage response
microtubule organization
spindle organization
DNA replication initiation
GeneRatio
p.adjust
Count
D
Co-culture
Mono-culture
Levels in media (fold vs control)
IL-6
IL-8
Angiogenin
ENA-78
IGFBP-2
GRO
GRO-alpha
TIMP-1
TIMP-2
IGF-1
Osteopontin
MCP-1
BDNF
VEGF-a

Figure 5. Communication between GBM cells and endothelial cells enhances aggressive GBM characteristics.
(A) Heat map depicting differential expression of anti-tumor signaling molecules in glioblastoma (GBM) cells cultured alone (monoculture) versus in co-culture with endothelial cells, highlighting suppressed tumor-suppressive signaling in the co-culture condition. (B) Volcano plot showing transcriptomic changes between GBM monoculture and co-culture conditions, identifying significantly upregulated (right) and downregulated (left) genes. Significant genes are labelled on the plot. N=3 (C) Gene ontology (GO) enrichment analysis of differentially expressed genes reveals co-culture-driven activation of pro-tumorigenic pathways and suppression of homeostatic processes. (D) Cytokine array comparing secreted factors in GBM-EC co-culture versus GBM monoculture, illustrating increased levels of pro-inflammatory and pro-angiogenic cytokines in the co-culture setting. N=3,
* < p - 0.05, ** < p - 0.01, *** < p - 0.001, **** < p - 0.0001.

Effect of co-culture on the migratory potential and stemness of rGBM cells

Functional assays were used to assess the impact of endothelial co-culture on key tumor N=3 behaviours. Transwell migration assays demonstrated a significant increase in motility for both BT241 and BT972 rGBM patient-derived cells in the presence of endothelial cells (Figure 5A-B). This finding suggests that endothelial cells release factors that promote chemotactic responses and cytoskeletal reorganization in rGBM cells. Sphere formation assays, a proxy for self-renewal capacity, revealed a similar trend, with both rGBM lines showing increased sphere number and size under co-culture conditions (Figure 5C-D). This suggests that endothelial signals support the expansion or maintenance of glioma-initiating stem-like cells. Invasion assays using spheroids embedded in extracellular matrix showed markedly increased invasive outgrowth in co-cultured spheroids (Figure 5E). This enhanced invasion is consistent with the transcriptional and secretory changes observed in Figure 1. Mechanistically, Western blot analysis of BT241 lysates showed upregulation of stemness and mesenchymal markers, including SOX2, BMI1, and N-Cadherin, under co-culture conditions (Figure 5F). These molecular changes align with the increased motility and self-renewal observed in functional assays. Collectively, these results indicate that endothelial interaction enhances multiple malignant phenotypes, including migration, invasion, and stemness of recurrent GBM tumors.

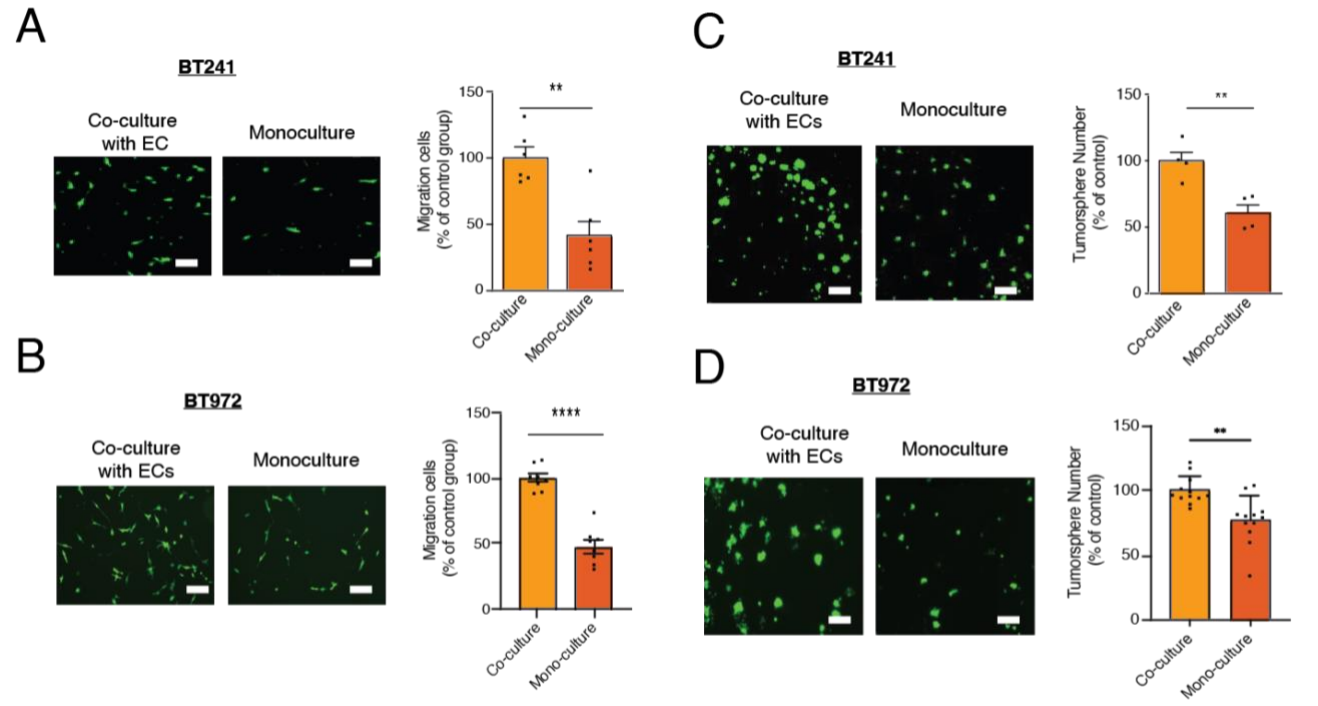
A
BT241
Co-culture with EC
Monoculture
Migration cells (% of control group)
Co-culture
Mono-culture
B
BT972
Co-culture with ECs
Monoculture
Migration cells (% of control group)
C
BT241
Co-culture with ECs
Monoculture
Tumorsphere Number (% of control)
D
BT972
Co-culture with ECs
Monoculture
Tumorsphere Number (% of control)

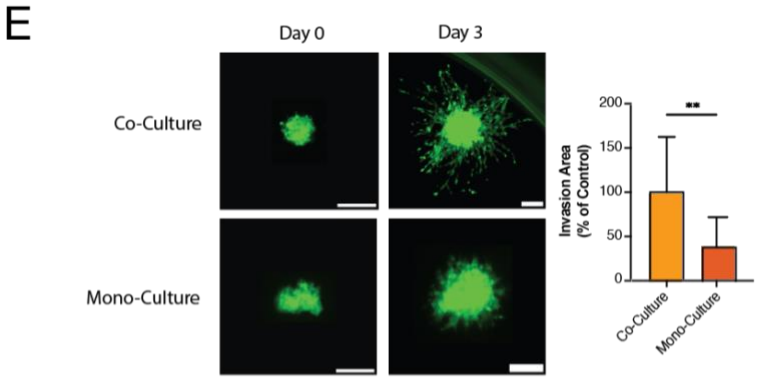
E
Day 0
Day 3
Co-Culture
Mono-Culture
Invasion Area (% of Control)

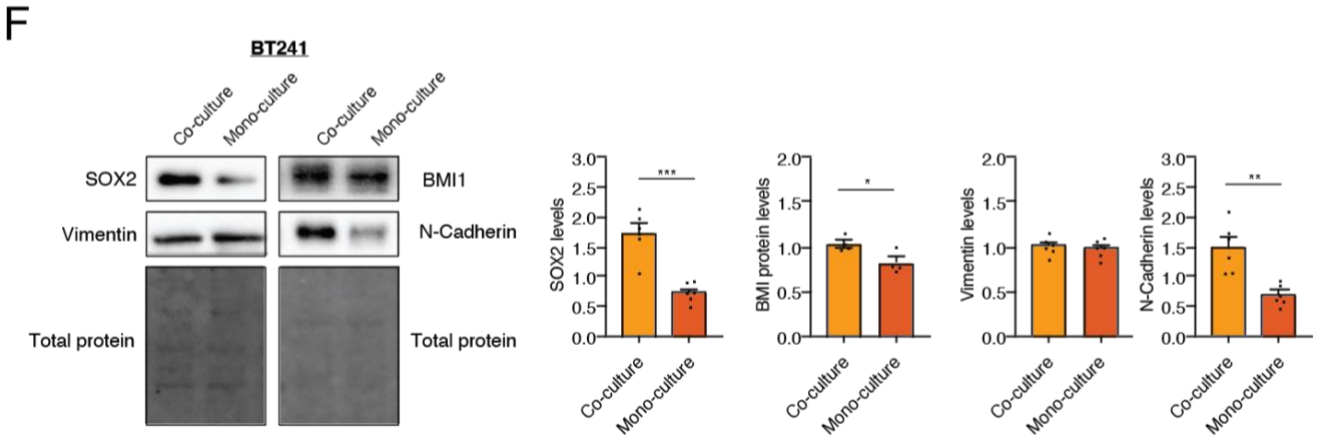
F
BT241
Co-culture
Mono-culture
SOX2
Vimentin
Total protein
BMI1
N-Cadherin
Total protein
SOX2 levels
BMI protein levels
Vimentin levels
N-Cadherin levels

Figure 6. Endothelial cell interaction enhances rGBM cell migration, self-renewal, invasion, and mesenchymal transition.
Migration of GBM cells was significantly enhanced in co-culture with endothelial cells, as shown by increased migration of BT241 (A) and BT972 (B) recurrent cells in transwell assays. Sphere formation was also elevated in both GBM cell types when cultured with endothelial cells, indicating enhanced self-renewal capacity (C, D). GBM spheroid invasion was markedly increased in the presence of endothelial cells over 3 days. N=4 (E). (F) Western blot analysis of BT241 cells revealed upregulation of mesenchymal and stemness-associated proteins (Sox2, BMI1, and N-Cadherin) in the co-culture condition compared to monoculture. The scale bar is 150 μm in Fig. A and B, 1 mm in Fig. C-D, and 200 μm in Fig. E. * < p - 0.05, ** < p - 0.01, *** < p - 0.001, **** < p - 0.0001.

Elevated SRR expression in patient samples and patient-derived rGBM cells associated with poor outcome

To assess the clinical relevance of SRR in human glioblastoma, transcriptomic data from multiple independent datasets were analyzed. Across the TCGA TARGET GTEx, Rembrandt, TCGA GBM-LGG, and CGGA datasets, SRR transcript levels were significantly elevated in tumor tissue compared to non-tumor brain, with expression increasing further in higher-grade gliomas (Figure 6A). This trend was consistent across both primary and recurrent glioblastoma samples, suggesting that SRR upregulation is a common feature of malignant recurrent gliomas.

To determine whether SRR expression correlates with clinical outcome, patients were stratified into high- and low-SRR expression groups using the median expression level as the cutoff. Use of the median as the cutoff for SRR expression allowed patients to be stratified into high- and low-expression groups using a non-arbitrary threshold derived directly from the dataset. This method is commonly applied in survival analyses because it yields comparably sized groups, reduces sensitivity to extreme values, and facilitates clear interpretation of Kaplan-Meier differences, while acknowledging that gene expression exists on a continuous spectrum. Kaplan-Meier survival analysis demonstrated that high SRR expression was significantly associated with reduced overall survival (Figure 6B). Patients with low SRR expression survived longer, with a hazard ratio (HR) of 0.55 (95% CI: 0.39–0.79, p = 0.0014), indicating that SRR may serve as a negative prognostic biomarker in rGBM.

GBM cells secrete D-Serine into the tumor microenvironment in a time-dependent manner

To determine how glioblastoma cells regulate extracellular D-serine within an endothelial-supported microenvironment, D-serine concentrations were measured in conditioned media collected from rGBM-endothelial co-culture over time. In BT241 cells (Figure 6C), D-serine levels increased steadily from the initial co-culture time point, showing a significant rise by 12 hours and continuing to elevate through 48 hours. D-serine increase reached approximately threefold by 24 hours and nearly fourfold by 48 hours, indicating a sustained accumulation of D-serine in the shared microenvironment. A similar pattern was observed in BT972 cells (Figure 6D). In BT972, D-serine levels increased progressively, beginning at early time points, with significant changes detected by 24 hours and continuing to rise through 72 hours. By the final time point, extracellular D-serine approached a four- to fivefold increase compared to baseline. Together, these results demonstrate that two distinct recurrent patient-derived GBM lines progressively release D-serine when co-cultured with endothelial cells, supporting the idea that D-serine can serve as a paracrine signaling mediator.

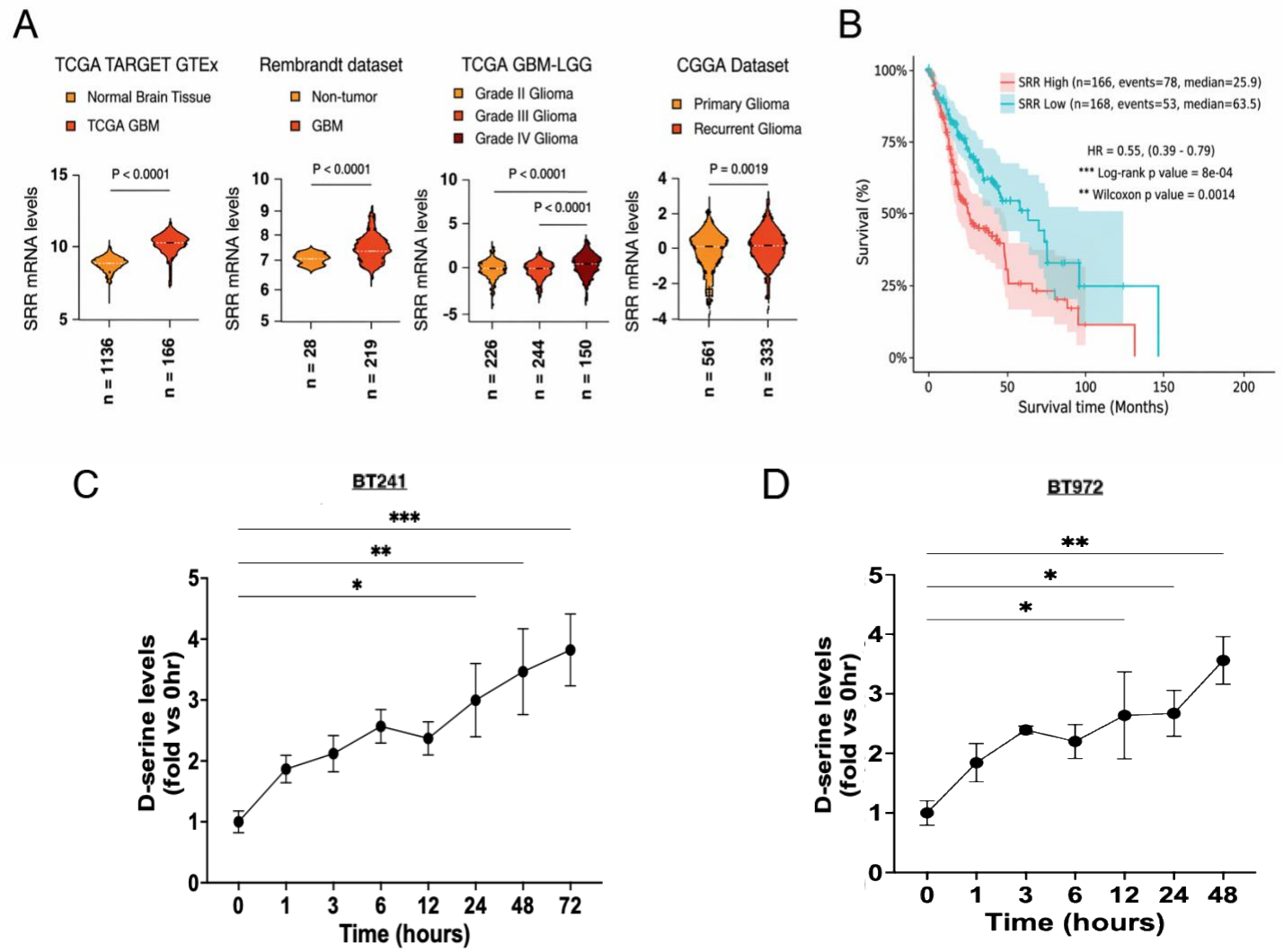

Figure 7. SRR upregulation in human GBM has prognostic significance, and there is time-dependent accumulation of extracellular D-serine in rGBM–endothelial co-cultures.

(A) SRR transcript levels were compared across four independent clinical datasets. (B) Kaplan Meier survival analysis of TCGA glioblastoma samples stratified by median SRR expression. High SRR expression correlated with shorter overall survival. (C-D) Time-course analysis of extracellular D-serine in conditioned media from BT241 and BT 972 rGBM cells co-cultured with endothelial cells. N=3. * < p - 0.05, ** < p - 0.01, *** < p - 0.001, **** < p - 0.0001.

Depleting of extracellular D-serine reverses migration and stemness

To test the functional relevance of extracellular D-serine in tumor progression, rGBM cells were exposed to extracellular DAAO, which degrades D-serine. Extracellular media were extracted and displayed a reduced D-serine concentration following DAAO treatment after 48 hours in both BT241 and BT972 when co-cultured with ECs (Figure 7A-B). This confirmed effective enzymatic depletion of extracellular D-serine in the co-culture system.

Transwell migration assays showed that DAAO treatment significantly reduced the migration of BT241 and BT972 cells (Figure 7C-D). This indicates that extracellular D-serine plays a role in supporting GBM migration. Sphere formation was also impaired, as demonstrated by fewer and smaller spheres in treated conditions (Figure 7E-F), suggesting that D-serine supports self-renewal in rGBM cells.

Invasion assays indicated that DAAO dramatically reduced spheroid outgrowth over 3 days (Figure 7G), highlighting the importance of D-serine in driving ECM invasion. Moreover, Western blot analysis showed decreased levels of mesenchymal and stemness markers (SOX2, Vimentin, BMI1, and N-Cadherin) following DAAO treatment (Figure 7H). These results demonstrate that extracellular D-serine is a driver of recurrent GBM aggressiveness, supporting migration, invasion, and self-renewal in the context of endothelial interaction. Enzymatic depletion of D-serine reverses these malignant phenotypes and reduces expression of mesenchymal and stemness markers, indicating that D-serine–dependent signaling is required to support rGBM malignancy.

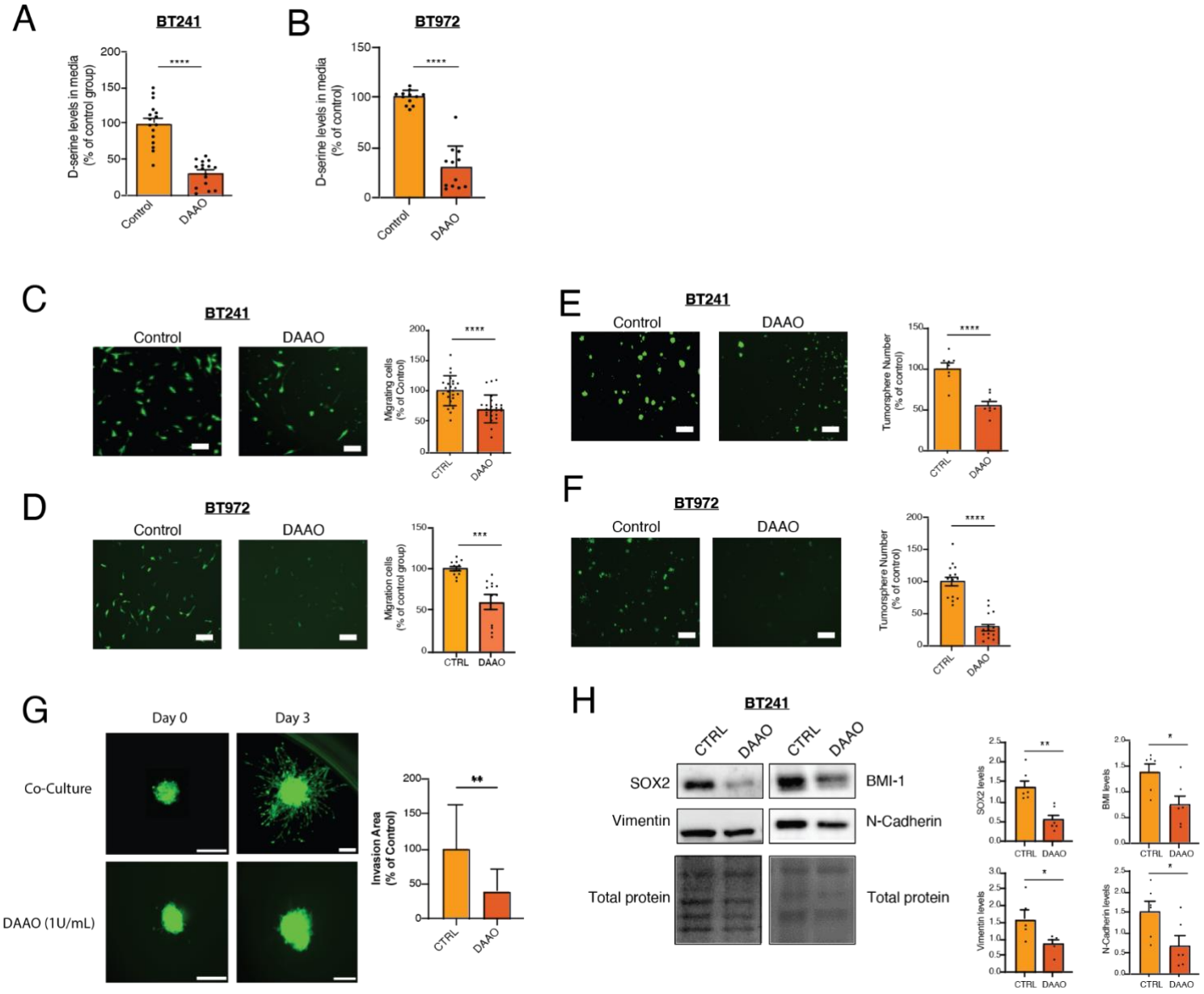

Figure 8. DAAO inhibits rGBM cell migration, self-renewal, invasion, and mesenchymal marker expression by degrading extracellular D-serine.

Quantification of extracellular D-serine levels in rGBM–hCMEC co-cultures revealed a reduction in D-serine following DAAO treatment for BT241 (A) and BT972 (B) cells. Migration assays showed a significant decrease in GBM cell motility in BT241 (C) and BT972 (D) after DAAO treatment. Sphere formation was also suppressed following DAAO treatment, with both BT241 (E) and BT972 (F). Invasion assays (G) revealed marked attenuation of GBM spheroid outgrowth over 3 days when DAAO was present in the co-culture system. N=3. Western blot analysis of BT241 cells (H) demonstrated decreased expression of mesenchymal and stemness-associated markers under DAAO treatment. The scale bar is 150 µm in Fig. C and D, 1 mm in Fig. E and F, and 200 µm in Fig. G. * < p - 0.05, ** < p - 0.01, *** < p - 0.001, **** < p - 0.0001.

Pharmacological inhibition or genetic knockout of SRR reduces rGBM migration and stemness

PMS is a phenazine derivative that directly inhibits SRR catalytic activity with an *in vitro* half-maximal inhibitory concentration (IC50) of about 3 μM[102]. Furthermore, other *in vivo* studies have used similar concentrations (3 mg/kg/day) to inhibit SRR, as we have in this study[103]. In SRR activity assays using purified enzyme, PMS and the related compound phenazine ethosulfate rank among the most potent known SRR inhibitors, whereas the parent phenazine scaffold does not inhibit SRR even at much higher concentrations, emphasizing structure-dependent selectivity within this chemical class. PrestoBlue is a resazurin-based metabolic viability assay in which viable cells convert the reagent to a fluorescent product; reduced signal reflects diminished metabolic activity and cell viability. In BT241 and BT972 rGBM cells, PMS produced a clear dose-dependent decrease in PrestoBlue signal, with BT972 displaying slightly greater sensitivity, indicating cell line–specific dependence on SRR activity while still maintaining acceptable viability at low micromolar doses (Figure 8A).

Extracellular media were collected and showed reduced extracellular D-serine concentration following PMS treatment in both BT241 and BT972 when co-cultured with ECs (Figure 8B-C). This confirms that PMS effectively inhibits SRR enzymatic function and reduces extracellular D-serine.

Pharmacologic inhibition of serine racemase using PMS was evaluated across multiple tumorigenic characteristics. Migration was significantly suppressed in a dose-dependent manner under PMS treatment (Figure 8D-E), aligning with prior results from DAAO treatment. Sphere formation assays showed a marked reduction in self-renewal following PMS treatment (Figure 8F-G), and spheroid invasion assays confirmed decreased invasive capacity in BT 241 cells (Figure 8H). Western blot analysis further validated the molecular effects of PMS, revealing

downregulation of key markers associated with mesenchymal transition and stemness (Figure 8I). These findings indicate that serine racemase activity is required for multiple tumor-supporting features in rGBM cells.

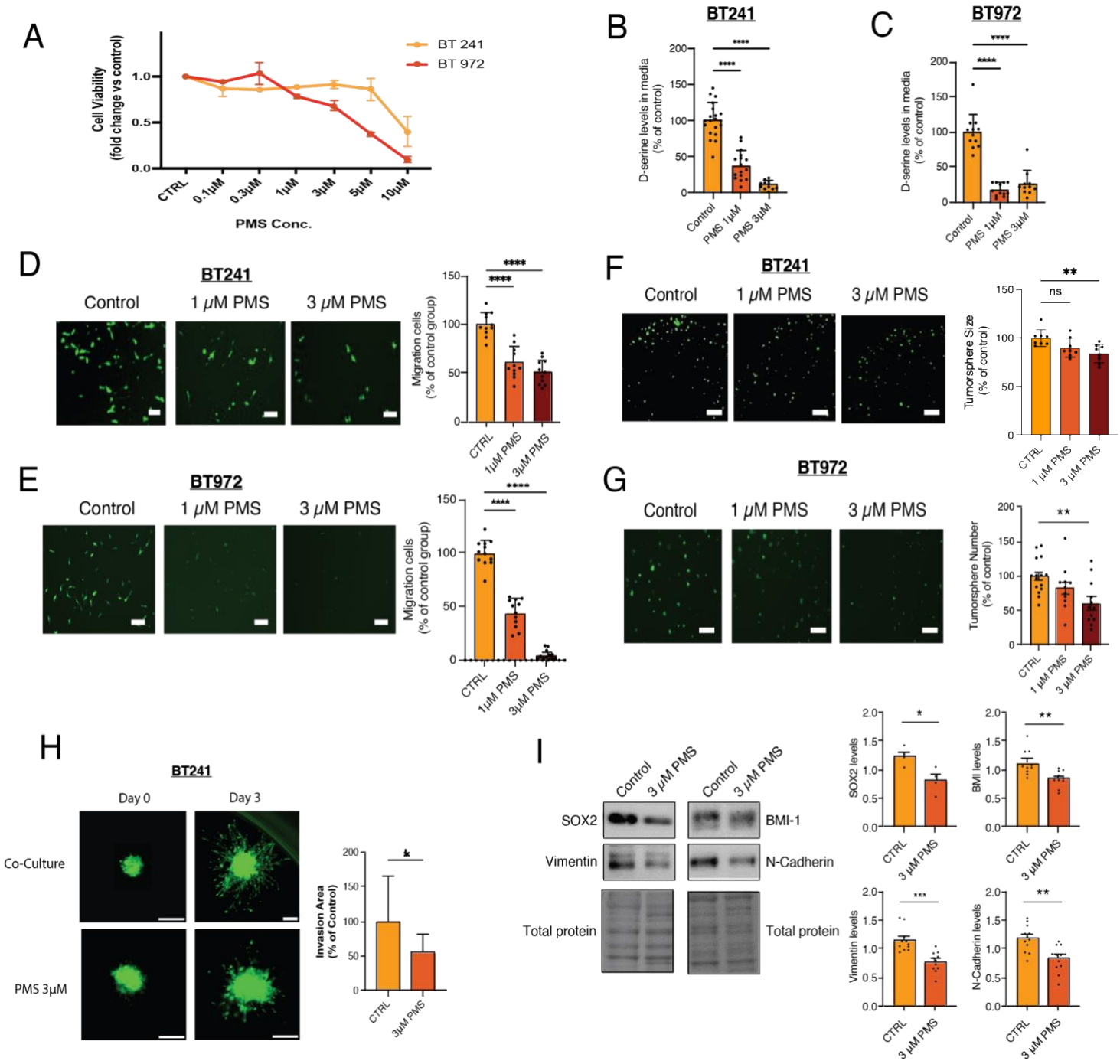

Figure 9. Pharmacological inhibition of serine racemase by PMS reduces rGBM cell viability, migration, invasion, and mesenchymal marker expression.

A) Cell viability, measured by the PrestoBlue assay, showed a dose-dependent decrease in metabolic activity in BT241 and BT972 cells following PMS treatment N=3. Quantification of extracellular D-serine levels in BT241–hCMEC co-cultures revealed a reduction in D-serine following DAAO for BT241 (B) and BT972 (C) cells. Migration assays showed significantly reduced GBM cell motility in BT241 (D) and BT972 (E) after treatment with 1 µM or 3 µM PMS. Sphere formation was also suppressed in both BT241 (F) and BT972 (G) cells at 3 µM PMS, indicating impaired self-renewal capacity under serine racemase inhibition. Invasion assays (H) showed reduced spheroid outgrowth in BT241 cells treated with PMS (3 µM) over 3 days. N=3. Western blot analysis (I) of BT241 cells demonstrated downregulation of mesenchymal and stemness-associated proteins. The scale bar is 150 µm in Fig. D and E, 1 mm in Fig. F and G, and 200 µm in Fig. H. * < p - 0.05, ** < p - 0.01, *** < p - 0.001, **** < p - 0.0001.

To genetically validate pharmacologic findings with PMS, serine racemase was deleted via CRISPR-Cas9 in BT241 and BT972 rGBM cells. Immunoblotting confirmed efficient knockout in both cell lines using two independent sgRNAs (Figure 9A), showing near complete loss of SRR protein.

Media from SRR KO/EC co-cultures had significantly lower extracellular D-serine levels, indicating loss of SRR enzymatic activity sufficient to suppress D-serine release (Figure 9B-C). Functional assays revealed a significant reduction in migration, sphere formation, and invasion in SRR KO cells across both lines (Figure 9D-H). The close alignment of these phenotypes with those observed under PMS treatment reinforces the role of SRR and D-serine in sustaining GBM malignancy. Western blot analysis further validated the role of SRR by detecting a reduction in pro-tumor phenotypes when SRR KO rGBM cells are co-cultured with ECs, revealing downregulation of key markers associated with mesenchymal transition and stemness (Figure 9I). These findings indicate that serine racemase activity is required for multiple tumor-supporting features in rGBM cells.

Endothelial SRR does not contribute to extracellular D-serine concentration in the TME

To determine the contribution of endothelial SRR to extracellular D-serine levels, SRR was knocked out in hCMEC/D3 endothelial cells using CRISPR-Cas9. Western blot confirmed efficient deletion (Figure 10A). Co-culture with rGBM cells showed no significant changes in extracellular D-serine concentrations, indicating that endothelial cells do not contribute substantially to D-serine production in this context (Figure 10B). GBM migration, sphere formation, and invasion were not affected when co-cultured with SRR KO endothelial cells (Figure 10C-E). These data confirm that rGBM cells are the predominant source of D-serine within the tumor microenvironment and that this signaling axis is initiating from rGBM release.

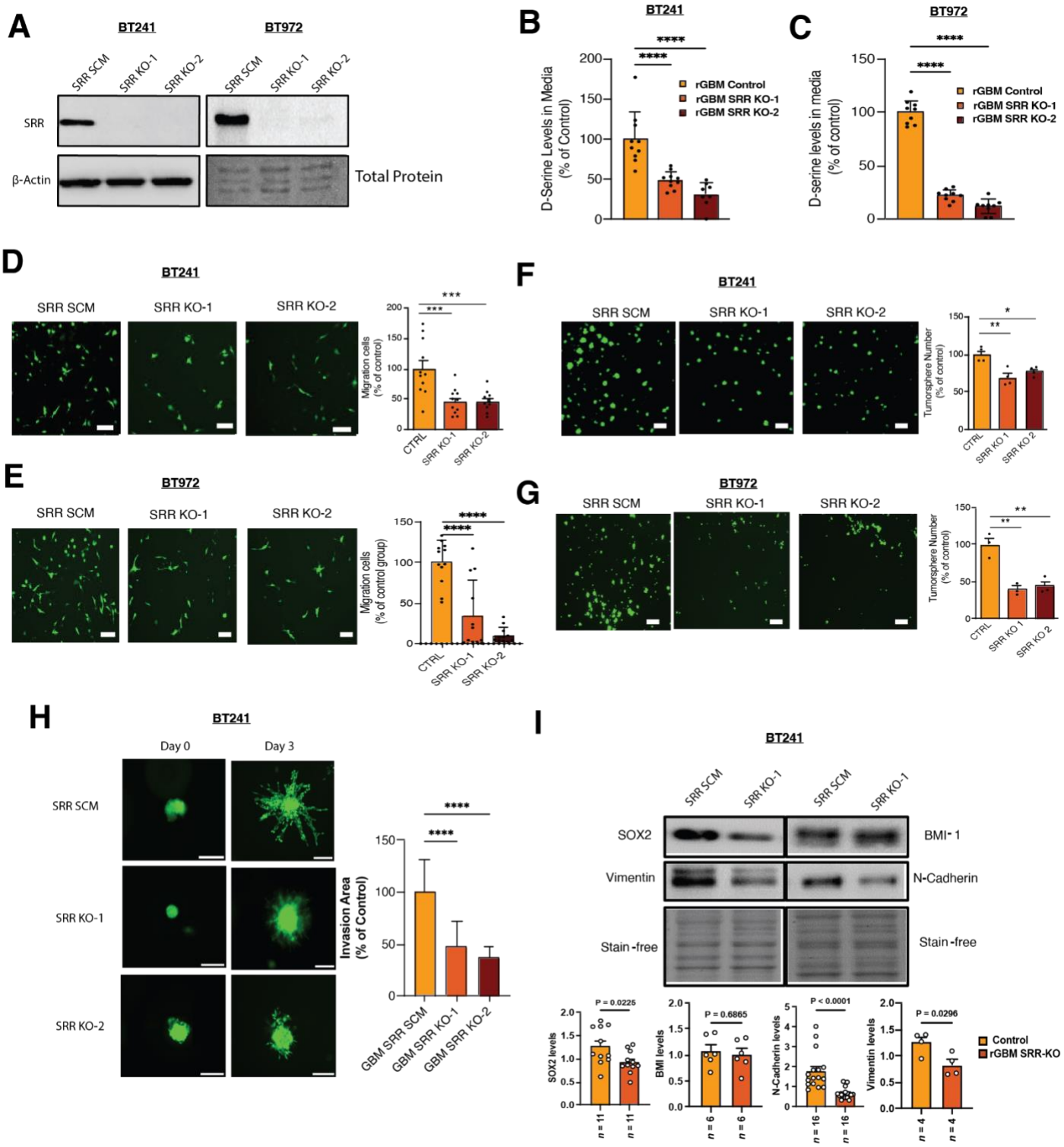
A
BT241
BT972
SRR SCM
SRR KO-1
SRR KO-2
SRR
β-Actin
Total Protein
B
BT241
D-Serine Levels in Media (% of Control)
rGBM Control
rGBM SRR KO-1
rGBM SRR KO-2
C
BT972
D-serine levels in media (% of control)
D
BT241
Migration cells (% of control)
CTRL
SRR KO-1
SRR KO-2
E
BT972
Migration cells (% of control group)
F
BT241
Tumorsphere Number (% of control)
G
BT972
H
BT241
Day 0
Day 3
Invasion Area (% of Control)
GBM SRR SCM
GBM SRR KO-1
GBM SRR KO-2
I
BT241
SOX2
BMI-1
Vimentin
N-Cadherin
Stain-free
SOX2 levels
BMI levels
N-Cadherin levels
Vimentin levels
P = 0.0225
P = 0.6865
P < 0.0001
P = 0.0296
Control
rGBM SRR-KO

Figure 10. Genetic knock out of SRR impairs D-serine production and limits malignant behaviour in rGBM cells.
(A) CRISPR Cas9-mediated knockout of SRR in BT241 and BT972 recurrent glioblastoma cells. Immunoblotting confirmed efficient deletion using two independent sgRNAs in each line, with complete loss of SRR protein. (B–C) Conditioned media collected from SRR knockout GBM–endothelial co-cultures showed reduced extracellular D-serine. (D–H) Functional assays demonstrated that SRR deletion significantly diminished key malignant behaviours in both GBM cell lines. SRR knockout cells exhibited reduced migration, impaired sphere-forming capacity, and decreased invasion (N=4). (I) Western blot analysis of SRR knockout GBM cells co-cultured with endothelial cells revealed reduced expression of some mesenchymal and stemness-associated markers. The scale bar is 150 µm in Fig. D and E, 1 mm in Fig. F and G, and 200 µm in Fig. H. * < p - 0.05, ** < p - 0.01, *** < p - 0.001, **** < p - 0.0001.

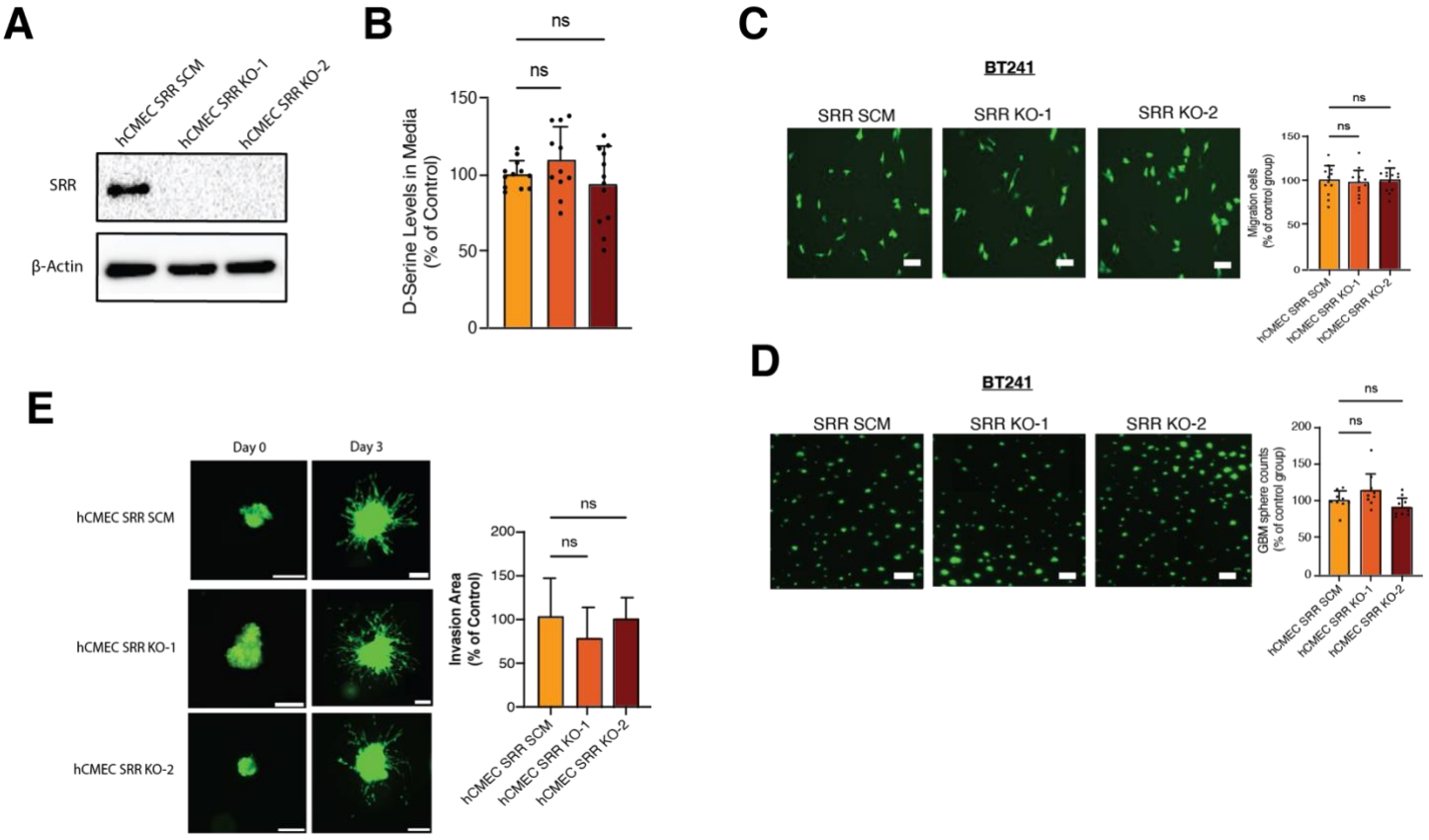

Figure 11. Endothelial-specific SRR knockout does not alter GBM cell behaviour in co-culture.
(A) Western blot confirming efficient knockout of serine racemase (SRR) in hCMEC/D3 cells using two independent sgRNAs. (B) Quantification of extracellular D-serine levels in BT241–hCMEC co-cultures revealed no significant changes with SRR knockout in hCMECs. (C) Transwell migration assays using BT241 co-cultured with SRR KO or control hCMECs showed no significant difference in cell migration. (D) Sphere formation assays demonstrated that BT241 self-renewal capacity was unaffected by the loss of endothelial SRR expression. (E) Invasion assays with BT241 spheroids co-cultured with SRR KO or control hCMECs showed comparable levels of invasive outgrowth over 3 days, N=4. The scale bar is 150 µm in Fig. C, 200 µm in Fig. E, and 1 mm in Fig. D. ns = not significant.

Extracellular D-Serine depletion improves outcomes *in vivo*

Given the established role of D-serine in promoting tumor–endothelial signalling and aggressive phenotypes in rGBM, we employed a patient-derived xenograft (PDX) intracranial model to evaluate the functional contribution of SRR to *in vivo* tumor progression. Patient-derived rGBM cells were stereotactically implanted into the forebrain of immunocompromised mice to recapitulate the human tumor microenvironment. To assess the effect of SRR loss of function on *in vivo* tumorigenesis, the pharmacologic SRR inhibitor PMS (3 mg/kg, daily) was administered beginning 10 days post-implantation (Figure 11A). MRI analysis at four weeks demonstrated that PMS-treated animals exhibited a marked reduction in tumor volume compared to vehicle-treated controls (Figure 11B-C). Tumor burden was significantly reduced as confirmed by volumetric quantification. Correspondingly, PMS-treated mice displayed extended survival in Kaplan-Meier analysis (Figure 11D), reinforcing the conclusion that pharmacologic SRR inhibition reduces tumor growth and improves outcome in an orthotopic rGBM model.

In a similar experiment, intracranial xenograft models were established using rGBM patient-derived SRR KO cells (Figure 12A). MRI imaging at four weeks post-injection revealed that tumors derived from SRR-KO cells had significantly smaller volumes compared to those from control rGBM cells (Figure 12B). Quantification of MRI-derived tumor volume confirmed a reduction in tumor burden in the SRR-KO cohort (Figure 12C). Kaplan-Meier survival analysis showed that mice implanted with SRR-KO cells had a significantly prolonged survival relative to controls (Figure 12D), indicating that SRR activity contributes to tumor progression *in vivo*.

Immunofluorescence staining of these *in vivo* tumors showed reduced expression of CD44, Nestin, Vimentin, Ki67, N-Cadherin, and Sox2, in PMS-treated tumors compared to controls (Figure 13).

The panel of markers used spans multiple oncogenic programs, including proliferation (Ki67), mesenchymal identity (Vimentin, N-Cadherin), and stemness (Sox2, CD44, Nestin). Quantitative analysis confirmed a significant reduction in fluorescence intensity for all markers, suggesting that PMS suppresses tumor cell proliferation, stemness, and mesenchymal features *in vivo*. These data validate the *in vitro* findings and demonstrate the efficacy of PMS in targeting rGBM cell phenotypes in an orthotopic tumor model.

Immunostaining of the SRR-KO tumors revealed decreased expression of stemness and mesenchymal markers, including CD44, Nestin, Sox2, and N-Cadherin, relative to controls. Quantification showed statistically significant reductions for all markers except Vimentin and Ki67, which did not differ significantly (Figure 14). These findings indicate that while SRR deletion impairs expression of several key regulators of stemness and cell adhesion, it may not strongly affect proliferation or Vimentin-driven mesenchymal identity in all tumor contexts. Nevertheless, the data support the conclusion that SRR is a necessary factor for maintaining a subset of aggressive rGBM phenotypes *in vivo*.

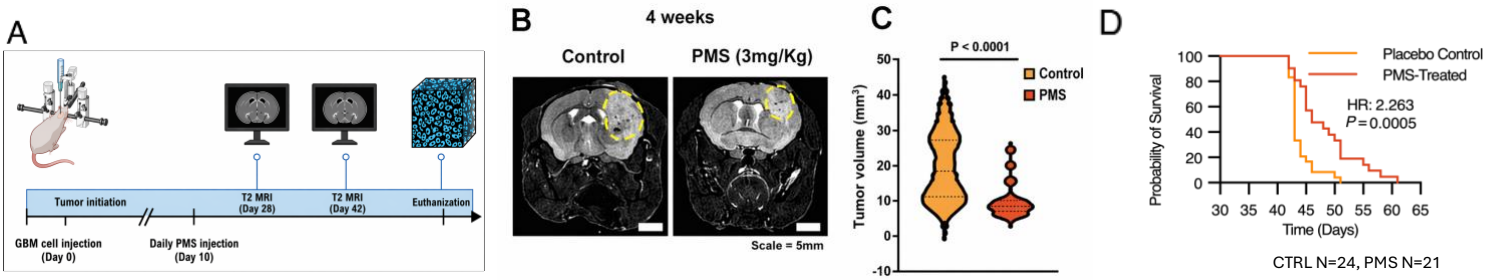

Figure 12. Inhibition of SRR reduces intracranial tumor growth and extends survival in rGBM xenograft models.
(A) Experimental timeline for intracranial xenograft of patient-derived GBM cells, subsequent treatment and MRI monitoring. (B) Representative MRI scans at four weeks post-implantation. Tumors treated with PMS were smaller than those formed by control cells. (C) Quantification of MRI derived tumor volume showed a significant reduction in tumor burden in the PMS-treated mice. (D) Kaplan Meier survival analysis demonstrated that mice treated with PMS survived longer than controls. The scale bar is 5mm in Fig. B. N=24 (control), N=21 (PMS)

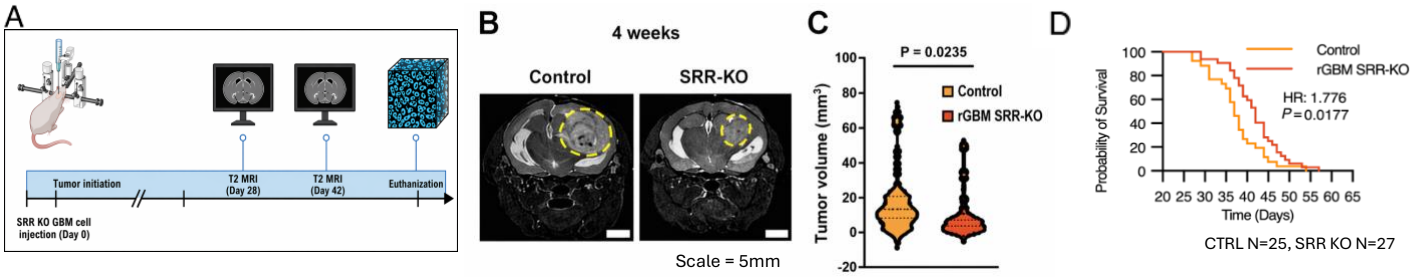

Figure 13. Loss of SRR reduces intracranial tumor growth and extends survival in rGBM xenograft models.
(A) Experimental timeline for intracranial xenograft of patient-derived GBM cells and subsequent MRI monitoring. (B) Representative MRI scans at four weeks post-implantation. Tumors derived from SRR knockout (SRR KO) cells were smaller than those formed by control cells. (C) Quantification of MRI derived tumor volume showed a significant reduction in tumor burden in the SRR KO cohort. (D) Kaplan Meier survival analysis demonstrated that mice implanted with SRR KO cells survived longer than controls. The scale bar is 5mm in Fig. B. N=25 (control), N=27 (SRR-KO)

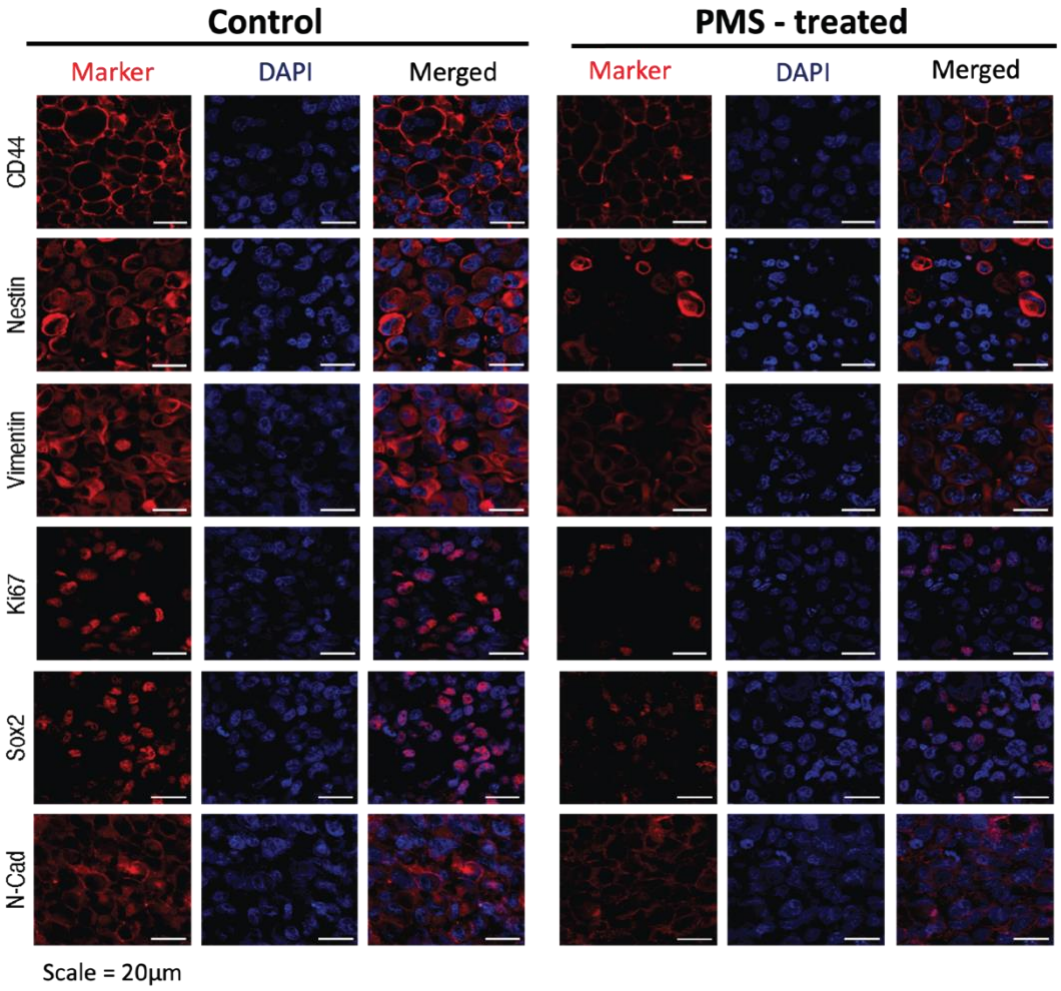
Control
PMS - treated
Marker
DAPI
Merged
Marker
DAPI
Merged
CD44
Nestin
Vimentin
Ki67
Sox2
N-Cad
Scale = 20µm

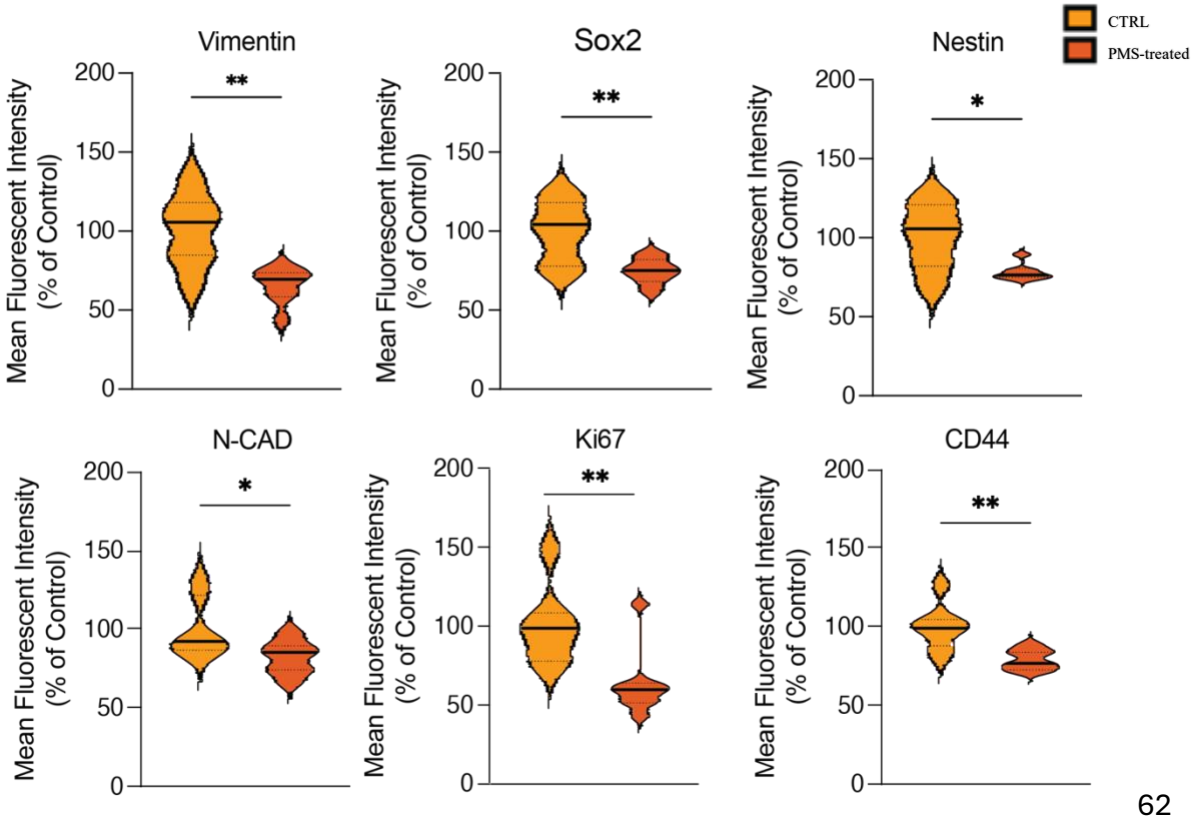
CTRL
PMS-treated
Vimentin
Sox2
Nestin
N-CAD
Ki67
CD44
Mean Fluorescent Intensity (% of Control)
200
150
100
50
0
**
**
*
*
**
**

Figure 14. PMS treatment reduces expression of stemness, proliferation, and mesenchymal markers in PDX glioblastoma tumors.
Immunohistochemical analysis of patient-derived xenograft (PDX) tumor sections from mice treated daily with PMS (3 mg/kg) or vehicle control revealed a marked reduction in the expression of multiple GBM-associated markers. Representative images show immunofluorescence staining (red) for CD44, Nestin, Vimentin, Ki67, N-Cadherin (N-CAD), and Sox2, with nuclear counterstaining using DAPI (blue). Quantification of mean fluorescence intensity revealed significantly lower levels of all markers in PMS-treated tumors compared to controls. Data are represented as violin plots showing intensity values normalized to control levels (% of control). The scale bar is 20 μm. N= 7 for both groups. * < p - 0.05, ** < p - 0.01, *** < p - 0.001, **** < p - 0.0001.

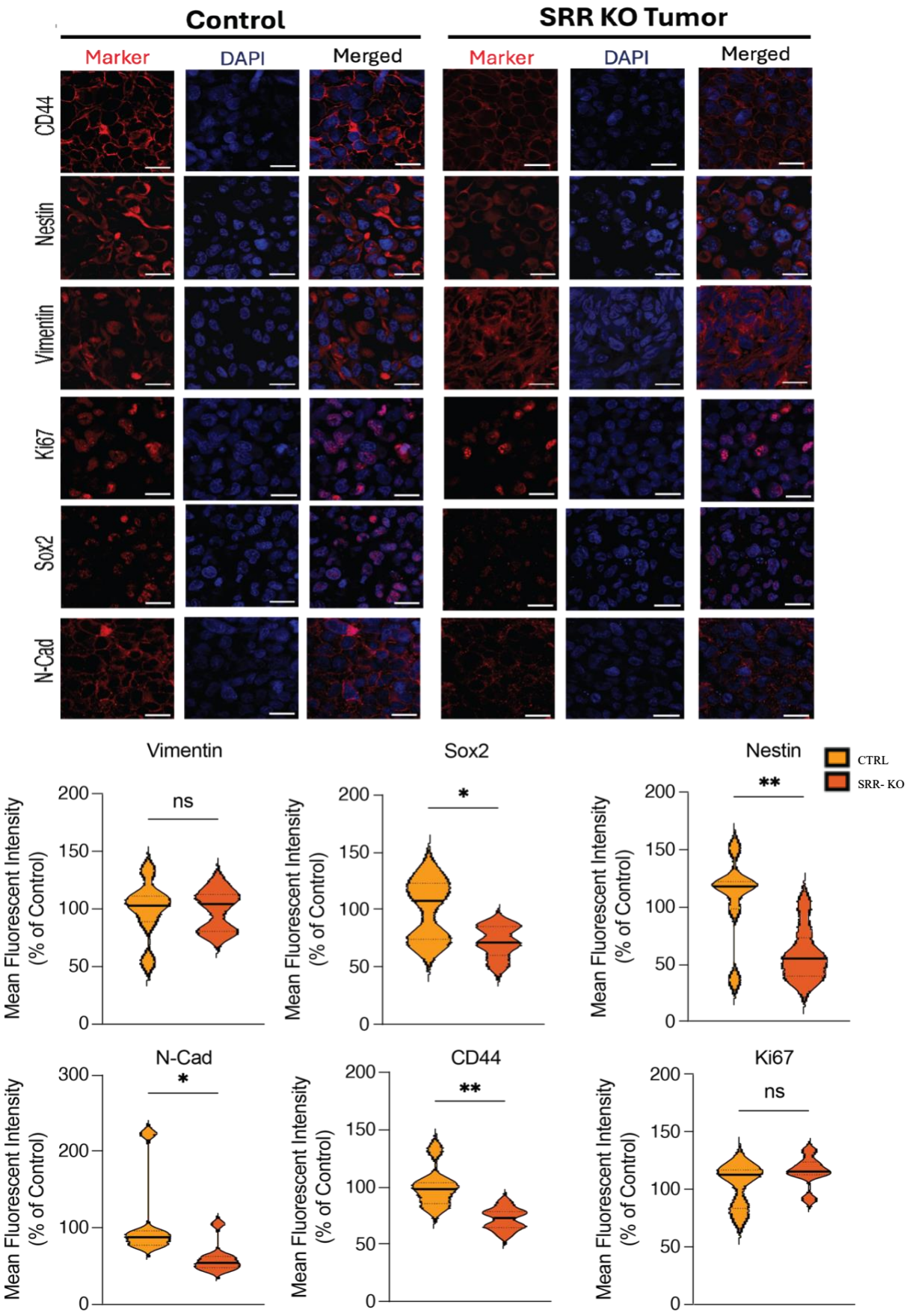
Control
SRR KO Tumor
Marker
DAPI
Merged
CD44
Nestin
Vimentin
Ki67
Sox2
N-Cad
Vimentin
Sox2
Nestin
CTRL
SRR- KO
Mean Fluorescent Intensity (% of Control)
ns
*
**
N-Cad
CD44
Ki67

Figure 15. SRR KO cells had reduced expression of stemness, migratory, and mesenchymal markers in PDX glioblastoma tumors.
Immunohistochemical analysis of patient-derived xenograft (PDX) tumor sections from mice giving SRR KO rGBM cells or control cells revealed a marked reduction in the expression of multiple GBM-associated markers. Representative images show immunofluorescence staining (red) for CD44, Nestin, Vimentin, Ki67, N-Cadherin (N-CAD), and Sox2, with nuclear counterstaining using DAPI (blue). Quantification of mean fluorescence intensity revealed significantly lower levels of all markers in PMS-treated tumors compared to controls. Data are represented as violin plots showing intensity values normalized to control levels (% of control). The scale bar is 20 μm. N= 7 for SRR KO and N=6 for control. * < p - 0.05, ** < p - 0.01, *** < p - 0.001, **** < p - 0.0001.

SRR activity supports endothelial network in the rGBM microenvironment

To determine whether disruption of rGBM/endothelial cell crosstalk alters vascular structure *in vivo*, we examined the effects of SRR inhibition on tumor-associated vasculature. tumor sections from PMS-treated mice were stained for CD31, an endothelial cell marker. Along with CD31, tumors were stained with LDHA (tumor-specific marker), and a nuclear stain. Low-magnification images revealed preserved tumor architecture, while high-magnification images showed a significant reduction in CD31-positive vascular structures in PMS-treated tumors (Figure 15A). Vessel profiles appeared less frequent and showed reduced branching compared to controls. Quantification of CD31-positive area confirmed a significant decrease in vascular density in PMS-treated tumors (Figure 15B), demonstrating that SRR activity contributes to the maintenance of endothelial networks within the rGBM microenvironment.

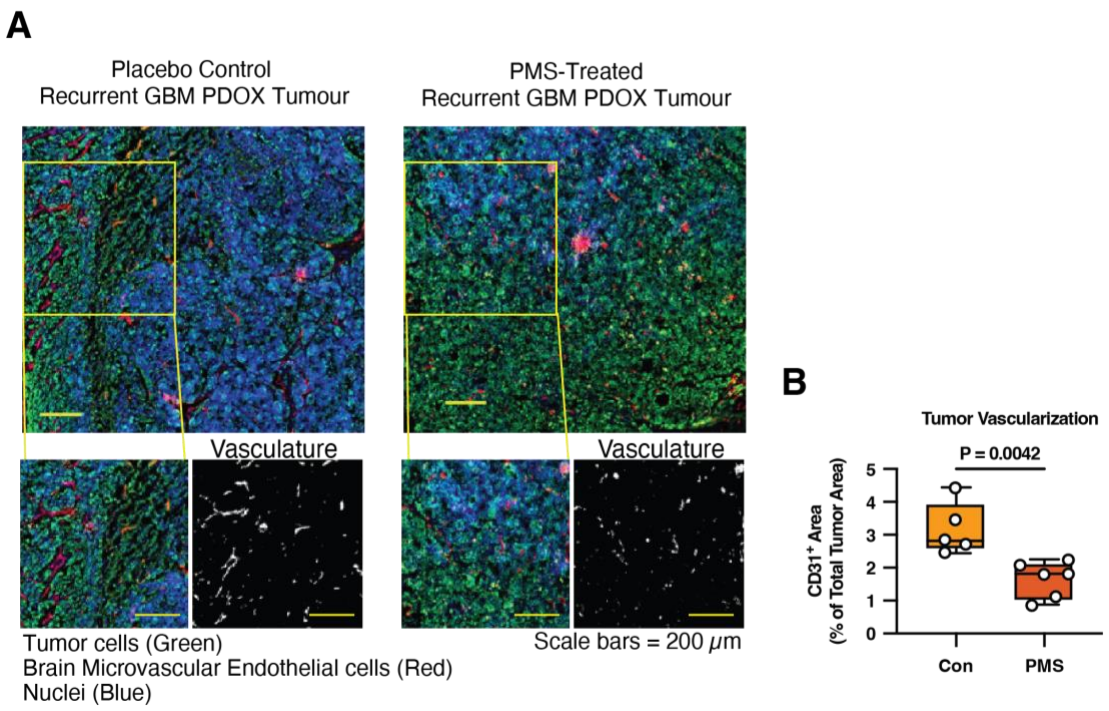

Figure 16. PMS treatment reduces tumor-associated vasculature.
(A) Immunohistochemistry staining of tumor sections following PMS treatment. Higher-magnification inset highlighting intratumoral vasculature labelled with the endothelial marker CD31, 20X. (B) Quantification of CD31-positive vascular density within the tumor region was done at 40x. N=2 per group, n=6.

Loss of SRR activity disrupts angiogenic and proliferative gene expression

Given the strong evidence that SRR-dependent signaling shapes tumor/endothelial interactions *in vitro*, we next sought to determine whether disruption of this crosstalk alters transcriptional programs that support vascular maintenance and tumor growth *in vivo*. In particular, we aimed to assess whether SRR activity influences gene expression within spatially distinct tumor regions characterized by differing vascular densities. Spatial transcriptomics was therefore employed to investigate compartment-specific signaling within PMS-treated and SRR knockout tumors by using the GeoMx digital profiler workflow (Figure 16). Tumor sections were segmented by cell type using CD31, DAPI, and tumor marker LDHA, allowing for compartment-specific analysis (Figure 17A, D). Volcano plots identified significantly downregulated genes in both PMS-treated and SRR-KO tumors, with substantial overlap of similar genes (Figure 17B, E). Expression of

genes involved in angiogenesis (*VEGFA*), hypoxia (*HIF1A*), stemness (*ITGB8, CD44*) and proliferation (*Mki67*) were all reduced in response to PMS and SRR KO (Figure 17C, F). These results demonstrate that SRR supports a transcriptional program beneficial to tumor progression and that its inhibition or deletion disrupts this state. A substantial set of genes was jointly suppressed across the two conditions, indicating convergence on a shared molecular response when SRR activity is reduced.

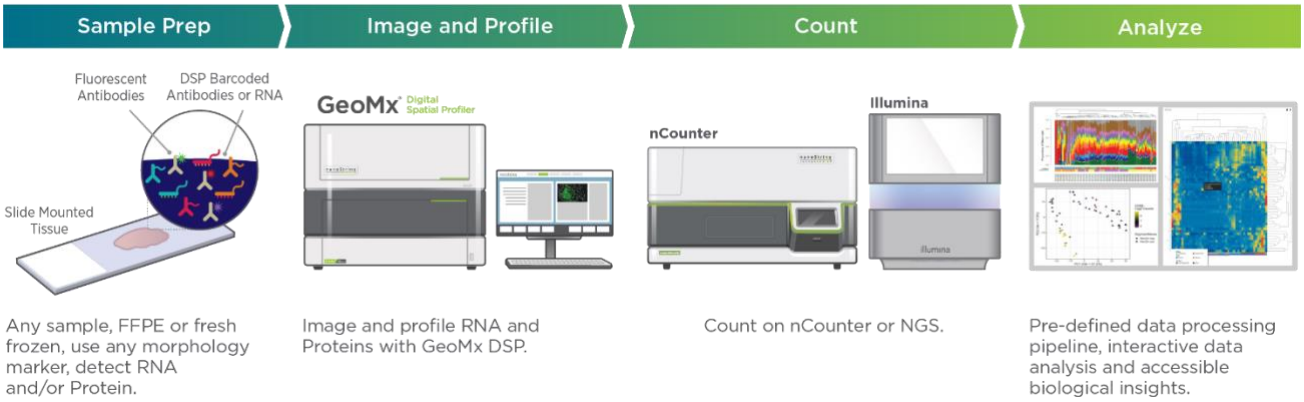

Figure 17. Spatial transcriptomic experimental workflow.
[Bruker Spatial Biology/Nanostring] https://nanostring.com/products/geomx-digital-spatial-profiler/geomx-dsp-overview/

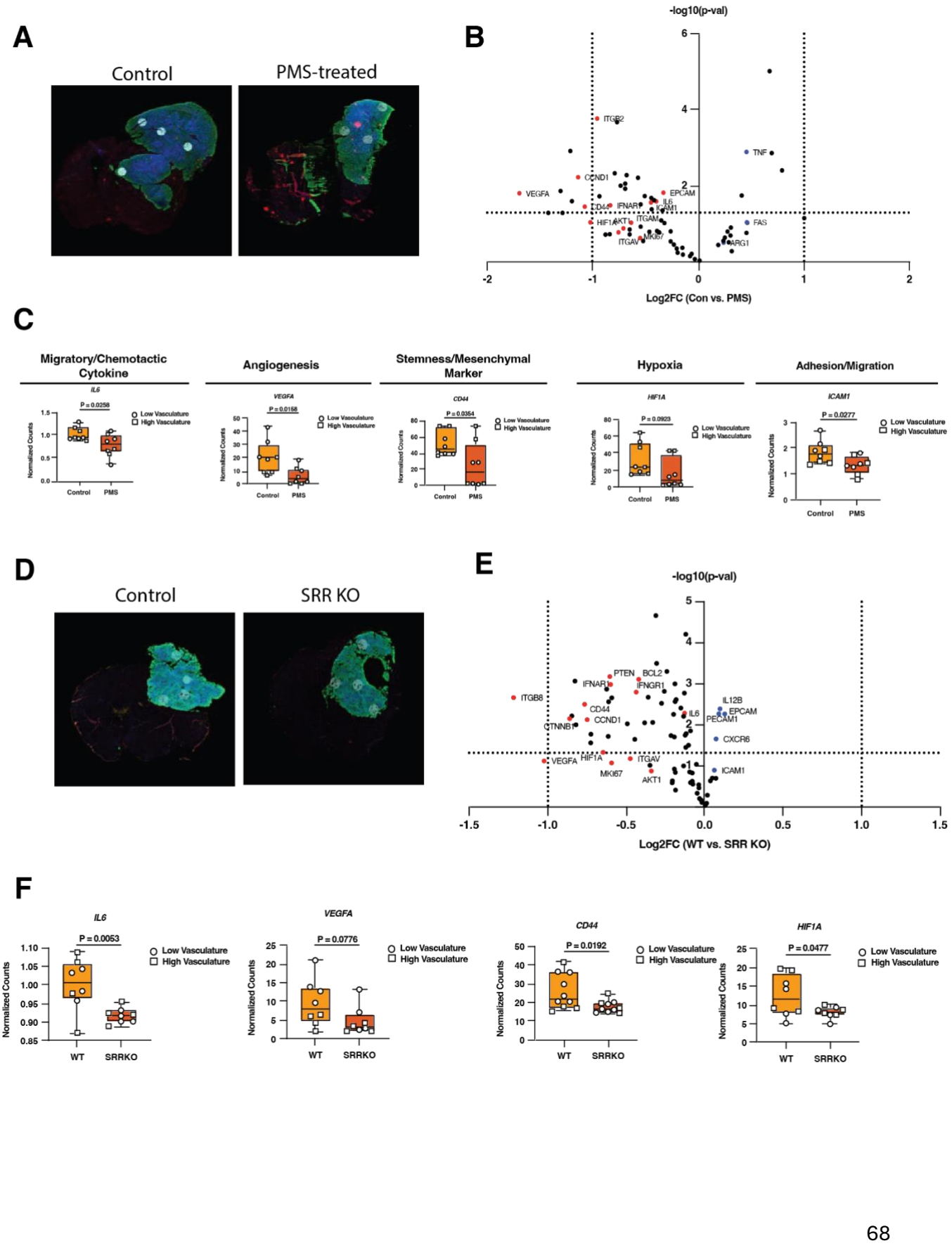
A
Control
PMS-treated
B
-log10(p-val)
Log2FC (Con vs. PMS)
ITGB2
TNF
CCND1
VEGFA
EPCAM
CD44
IFNAR1
IL6
ICAM1
HIF1A
AKT1
ITGAM
FAS
ITGAV
MKI67
ARG1
C
Migratory/Chemotactic Cytokine
Angiogenesis
Stemness/Mesenchymal Marker
Hypoxia
Adhesion/Migration
IL6
VEGFA
CD44
HIF1A
ICAM1
P = 0.0258
P = 0.0168
P = 0.0354
P = 0.0923
P = 0.0277
Low Vasculature
High Vasculature
Normalized Counts
Control
PMS
D
Control
SRR KO
E
-log10(p-val)
Log2FC (WT vs. SRR KO)
PTEN
BCL2
IFNAR1
IFNGR1
ITGB8
IL12B
CD44
IL6
EPCAM
CCND1
PECAM1
CTNNB1
CXCR6
VEGFA
HIF1A
ITGAV
ICAM1
MKI67
AKT1
F
IL6
VEGFA
CD44
HIF1A
P = 0.0053
P = 0.0776
P = 0.0192
P = 0.0477
Low Vasculature
High Vasculature
Normalized Counts
WT
SRRKO

Figure 18. Spatial transcriptomic profiling reveals transcriptional suppression after SRR inhibition or deletion in GBM tumors.
(A, D) Spatial transcriptomics was performed on tumor sections from PMS-treated and SRR-KO tumors. Tissue regions were segmented by cell type using CD31 to identify vasculature, LDHA to define tumor compartments, and DAPI for nuclei. (B, E) Volcano plot analysis showed broad transcriptional downregulation in both PMS-treated and SRR-KO tumors log2FC is used to show the magnitude and direction of gene expression differences between two conditions, with positive values indicating upregulation and negative values indicating downregulation. (C, F) Targeted analysis of key pathways revealed consistent decreases in genes associated with angiogenesis (*VEGFA, ANGPT2*), hypoxia response (*HIF1A*), cell migration (C*D44*), adhesion signaling (*CXCL4*), and proliferation (*Mki67*). Each data point represents a ROI from a unique region within the tumor. N=2 per group, n=8

GBM-Derived D-Serine signals through endothelial NMDARs to promote tumor aggressiveness

Given our findings that recurrent GBM cells produce and release D-serine in an SRR-dependent manner, and that extracellular D-serine supports endothelial activation and tumor aggressiveness, we sought to determine whether tumor-derived D-serine is directly detected by endothelial cells through NMDA receptor. To test this, we generated an endothelial-specific knockout of the D-serine binding site, NMDAR subunit GluN1 and evaluated its impact on rGBM–EC interactions. Immunoblot analysis confirmed efficient GluN1 deletion in hCMECs, with complete loss of protein in GluN1-KO hCMECs compared to scramble controls (Figure 18A).

To test whether eNMDAR signaling influences the cytokine secretion established during tumor–vascular interactions, rGBM cells were co-cultured with either control or GluN1-KO hCMECs, and secreted factors were quantified using a cytokine array. Loss of eGluN1 altered the cytokine profile in the co-culture environment (Figure 18B). Several cytokines that were upregulated in control rGBM–EC co-cultures were significantly reduced upon GluN1 deletion, indicating that activation of eNMDARs contributes to a pro tumor signaling cascade. These included molecules associated with angiogenesis, inflammation, and tumor support.

We next examined whether disrupting eNMDAR signaling alters rGBM cell behaviour. Across two patient-derived rGBM lines, BT241 and BT972, co-culture with GluN1-KO hCMECs significantly reduced tumor cell migration (Figure 18 C–D). Loss of eGluN1 also impaired the

self-renewal capacity of rGBM cells. In BT241 and BT972 sphere formation assays, GluN1-KO hCMECs significantly decreased tumorsphere number relative to scramble control hCMECs (Figure 18 E–F). We then assessed whether eGluN1 influences tumor cell invasiveness within the microenvironment. Invasion assays showed that rGBM cells co-cultured with GluN1-KO hCMECs exhibited a reduction in invasive outgrowth compared to those cultured with GluN1 control hCMECs (Figure 18G). Tumor cells formed smaller, less outwardly projecting structures over three days, demonstrating that eNMDAR signaling facilitates rGBM migration, self-renewal, and invasive properties. Finally, Western blot analysis further validated the role of eGluN1 by detecting a reduction in pro-tumor phenotypes when rGBM were co-cultured with GluN1 knockout ECs, revealing downregulation of key markers associated with mesenchymal transition and stemness (Figure 18H).

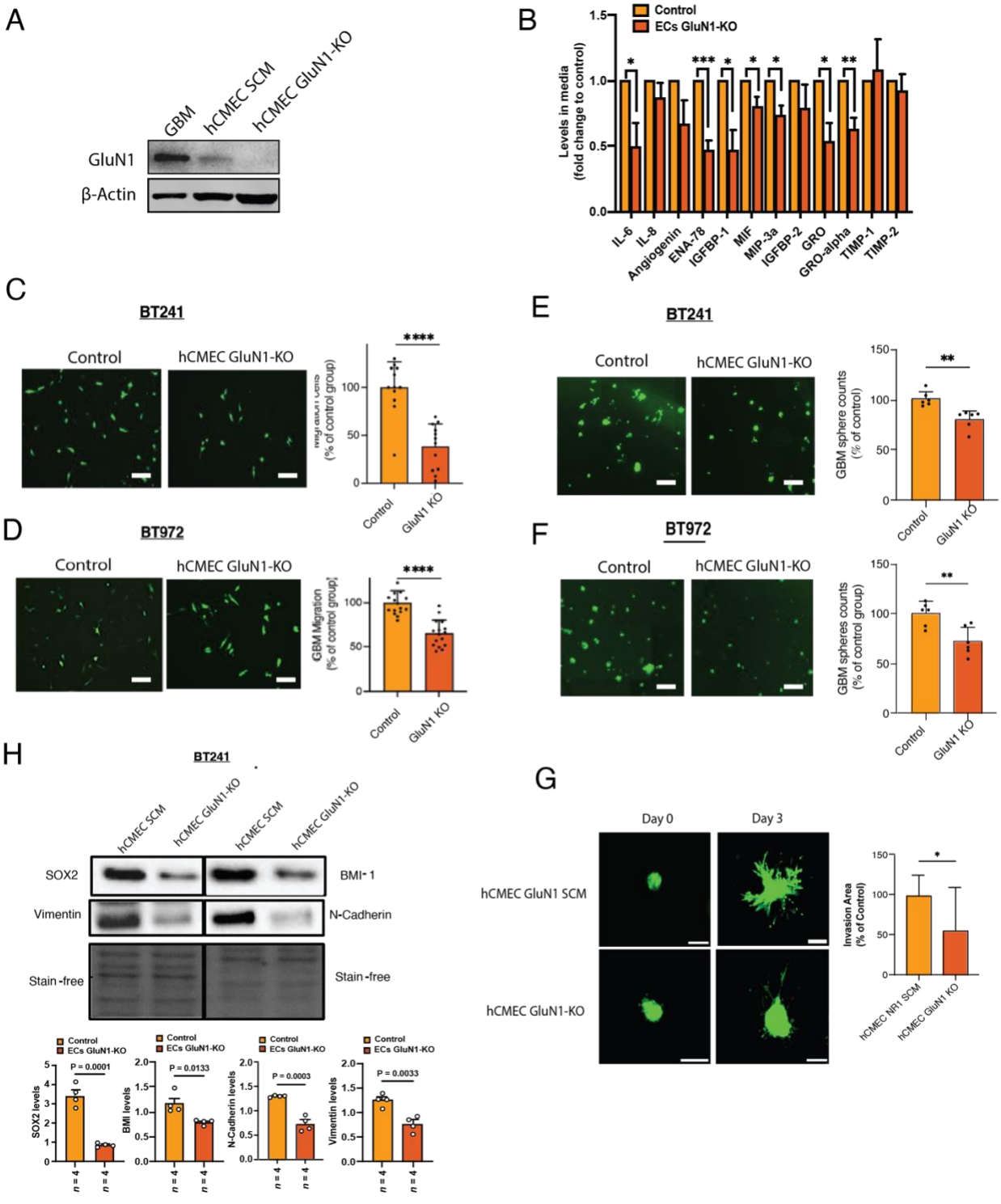
A
GBM
hCMEC SCM
hCMEC GluN1-KO
GluN1
β-Actin
B
Control
ECs GluN1-KO
Levels in media (fold change to control)
IL-6
IL-8
Angiogenin
ENA-78
IGFBP-1
MIF
MIP-3a
IGFBP-2
GRO
GRO-alpha
TIMP-1
TIMP-2
C
BT241
Control
hCMEC GluN1-KO
Migration (% of control group)
Control
GluN1 KO
D
BT972
GBM Migration (% of control group)
E
BT241
GBM sphere counts (% of control)
F
BT972
GBM spheres counts (% of control group)
G
Day 0
Day 3
hCMEC GluN1 SCM
hCMEC GluN1-KO
Invasion Area (% of Control)
hCMEC NR1 SCM
hCMEC GluN1 KO
H
BT241
SOX2
Vimentin
Stain-free
BMI-1
N-Cadherin
SOX2 levels
BMI levels
N-Cadherin levels
Vimentin levels
P = 0.0001
P = 0.0133
P = 0.0003
P = 0.0033
n = 4

Figure 19. Endothelial GluN1 deletion reduces rGBM/vascular signaling and limits tumor aggressiveness.
(A) Immunoblot showing efficient loss of GluN1 protein in GluN1-KO hCMECs compared to scramble controls. (B) Cytokine array of GBM–EC co-cultures showing that GluN1 deletion shifts the secreted cytokine profile and reduces multiple pro-tumor factors N=3. (C–D) Loss of eGluN1 reduces rGBM cell migration in BT241 and BT972 lines. (E–F) Tumorsphere assays demonstrating reduced GBM self-renewal when cultured with GluN1-KO hCMECs. (G) Invasion assays show that GBM cells grown with GluN1-KO hCMECs form smaller, less invasive structures over three days, N=4. (H) Western blot analysis of rGBM co-cultured with GluN1 knockout ECs revealed reduced expression of mesenchymal and stemness-associated markers. Scale = 150μm for Fig C and D, Scale = 1mm for Fig E aF and Scale = 200μm for Fig G. * < p - 0.05, ** < p - 0.01, *** < p - 0.001, **** < p - 0.0001.

To affirm that results with genetic loss of eGluN1 reflect functional eNMDAR loss, we treated BT241 and BT972 rGBM cells with a panel of NMDAR antagonists, including AP5, DCKA, MK801, and evaluated their effects on migration and sphere-forming capacity. AP5 is a competitive antagonist at the glutamate-binding site of the NMDAR, located on the GluN2 subunit. By directly competing with glutamate, AP5 prevents receptor activation in a ligand-dependent manner. Its inhibitory effects are therefore contingent on extracellular glutamate concentration. DCKA acts as a competitive antagonist at the glycine/D-serine co-agonist binding site located on the GluN1 subunit. Unlike AP5, DCKA does not interfere with glutamate binding, but instead prevents receptor activation by eliminating the required co-agonist signal. This mechanism makes DCKA particularly informative in studies examining D-serine–dependent NMDAR activation and provides a functional readout of serine racemase activity and D-serine availability. MK801 is a non-competitive, use-dependent NMDAR antagonist that blocks the receptor's ion channel pore. Unlike AP5 and DCKA, MK-801 requires receptor activation and channel opening before it can bind, after which it becomes trapped within the channel. This results in a long-lasting and essentially irreversible blockade under physiological conditions. MK-801 therefore preferentially inhibits actively signaling NMDARs and produces a profound suppression of calcium influx. In migration assays, all three inhibitors reduced GBM motility (Figure 19A–B). In BT241 cells, DCKA, MK801, and AP5 each produced a significant reduction

in migratory cells relative to control, indicating that blockade of the NMDAR signaling cascade, whether at the D-serine/glycine co-agonist site, the ion channel pore, or at the glutamate agonist site, impairs GBM movement. BT972 cells showed a similar pattern when NMDARs were blocked with the same drugs.

We next tested whether NMDAR inhibition affects the self-renewal potential of rGBM using tumor sphere formation assays. NMDAR inhibition impaired sphere forming behaviour in BT241 cells (Figure 19D–E). DCKA, MK801, and AP5 significantly reduced the average tumor sphere size. In BT972 cells, sphere formation was more selectively affected. DCKA and AP5 significantly decreased the number of tumorspheres, whereas MK801 had no measurable effect in this line (Figure 19F).

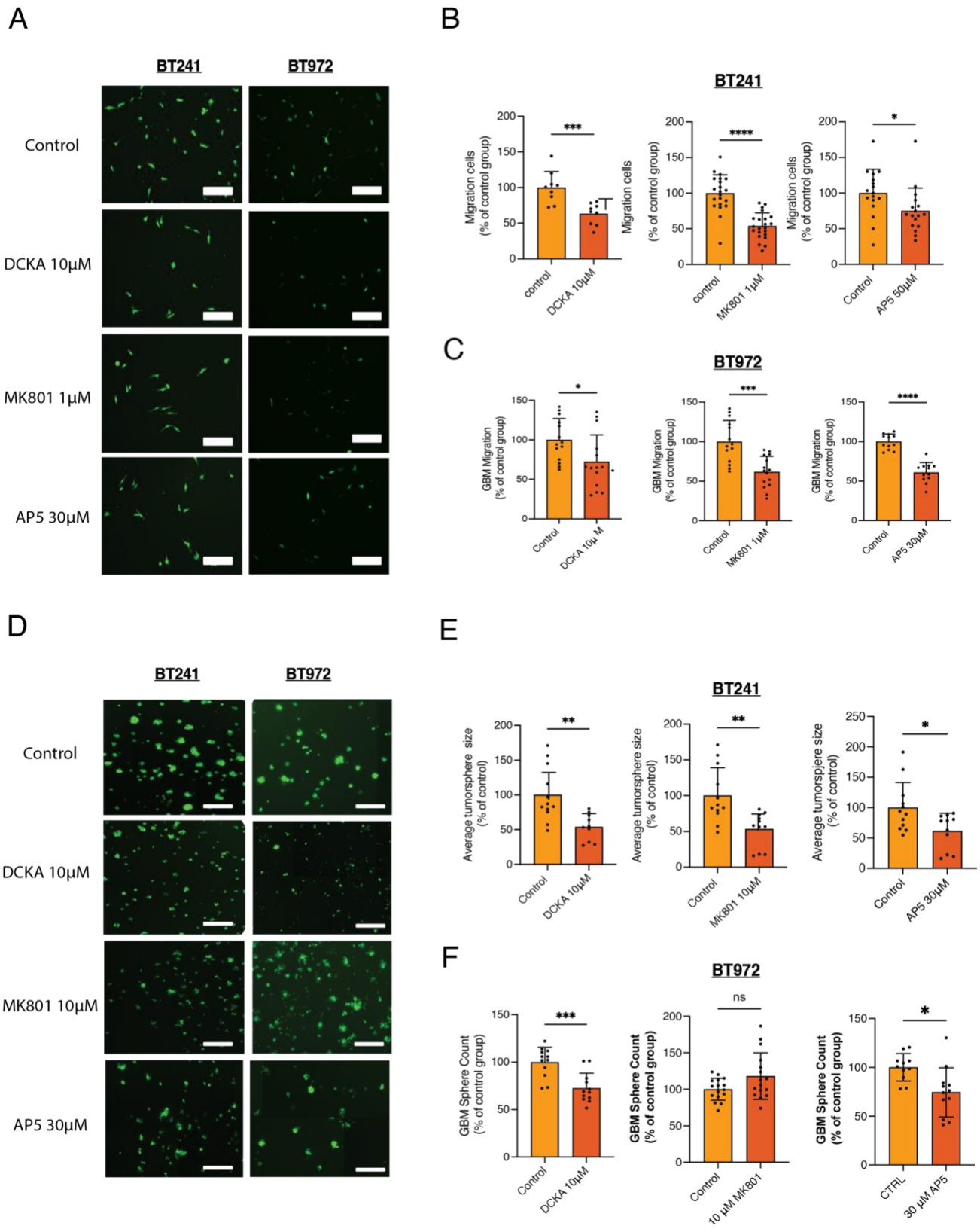
A
BT241
BT972
Control
DCKA 10µM
MK801 1µM
AP5 30µM
B
BT241
Migration cells (% of control group)
control
DCKA 10µM
MK801 1µM
Control
AP5 50µM
C
BT972
GBM Migration (% of control group)
Control
DCKA 10µ M
MK801 1µM
AP5 30µM
D
BT241
BT972
Control
DCKA 10µM
MK801 10µM
AP5 30µM
E
BT241
Average tumorsphere size (% of control)
Control
DCKA 10µM
MK801 10µM
AP5 30µM
F
BT972
GBM Sphere Count (% of control group)
ns
Control
DCKA 10µM
10 µM MK801
CTRL
30 µM AP5

Figure 20. Pharmacologic NMDAR inhibition reduces rGBM migration and self-renewal.
(A–C) Migration assays showing that DCKA, MK801, and AP5 each suppress motility in BT241 and BT972 rGBM cells. (D–F) Tumorsphere assays in BT241 cells demonstrate that NMDAR blockade reduces sphere-forming capacity. In BT972 cells, DCKA and AP5 reduce the number of tumor spheres, whereas MK801 has no measurable effect. Scale = 150μm for Fig A, Scale = 1mm for Fig D. * < p - 0.05, ** < p - 0.01, *** < p - 0.001, **** < p - 0.0001.

Endothelial IL-6 and nitric oxide signaling differentially regulate migratory and self-renewal phenotypes in recurrent GBM cells

To assess the contribution of endothelial-derived inflammatory and metabolic signals to recurrent GBM aggressiveness, we examined the effects of IL-6 neutralization and nitric oxide (NO) inhibition on GBM cell migration and self-renewal using co-culture-based functional assays. We were interested in the role of IL-6 based on the previously shown cytokine arrays, which illustrated a significant reduction of IL-6 concentration in the media when BT241 was co-cultured with eGluN1 KO hCMECs. Further, our lab has previously shown that upon eNMDAR activation by Glutamate and D-serine caused endothelial NO generation[104]. We wanted to investigate if these findings could be expanded to the TME, where ECs could be creating a tumor-permissive environment through NO release.

A neutralization of IL-6 significantly reduced the migratory capacity of recurrent BT241 GBM cells in endothelial co-culture. Compared to control conditions, the addition of an anti–IL-6–neutralizing antibody resulted in a marked decrease in GBM cell migration (Figure 20A), indicating that IL-6 present in the co-culture environment contributes to the migratory phenotype of recurrent GBM cells. To determine whether this effect was specifically attributable to IL-6 signaling, recombinant IL-6 was added following IL-6 neutralization. Exogenous IL-6 restored GBM cell migration to levels comparable to control conditions (Figure 20B), demonstrating that IL-6 is both necessary and sufficient to support migration in this context. These findings indicate

that IL-6 acts as a paracrine mediator within the endothelial–GBM co-culture to promote tumor cell motility. Importantly, IL-6 manipulation did not significantly alter GBM sphere-forming capacity under these experimental conditions, indicating that IL-6 selectively regulates migratory behaviour rather than self-renewal.

We next examined the role of nitric oxide signaling by pharmacologically inhibiting nitric oxide synthase (NOS) using L-NIO. In contrast to IL-6 neutralization, NOS inhibition did not significantly affect GBM cell migration in co-culture assays (data not shown). However, blockade of NO production resulted in a significant reduction in tumorsphere size, reflecting impaired self-renewal capacity of recurrent GBM cells (Figure 20C). These data indicate that NO signaling contributes to the maintenance of stem-like properties rather than migratory behaviour in this setting. Together, these results demonstrate that endothelial-derived IL-6 and NO regulate distinct aspects of recurrent GBM aggressiveness. IL-6 selectively promotes tumor cell migration, whereas NO signaling supports self-renewal capacity.

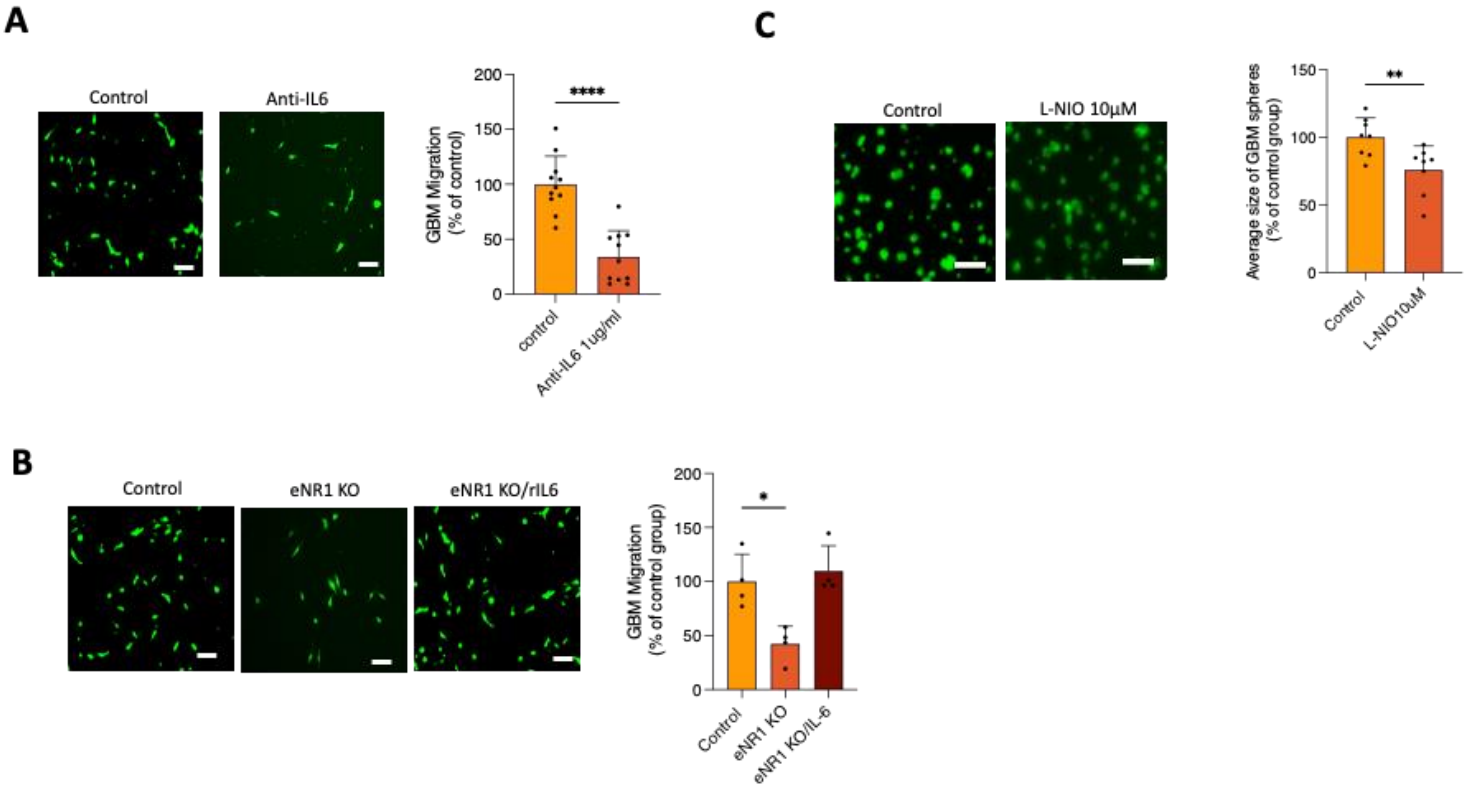

Figure 21. Downstream Modulators of Endothelial Activation: IL-6 and NO Pathways Influence GBM Aggressiveness. (A) Migration assays showing that neutralizing IL-6 suppresses motility in BT241 rGBM cells. (B) Migration assays in BT241 cells demonstrate that migration capability can be rescued with the addition of exogenous recombinant IL-6. (C) Tumorsphere assays in BT241 cells demonstrate that NOS blockade reduces sphere-forming capacity. Scale = 150µm for Fig A,B, Scale = 1mm for Fig C. * < p - 0.05, ** < p - 0.01, *** < p - 0.001, **** < p - 0.0001.

Chapter 5: Discussion

Study Overview

GBM remains one of the most treatment-resistant human malignancies, driven by cellular heterogeneity, an adaptive metabolic landscape, and a supportive tumor microenvironment that supports malignant traits. The data presented identify SRR and its product, D-serine, as regulators of a paracrine communication axis between GBM cells and the endothelial compartment. This work reveals that GBM cells are the dominant producers of D-serine within the tumor vascular niche, and that SRR activity is required to maintain multiple hallmarks of aggressive tumor behaviour, including migration, invasion, stemness, angiogenic signaling, and *in vivo* tumor expansion. These findings identify the GBM-derived D-serine/endothelial NMDAR axis as a previously unrecognized driver of aggressive tumor–vascular crosstalk in recurrent GBM. Notably, disruption of this signaling pathway through multiple independent experimental approaches consistently attenuated the aggressive tumor phenotype (Figure 21).

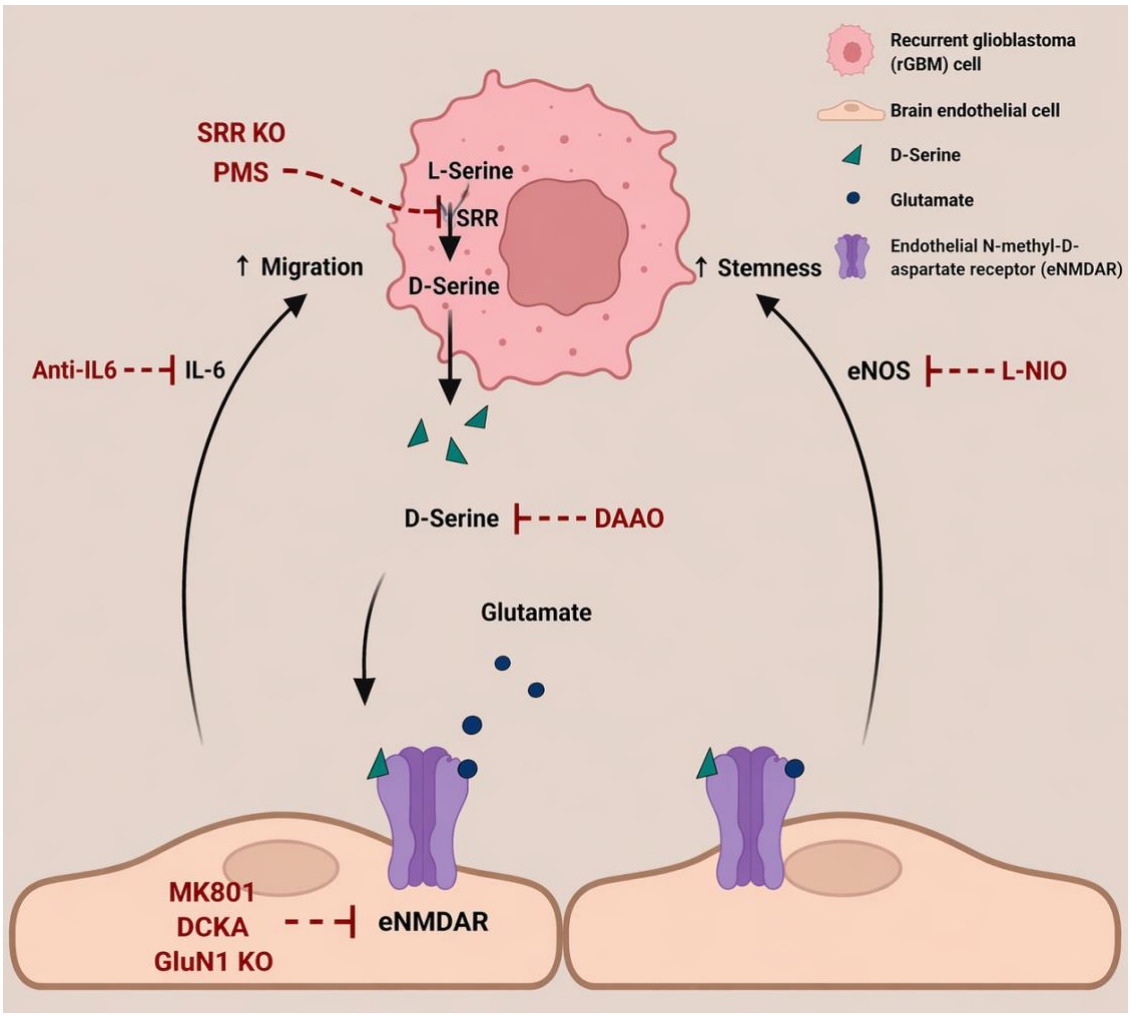

Figure 22. Study Overview: GBM-derived D-serine drives endothelial NMDAR-mediated tumor–vascular crosstalk in recurrent GBM.
Schematic of the proposed mechanism in which recurrent GBM (rGBM) cells convert L-serine to D-serine via serine racemase (SRR), increasing extracellular D-serine levels. In combination with tumor-derived glutamate, D-serine activates endothelial NMDARs (eNMDARs) on brain endothelial cells, promoting signalling that enhances tumor migration and stemness. Disruption of this axis is shown through multiple approaches: SRR inhibition or knockout (PMS, SRR KO) reduces D-serine production; DAAO degrades extracellular D-serine; eNMDAR blockade (MK-801, DCKA, GluN1 KO) prevents receptor activation; and eNOS inhibition (L-NIO) targets downstream signalling. IL-6 also contributes to migration and is attenuated by anti-IL-6 treatment.

SRR was found to be consistently upregulated across several independent patient datasets, including the TCGA, Rembrandt, and CGGA cohorts. Higher SRR expression correlated with increased tumor grade and poorer overall survival, suggesting that SRR is not purely a metabolic enzyme upregulated during oncogenesis but may contribute directly to the malignant phenotype. Historically, SRR has been studied primarily within the context of neuronal NMDAR regulation, where D-serine acts as a co-agonist with glutamate. This work extends SRR neurobiology into a cancer setting, demonstrating that GBM cells co-opted this metabolic pathway to sustain a niche dependent growth system. Elevated extracellular D-serine accumulated in GBM–EC co-culture systems, and genetic deletion or inhibition of SRR eliminated this accumulation and diminished aggressive tumor behaviours. These observations confirm that endogenous D-serine production supports tumor progression rather than acting as a metabolic byproduct.

Further, ECs, through their expression of the NMDARs, act as a critical receptor of GBM TME signaling. Previous work has highlighted that endothelial cells form a specialized stem cell–like niche for glioma propagation, mediated through Notch ligands, angiogenic signals, and structural protection within the perivascular zone[90]. Endothelial cells lacking GluN1 exhibited altered cytokine secretion, decreased production of angiogenic mediators, and significantly reduced capacity to promote GBM migration, invasion, and tumorsphere formation. These changes mirror the effects seen with SRR inhibition in GBM cells, demonstrating that SRR derived D-serine acts upstream of eNMDAR activation, and the downstream release of modulators can fuel GBM malignancy. Pharmacologic NMDAR antagonism further validated this signaling axis, although with cell line specific differences that reflect the heterogeneity intrinsic to GBM.

Spatial transcriptomics provided insight into how SRR inhibition reshapes transcriptional states within the tumor microenvironment. The use of spatial profiling was important because it allowed gene expression changes to be mapped within discrete tumor regions defined by vascular density and cellular composition. This compartment-specific approach revealed that SRR inhibition or knockout suppresses transcriptional programs associated with vascular maintenance and tumor growth, thereby strengthening the conclusion that SRR plays a key role in sustaining pro-tumorigenic signalling within the glioblastoma microenvironment. Both pharmacologic and genetic suppression of SRR led to downregulation of genes associated with angiogenesis, hypoxia responses, adhesion, migration, and proliferation. These findings align with evolving spatial transcriptomic maps showing that GBM-associated vasculature is molecularly distinct from normal endothelium and plays a critical role in supporting tumor stemness, growth, and immune evasion[105]. By demonstrating that SRR activity is required to maintain these vascular niche signatures, this work broadens the understanding of how metabolic signaling integrates with transcriptional programs to sustain GBM progression.

Importance of the study

Although SRR has not traditionally been studied within oncology, its role in human disease has been extensively documented in neurological and neuropsychiatric disorders. SRR is best known for its regulation of D-serine production in the central nervous system, where D-serine functions as a key co-agonist of NMDA receptors and modulates synaptic plasticity, learning, and memory. Dysregulation of SRR or D-serine signaling has been implicated in schizophrenia, amyotrophic lateral sclerosis, Alzheimer's disease, epilepsy, and ischemic brain injury, where aberrant NMDA receptor activity contributes to excitotoxicity, neuronal dysfunction, or altered circuit

development. In these contexts, SRR has been viewed primarily as a neuronal or glial enzyme whose pathological relevance is confined to the nervous system.

Beyond classical neurobiology, emerging studies have begun to suggest broader roles for SRR and D-serine signaling in non-neuronal tissues. Endothelial NMDA receptor expression has been described in vascular beds, where it regulates calcium signaling, permeability, and angiogenic responses. In parallel, D-serine has been implicated in inflammatory regulation, immune cell activation, and oxidative stress responses, indicating that SRR-dependent pathways may participate in systemic signaling processes beyond synaptic transmission. However, these observations have remained largely disconnected from cancer biology, and SRR has not been widely recognized as a contributor to tumor progression.

A defining feature of SRR, particularly relevant to cancer, is its bifunctional enzymatic activity. In addition to racemization, SRR catalyzes the β-elimination of serine to produce pyruvate and ammonia. This reaction provides a direct metabolic connection between serine availability and central carbon metabolism. Ohshima et al. demonstrated that colorectal cancer cells exploit this catalytic property to sustain proliferation, mitochondrial mass, and survival[106]. Their work showed that SRR-derived pyruvate contributes to acetyl-CoA pools, thereby influencing histone H3 acetylation and transcriptional regulation of growth-promoting programs. Pharmacologic or genetic inhibition of SRR suppressed tumor growth in vivo and enhanced sensitivity to 5-fluorouracil, establishing SRR as an active metabolic driver in colorectal cancer[106].

While serine canonically fuels one-carbon metabolism and S-adenosylmethionine (SAM)–dependent methylation, SRR introduces an alternative metabolic branch that diverts serine carbon toward pyruvate production and mitochondrial acetyl-CoA generation. Although direct SRR-

focused studies in GBM remain limited, work in other tumor types demonstrates that SRR-mediated serine dehydration sustains mitochondrial function, preserves acetyl-CoA pools, and promotes histone acetylation, thereby supporting transcriptional programs associated with proliferation and tumor fitness[85]. In GBM, where acetyl-CoA availability is a known regulator of chromatin accessibility and lineage plasticity, loss of SRR activity or reduced serine flux into acetyl-CoA would be expected to preferentially impair histone acetylation–dependent transcriptional programs[107,108]. Thus, SRR knockout in GBM is most plausibly linked to altered epigenetic control through reduced acetyl-CoA–driven histone acetylation, with downstream effects on gene expression programs that maintain stem-like or therapy-resistant states.

By contrast, the epigenetic consequences of D-serine deficiency in GBM are likely to play an indirect role. D-serine itself is not a methyl donor, and there is currently no strong evidence that D-serine depletion directly alters DNA or RNA methylation programs in cancer. However, SRR loss might alters how intracellular serine is partitioned between one-carbon metabolism and other fates. Serine availability is a critical determinant of SAM production, and serine restriction has been shown to reduce DNA and RNA methylation and to remodel transcription via SAM-sensitive epigenetic and epitranscriptomic pathways[109]. In GBM, where serine uptake and synthesis are frequently upregulated, SRR knockout could bias serine utilization toward one-carbon pathways while limiting acetyl-CoA production, or conversely create metabolic stress that limits both acetylation and methylation capacity.

Importantly, the role of SRR appears to be context dependent across cancer types. In pancreatic cancer, clinical data suggest that SRR expression correlates with patient outcomes, positioning it as a potential prognostic marker[110]. Given the metabolic heterogeneity of pancreatic tumors, it is

plausible that SRR contributes selectively to subsets of tumors that rely on oxidative metabolism or serine-rich microenvironments. Similarly, bioinformatic analyses in endometrial cancer have identified SRR as an independent prognostic factor and implicated it in regulatory networks involving noncoding RNAs and immune-associated pathways[111]. While such studies provide valuable correlative insights, they also highlight a limitation inherent to expression-based analyses: SRR protein abundance does not necessarily reflect its catalytic output or the balance between racemization and elimination reactions, both of which are likely influenced by substrate availability and cellular redox state. Evidence from osteosarcoma further supports a functional role for SRR in tumor progression. Pu et al. reported that miR-193a-5p suppresses osteosarcoma cell migration and invasion by directly targeting SRR, implicating the enzyme in metastatic behaviour[112]. Although the precise downstream mechanisms were not fully outlined, these findings are consistent with a model in which SRR supports invasive phenotypes through metabolic or signaling pathways.

Beyond metabolism, SRR may also influence cancer through D-serine–mediated signaling. Functional NMDARs have been identified in multiple tumor types, and glutamatergic signaling has been implicated in cancer cell proliferation, survival, and invasion[113]. In this context, SRR-derived D-serine may act in an autocrine or paracrine manner to modulate tumor–microenvironment interactions. Although these signaling mechanisms remain incompletely characterized, they align with a broader hypothesis in which cancers co-opt neuronal signaling pathways to support growth and invasion[113].

Regulation of SRR activity adds an additional layer of complexity. SRR is sensitive to post-translational modifications, including S-nitrosylation, linking its activity to nitric oxide signaling and redox balance[114]. Given that oxidative and nitrosative stress are hallmarks of the tumor

microenvironment, SRR may function as a redox-responsive metabolic switch, dynamically adjusting serine utilization in response to environmental cues. This regulatory flexibility may partly explain why SRR exerts divergent effects across tumor types and stages.

The present study extends the functional scope of SRR by demonstrating that glioblastoma cells co-opt a neurobiological signaling pathway to promote tumor growth through microenvironmental manipulation. Unlike prior work that frames SRR activity within neurons or astrocytes, this study identifies malignant cells as the dominant source of D-serine within the tumor vascular niche. Importantly, SRR-driven D-serine production does not act in an autocrine neuronal-like fashion, but instead activates endothelial NMDA receptors to reprogram the vascular compartment toward a tumor-supportive state. This represents a shift in how SRR biology is understood, reframing it as a mediator of paracrine metabolic signaling.

These findings highlight a characteristic of brain tumors, in which tumors arising within the central nervous system repurpose developmental and synaptic signaling pathways to sustain malignancy. Similar examples have been described for glutamate release, synapse-like tumor–neuron interactions, and activity-dependent tumor growth. The identification of SRR and D-serine as components of this signaling landscape further expands the collection of neurobiological mechanisms hijacked by GBM. By linking D-serine metabolism to endothelial activation and vascular niche maintenance, this work bridges previously distinct fields of neurotransmitter biology, tumor metabolism, and microenvironmental regulation.

Importantly, this study also suggests that SRR may represent a more generalizable disease modifier beyond GBM. Given the expression of NMDA receptors in vascular and stromal cells across multiple tissues, SRR-dependent signaling could plausibly influence angiogenesis, inflammation,

or tumor–stroma interactions in other cancer types. While speculative at this stage, these findings open new avenues for investigating SRR as a context-dependent regulator of pathological signaling rather than a neuron-restricted enzyme.

Limitations

Several limitations should be considered within this study. Only two patient-derived GBM models were used as the primary experimental systems. Although these models capture key features of recurrent GBM, tumor-intrinsic heterogeneity remains a major challenge, and SRR dependence may vary across molecular subtypes, including IDH mutant and primary versus recurrent tumors. Additionally, the endothelial co-culture does not fully recapitulate the complexity of the human tumor microenvironment, particularly with respect to immune populations that influence vascular structure and tumor behaviour. A limitation of the spatial transcriptomic analysis is the low number of biological replicates, which may reduce statistical power and limit the generalizability of the observed transcriptional changes. While the inclusion of multiple ROIs from the same tumor allowed assessment of spatial heterogeneity and strengthened within-sample comparisons, these measurements are not equivalent to independent biological replication; moreover, the absence of multiple testing correction should be considered when interpreting the significance of differential gene expression. Other limitations exists when interpreting the pharmacological arm of this study. Although the inhibitor and antagonist experiments strongly support the biological importance of the SRR–D-serine–eNMDAR axis, the compounds used here function primarily as mechanistic tools rather than clinical therapeutics. This is particularly relevant for PMS, which served as a proof-of-concept SRR inhibitor in our model. The specificity and translational suitability of PMS remain incompletely defined. Beyond its use in SRR studies, PMS is also a redox-active electron-transfer reagent that has been used experimentally to generate superoxide, and prior toxicology

work has linked phenazine methosulfate-associated cytotoxicity to oxidative stress and altered calcium homeostasis[115]. Accordingly, some component of the phenotype observed with PMS may reflect broader redox perturbation in addition to SRR inhibition itself. Similarly, DAAO was highly informative as an experimental strategy for depleting extracellular D-serine, but this enzyme degrades D-amino acids via oxidative deamination, generating hydrogen peroxide and ammonia as reaction products. This introduces an important interpretive limitation, because some effects attributed to D-serine depletion could also be influenced by secondary oxidative or metabolic stress.

The NMDAR antagonist studies should also be interpreted in the context of the broader translational history of this drug class. Although AP5, DCKA, and MK-801 were highly informative mechanistic tools in the present study, they are not ideal therapeutic leads in their current forms, and the clinical history of broad NMDA receptor antagonism has been mixed. The most successful NMDA antagonists in clinical medicine have been agents such as memantine, ketamine, and esketamine, which are approved for non-oncology indications and are used under pharmacologic contexts very different from the broad experimental blockade achieved by classical preclinical antagonists[116]. By contrast, several direct NMDA antagonist programs in neurology failed to translate despite promising preclinical rationale. In severe head injury, phase III trials of selfotel were halted early after concerns about possible increased deaths and serious brain-related adverse events[117], and the final analysis showed no clinical benefit. In acute ischemic stroke, aptiganel was not efficacious and may have been harmful, with placebo performing at least as well or better on several outcomes and with adverse effects including cerebral edema, stupor, somnolence, vomiting, and cardiovascular toxicity[118]. A widely cited explanation for these disappointments is that broad NMDAR blockade may suppress physiologic glutamatergic

signaling required for neuronal survival, plasticity, and recovery, thereby narrowing or even negating the therapeutic window. This point is particularly relevant in GBM, where patients may already have substantial neurologic vulnerability from the tumor itself, seizures, edema, prior surgery, radiation, and systemic therapy. Importantly, the clinical record is not uniformly negative: in patients receiving whole-brain radiotherapy for brain metastases, memantine was well tolerated, had a toxicity profile similar to placebo, and delayed time to cognitive decline, suggesting that lower-affinity or more clinically tractable forms of NMDA antagonism can be used safely in selected CNS settings[119]. However, this benefit was neuroprotective rather than anti-tumor. These data suggest that while NMDAR dependency is mechanistically important, broad receptor blockade is difficult to translate directly into a cancer treatment strategy. Future therapeutic development may therefore be better served by targeting the pathway more selectively upstream, such as through SRR inhibition or other approaches that disrupt tumor–vascular D-serine signaling while minimizing interference with physiologic NMDAR function in the normal brain.

Future investigations

These limitations open possibilities for future investigation. A major next step will involve testing SRR inhibition in combination with the current standard of care for recurrent GBM, which includes radiotherapy and temozolomide administration. Because SRR depletion reduces stemness markers, angiogenesis, and hypoxia-driven transcriptional states, SRR inhibitors may sensitize tumors to DNA-damaging therapies. Importantly, prior work has shown that NMDAR activation can induce temozolomide resistance through MGMT upregulation[120], suggesting that targeting SRR or NMDAR signaling could enhance the efficacy of chemoradiotherapy. Extending these studies into patient-derived organoids, ex vivo slice cultures, and eNMDAR-deficient mouse models will be essential for elucidating the broader impact of SRR inhibition on immune infiltration, tumor vascular remodelling, and tumor expansion. The development of more selective,

brain penetrant SRR inhibitors and controlled-release delivery systems may further improve therapeutic potential while minimizing off-target neurocognitive effects.

The emphasis on recurrent glioblastoma is particularly important. Most mechanistic studies focus on treatment-naïve tumors, despite the fact that recurrence accounts for the majority of glioblastoma-related mortality. The enrichment and functional relevance of SRR and D-serine–eNMDAR signaling after radiotherapy and temozolomide suggest that therapeutic pressure selects for metabolic communication pathways that promote aggressiveness, invasiveness, and resistance. This provides a plausible explanation for the aggressive phenotype of recurrent disease and highlights how standard treatments may inadvertently reshape the tumor microenvironment in ways that favor relapse.

The therapeutic implications of these findings are based on disrupting SRR activity, which destabilizes the tumor-promoting vascular niche and enhances sensitivity to radiotherapy and temozolomide, targeting an adaptive mechanism that emerges after initial treatment rather than primary tumor growth alone. In a clinical landscape where options for recurrent glioblastoma remain limited and largely ineffective, identifying SRR as a modifiable metabolic vulnerability is a meaningful advance.

An important future direction arising from these pharmacological studies is to determine whether SRR inhibition could be incorporated into a treatment regimen for GBM not only as a salvage strategy at recurrence, but also as an adjunct during initial therapy. In this thesis, pharmacologic and genetic suppression of SRR reduced migration, invasion, stemness-associated features, vascular density, and in vivo tumor growth while prolonging survival, supporting the concept that SRR is a functional driver of aggressive tumor–vascular crosstalk in rGBM. This raises the

possibility that an optimized SRR inhibitor could be administered following maximal safe resection and alongside standard chemoradiotherapy to target residual, therapy-resistant cells that persist within the perivascular niche. In that setting, SRR inhibition may be most valuable as a niche-disrupting strategy designed to suppress D-serine-mediated endothelial support, reduce invasive outgrowth, and limit the re-establishment of stem-like tumor populations that contribute to recurrence. From a translational perspective, this approach could theoretically delay recurrence by targeting biological programs that are not adequately addressed by surgery, radiation, or temozolomide alone.

SRR inhibition may also have clinical relevance in the recurrent setting, where there is currently no clearly effective standard treatment and where therapeutic decisions are often balanced against preservation of neurologic function and quality of life. Given that SRR blockade in this study limited malignant phenotypes linked to vascular support, tumor aggressiveness, and survival, an SRR-targeted therapy at relapse may help restrain progression even if it does not fully eradicate tumor burden. In practice, this could position SRR inhibitors as adjuncts to repeat surgery, re-irradiation, or systemic salvage therapies, or potentially as a less intensive biologically targeted option for patients who are not candidates for further aggressive intervention. In this context, the benefit may lie in slowing disease progression, delaying further neurologic decline, and modestly extending survival by disrupting the tumor microenvironmental support that sustains recurrent disease. However, these possibilities remain speculative and would require substantial preclinical and translational validation, particularly because PMS serves here as a proof-of-concept inhibitor and is not a clinically optimized drug. Future studies should therefore focus on development of more selective and brain-penetrant SRR inhibitors, define the optimal timing of administration

relative to the STUPP regimen and recurrence, and carefully evaluate toxicity, since D-serine and NMDAR signaling also serve important physiological roles in the central nervous system.

Overall, this work uncovers a previously unrecognized mode of metabolic crosstalk between glioblastoma cells and the endothelium that supports tumor maintenance after therapy. By showing how SRR-driven D-serine signaling sustains a permissive vascular niche in recurrent disease, the study adds a new layer to our understanding of glioblastoma recurrence and provides a strong rationale for pursuing SRR-targeted strategies in combination with existing treatments.

References

1. Grochans, S. *et al.* Epidemiology of Glioblastoma Multiforme–Literature Review. *Cancers (Basel)* **14**, 2412 (2022).
2. Rong, L., Li, N. & Zhang, Z. Emerging therapies for glioblastoma: current state and future directions. *Journal of Experimental & Clinical Cancer Research* **41**, 142 (2022).
3. Kim, M. *et al.* Glioblastoma as an age-related neurological disorder in adults. *Neuro-Oncology Advances* **3**, vdab125 (2021).
4. Johnson, M. *et al.* Advanced Age in Humans and Mouse Models of Glioblastoma Show Decreased Survival from Extratumoral Influence. *Clin Cancer Res* **29**, 4973–4989 (2023).
5. Colopi, A. *et al.* Impact of age and gender on glioblastoma onset, progression, and management. *Mechanisms of Ageing and Development* **211**, 111801 (2023).
6. Yang, W. *et al.* Sex differences in GBM revealed by analysis of patient imaging, transcriptome, and survival data. *Sci Transl Med* **11**, eaao5253 (2019).
7. Prosperetti, C. *et al.* Sex-Related Differences in Glioblastoma: A Single-Center Retrospective Cohort Study. *Biomedicines* **13**, 1715 (2025).
8. Wang, G.-M. *et al.* Importance of the intersection of age and sex to understand variation in incidence and survival for primary malignant gliomas. *Neuro Oncol* **24**, 302–310 (2021).
9. Jovanovich, N. *et al.* Sex-specific molecular differences in glioblastoma: assessing the clinical significance of genetic variants. *Front. Oncol.* **13**, (2024).

10. Tournant, F. Immunological sex differences in glioblastoma. *Nat Cancer* **4**, 1636–1636 (2023).
11. Davis, M. E. Glioblastoma: Overview of Disease and Treatment. *Clin J Oncol Nurs* **20**, S2–S8 (2016).
12. Rogers, S. *et al.* Re-irradiation for recurrent glioblastoma: a pattern of care analysis. *BMC Neurology* **24**, 462 (2024).
13. Osuka, S. & Meir, E. G. V. Overcoming therapeutic resistance in glioblastoma: the way forward. *J Clin Invest* **127**, 415–426 (2017).
14. Davis, F. G. *et al.* Glioblastoma incidence rate trends in Canada and the United States compared with England, 1995–2015. *Neuro Oncol* **22**, 301–302 (2020).
15. Djamel-Eddine, Y.-C., De Witte, O., Mélot, C. & Lefranc, F. Recurrent glioblastomas: Should we operate a second and even a third time? *Interdisciplinary Neurosurgery* **18**, 100551 (2019).
16. Albano, D. *et al.* Imaging side effects and complications of chemotherapy and radiation therapy: a pictorial review from head to toe. *Insights into Imaging* **12**, 76 (2021).
17. Yang, X., Ren, H. & Fu, J. Treatment of Radiation-Induced Brain Necrosis. *Oxid Med Cell Longev* **2021**, 4793517 (2021).
18. Ortensi, B., Setti, M., Osti, D. & Pelicci, G. Cancer stem cell contribution to glioblastoma invasiveness. *Stem Cell Research & Therapy* **4**, 18 (2013).
19. Liu, F. *et al.* EGFR Mutation Promotes Glioblastoma through Epigenome and Transcription Factor Network Remodeling. *Molecular Cell* **60**, 307–318 (2015).

20. Sigismund, S., Avanzato, D. & Lanzetti, L. Emerging functions of the EGFR in cancer. *Mol Oncol* **12**, 3–20 (2018).

21. Carrillo-García, C. *et al.* Growth/differentiation factor 15 promotes EGFR signalling, and regulates proliferation and migration in the hippocampus of neonatal and young adult mice. *Development* **141**, 773–783 (2014).

22. Xu, H. *et al.* Epidermal growth factor receptor in glioblastoma. *Oncol Lett* **14**, 512–516 (2017).

23. Han, S. *et al.* IDH mutation in glioma: molecular mechanisms and potential therapeutic targets. *Br J Cancer* **122**, 1580–1589 (2020).

24. Alzial, G. *et al.* Wild-type isocitrate dehydrogenase under the spotlight in glioblastoma. *Oncogene* **41**, 613–621 (2022).

25. Zhang, Y. *et al.* The p53 Pathway in Glioblastoma. *Cancers (Basel)* **10**, 297 (2018).

26. Liu, Y. *et al.* Dual targeting macrophages and microglia is a therapeutic vulnerability in models of *PTEN*-deficient glioblastoma. *J Clin Invest* **134**, (2024).

27. Verhaak, R. G. W. *et al.* Integrated genomic analysis identifies clinically relevant subtypes of glioblastoma characterized by abnormalities in PDGFRA, IDH1, EGFR, and NF1. *Cancer Cell* **17**, 98–110 (2010).

28. Wang, L. *et al.* A single-cell atlas of glioblastoma evolution under therapy reveals cell-intrinsic and cell-extrinsic therapeutic targets. *Nat Cancer* **3**, 1534–1552 (2022).

29. Butler, M. *et al.* MGMT status as a clinical biomarker in glioblastoma. *Trends Cancer* **6**, 380–391 (2020).

30. Faisal, S. M. *et al.* The complex interactions between the cellular and non-cellular components of the brain tumor microenvironmental landscape and their therapeutic implications. *Front Oncol* **12**, 1005069 (2022).
31. Tang, J., Amin, M. A. & Campian, J. L. Glioblastoma Stem Cells at the Nexus of Tumor Heterogeneity, Immune Evasion, and Therapeutic Resistance. *Cells* **14**, 562 (2025).
32. Liu, J. H., Horiachok, M., Guru, S. & Maire, C. L. Unraveling Glioblastoma Heterogeneity: Advancing Immunological Insights and Therapeutic Innovations. *Brain Sci* **15**, 833 (2025).
33. Groblewska, M. & Mroczko, B. Pro- and Antiangiogenic Factors in Gliomas: Implications for Novel Therapeutic Possibilities. *Int J Mol Sci* **22**, 6126 (2021).
34. Wang, G. *et al.* Tumor-associated microglia and macrophages in glioblastoma: From basic insights to therapeutic opportunities. *Front Immunol* **13**, 964898 (2022).
35. Lin, Y.-J., Wu, C. Y.-J., Wu, J. Y. & Lim, M. The Role of Myeloid Cells in GBM Immunosuppression. *Front Immunol* **13**, 887781 (2022).
36. Winkler, J., Abisoye-Ogunniyan, A., Metcalf, K. J. & Werb, Z. Concepts of extracellular matrix remodelling in tumour progression and metastasis. *Nat Commun* **11**, 5120 (2020).
37. Rushin, A., Shaikh, A., Hardin, C., Deleyrolle, L. P. & Merritt, M. E. Metabolic flux analysis of glioblastoma neural stem cells reveals distinctive metabolic phenotypes in ketogenic conditions. *Sci Rep* **15**, 18736 (2025).
38. Clay, R., Li, K. & Jin, L. Metabolic Signaling in the Tumor Microenvironment. *Cancers (Basel)* **17**, 155 (2025).

39. Cortes Ballen, A. I. *et al.* Metabolic Reprogramming in Glioblastoma Multiforme: A Review of Pathways and Therapeutic Targets. *Cells* **13**, 1574 (2024).
40. Campos-Sandoval, J. A. *et al.* Antioxidant responses related to temozolomide resistance in glioblastoma. *Neurochem Int* **149**, 105136 (2021).
41. Olivier, C., Oliver, L., Lalier, L. & Vallette, F. M. Drug Resistance in Glioblastoma: The Two Faces of Oxidative Stress. *Front Mol Biosci* **7**, 620677 (2020).
42. Ali, M. Y. *et al.* Radioresistance in Glioblastoma and the Development of Radiosensitizers. *Cancers (Basel)* **12**, 2511 (2020).
43. Rocha, C. R. R., Kajitani, G. S., Quinet, A., Fortunato, R. S. & Menck, C. F. M. NRF2 and glutathione are key resistance mediators to temozolomide in glioma and melanoma cells. *Oncotarget* **7**, 48081–48092 (2016).
44. Almeida Lima, K. *et al.* Temozolomide Resistance in Glioblastoma by NRF2: Protecting the Evil. *Biomedicines* **11**, 1081 (2023).
45. Bernhard, C., Reita, D., Martin, S., Entz-Werle, N. & Dontenwill, M. Glioblastoma Metabolism: Insights and Therapeutic Strategies. *Int J Mol Sci* **24**, 9137 (2023).
46. Morandi, A., Taddei, M. L., Chiarugi, P. & Giannoni, E. Targeting the Metabolic Reprogramming That Controls Epithelial-to-Mesenchymal Transition in Aggressive Tumors. *Front Oncol* **7**, 40 (2017).
47. Manni, W. & Min, W. Signaling pathways in the regulation of cancer stem cells and associated targeted therapy. *MedComm (2020)* **3**, e176 (2022).

48. Trog, D., Moenkemann, H., Haertel, N., Schüller, H. & Golubnitschaja, O. Expression of ABC-1 transporter is elevated in human glioma cells under irradiation and temozolomide treatment. *Amino Acids* **28**, 213–219 (2005).

49. Kaur, E., Ketkar, M. & Dutt, S. Glioblastoma recurrent cells switch between ATM and ATR pathway as an alternative strategy to survive radiation stress. *Med Oncol* **39**, 50 (2022).

50. Lee, H. *et al.* Cancer stem cells: landscape, challenges and emerging therapeutic innovations. *Signal Transduct Target Ther* **10**, 248 (2025).

51. Hanif, F., Muzaffar, K., Perveen, K., Malhi, S. M. & Simjee, S. U. Glioblastoma Multiforme: A Review of its Epidemiology and Pathogenesis through Clinical Presentation and Treatment. *Asian Pac J Cancer Prev* **18**, 3–9 (2017).

52. Aitchison, E. E., Dimesa, A. M. & Shoari, A. Matrix Metalloproteinases in Glioma: Drivers of Invasion and Therapeutic Targets. *BioTech (Basel)* **14**, 28 (2025).

53. Nowak, E. & Bednarek, I. Aspects of the Epigenetic Regulation of EMT Related to Cancer Metastasis. *Cells* **10**, 3435 (2021).

54. Xia, P. The significance of epithelial–mesenchymal transition (EMT) in the initiation, plasticity, and treatment of glioblastoma. *Genes & Diseases* 101711 (2025) doi:10.1016/j.gendis.2025.101711.

55. Onubogu, U. *et al.* Spatial analysis of recurrent glioblastoma reveals perivascular niche organization. *JCI Insight* **9**, (2024).

56. Fidoamore, A. *et al.* Glioblastoma Stem Cells Microenvironment: The Paracrine Roles of the Niche in Drug and Radioresistance. *Stem Cells Int* **2016**, 6809105 (2016).

57. Zeppa, P. *et al.* Fluorescence-Guided Surgery in Glioblastoma: 5-ALA, SF or Both? Differences between Fluorescent Dyes in 99 Consecutive Cases. *Brain Sci* **12**, 555 (2022).

58. Read, R. D., Tapp, Z. M., Rajappa, P. & Hambardzumyan, D. Glioblastoma microenvironment—from biology to therapy. *Genes Dev.* **38**, 360–379 (2024).

59. Mi, L. *et al.* Elevated nonhomologous end-joining by AATF enables efficient DNA damage repair and therapeutic resistance in glioblastoma. *Nat Commun* **16**, 4941 (2025).

60. Alnasser, S. M. *et al.* Pharmacological modulation of stem cells signaling pathway for therapeutic applications. *Stem Cell Res Ther* **16**, 327 (2025).

61. Xiang, W. *et al.* Differentiation therapy targeting the stalled epigenetic developmental programs in pediatric high-grade gliomas. *Pharmacological Research* **212**, 107599 (2025).

62. Auffinger, B., Spencer, D., Pytel, P., Ahmed, A. U. & Lesniak, M. S. The role of glioma stem cells in chemotherapy resistance and glioblastoma multiforme recurrence. *Expert Rev Neurother* **15**, 741–752 (2015).

63. Cerretti, G. *et al.* Bevacizumab in recurrent glioblastoma: does dose matter? Our monocentric and comparative experience. *J Neurooncol* **173**, 449–456 (2025).

64. Chinot, O. L. *et al.* Bevacizumab plus radiotherapy-temozolomide for newly diagnosed glioblastoma. *N Engl J Med* **370**, 709–722 (2014).

65. Gilbert, M. R. *et al.* A randomized trial of bevacizumab for newly diagnosed glioblastoma. *N Engl J Med* **370**, 699–708 (2014).

66. Lu, K. V. *et al.* VEGF Inhibits Tumor Cell Invasion and Mesenchymal Transition Through a MET/VEGFR2 Complex. *Cancer Cell* **22**, 21–35 (2012).

67. Piao, Y. *et al.* Glioblastoma resistance to anti-VEGF therapy is associated with myeloid cell infiltration, stem cell accumulation, and a mesenchymal phenotype. *Neuro Oncol* **14**, 1379–1392 (2012).

68. Durga, Y. K. & Pusapati, R. V. Drug resistance in glioblastoma: Challenges, mechanisms and therapeutic strategies (Review). *Mol Clin Oncol* **24**, 4 (2025).

69. Sterner, R. C. & Sterner, R. M. EGFRVIII and EGFR targeted chimeric antigen receptor T cell therapy in glioblastoma. *Front Oncol* **14**, 1434495 (2024).

70. Singh, D. D., Haque, S., Singh, A. K. & Yadav, D. K. Advancing vaccine-based immunotherapy in glioblastoma treatment. *Neuro Oncol Adv* **7**, vdaf135 (2025).

71. Long, G. V. *et al.* Neoadjuvant triplet immune checkpoint blockade in newly diagnosed glioblastoma. *Nat Med* **31**, 1557–1566 (2025).

72. Begagić, E. *et al.* CRISPR/Cas9-Mediated Gene Therapy for Glioblastoma: A Scoping Review. *Biomedicines* **12**, 238 (2024).

73. Lim, S. H., Yee, G. T. & Khang, D. Nanoparticle-Based Combinational Strategies for Overcoming the Blood-Brain Barrier and Blood-Tumor Barrier. *Int J Nanomedicine* **19**, 2529–2552 (2024).

74. Takeuchi, S. *et al.* Increased xCT Expression Correlates With Tumor Invasion and Outcome in Patients With Glioblastomas. *Neurosurgery* **72**, 33 (2013).

75. Dupuis, J. P., Nicole, O. & Groc, L. NMDA receptor functions in health and disease: Old actor, new dimensions. *Neuron* **111**, 2312–2328 (2023).

76. Papouin, T., Dunphy, J. M., Tolman, M., Dineley, K. T. & Haydon, P. G. Septal Cholinergic Neuromodulation Tunes the Astrocyte-Dependent Gating of Hippocampal NMDA Receptors to Wakefulness. *Neuron* **94**, 840-854.e7 (2017).

77. Li, C. *et al.* A functional role of NMDA receptor in regulating the differentiation of oligodendrocyte precursor cells and remyelination. *Glia* **61**, 732–749 (2013).

78. Miglio, G., Varsaldi, F. & Lombardi, G. Human T lymphocytes express N-methyl-D-aspartate receptors functionally active in controlling T cell activation. *Biochem Biophys Res Commun* **338**, 1875–1883 (2005).

79. Sharp, C. D. *et al.* Glutamate causes a loss in human cerebral endothelial barrier integrity through activation of NMDA receptor. *Am J Physiol Heart Circ Physiol* **285**, H2592-2598 (2003).

80. Mehra, A. *et al.* Nonionotropic Action of Endothelial NMDA Receptors on Blood-Brain Barrier Permeability via Rho/ROCK-Mediated Phosphorylation of Myosin. *J Neurosci* **40**, 1778–1787 (2020).

81. Yu, Y. *et al.* NMDA mediates disruption of blood-brain barrier permeability via Rho/ROCK signaling pathway. *Neurochem Int* **154**, 105278 (2022).

82. Kim, K.-S., Jeon, M. T., Kim, E. S., Lee, C. H. & Kim, D.-G. Activation of NMDA receptors in brain endothelial cells increases transcellular permeability. *Fluids Barriers CNS* **19**, 70 (2022).

83. Ferguson, H. J. M. *et al.* Glutamate dependent NMDA receptor 2D is a novel angiogenic tumour endothelial marker in colorectal cancer. *Oncotarget* **7**, 20440–20454 (2016).

84. Moriarty, C., Gupta, N. & Bhattacharya, D. Role of Glutamate Excitotoxicity in Glioblastoma Growth and Its Implications in Treatment. *Cell Biol Int* **49**, 421–434 (2025).

85. Ohshima, K. *et al.* Serine racemase enhances growth of colorectal cancer by producing pyruvate from serine. *Nat Metab* **2**, 81–96 (2020).

86. Sikka, P. *et al.* D-Serine metabolism in C6 glioma cells: Involvement of alanine-serine-cysteine transporter (ASCT2) and serine racemase (SRR) but not D-amino acid oxidase (DAO). *J Neurosci Res* **88**, 1829–1840 (2010).

87. Henneberger, C., Papouin, T., Oliet, S. H. R. & Rusakov, D. A. Long term potentiation depends on release of D-serine from astrocytes. *Nature* **463**, 232–236 (2010).

88. Mondal, J. & Huse, J. T. Neurotransmitter power plays: the synaptic communication nexus shaping brain cancer. *Acta Neuropathol Commun* **13**, 85 (2025).

89. Calabrese, C. *et al.* A perivascular niche for brain tumor stem cells. *Cancer Cell* **11**, 69–82 (2007).

90. Zhu, T. S. *et al.* Endothelial cells create a stem cell niche in glioblastoma by providing Notch ligands that nurture self-renewal of cancer stem-like cells. *Cancer Res* **71**, 6061–6072 (2011).

91. Jain, R. K. *et al.* Angiogenesis in brain tumours. *Nat Rev Neurosci* **8**, 610–622 (2007).

92. Folkins, C. *et al.* Glioma tumor stem-like cells promote tumor angiogenesis and vasculogenesis via vascular endothelial growth factor and stromal-derived factor 1. *Cancer Res* **69**, 7243–7251 (2009).

93. Charles, N. *et al.* Perivascular Nitric Oxide Activates Notch Signaling and Promotes Stem-like Character in PDGF-induced Glioma Cells. *Cell Stem Cell* **6**, 10.1016/j.stem.2010.01.001 (2010).

94. Wang, Q. *et al.* Vascular niche IL-6 induces alternative macrophage activation in glioblastoma through HIF-2α. *Nat Commun* **9**, 559 (2018).

95. Yang, F. *et al.* Synergistic immunotherapy of glioblastoma by dual targeting of IL-6 and CD40. *Nat Commun* **12**, 3424 (2021).

96. Wang, H. *et al.* Targeting interleukin 6 signaling suppresses glioma stem cell survival and tumor growth. *Stem Cells* **27**, 2393–2404 (2009).

97. El Hallani, S. *et al.* A new alternative mechanism in glioblastoma vascularization: tubular vasculogenic mimicry. *Brain* **133**, 973–982 (2010).

98. Ricci-Vitiani, L. *et al.* Tumour vascularization via endothelial differentiation of glioblastoma stem-like cells. *Nature* **468**, 824–828 (2010).

99. Soda, Y. *et al.* Transdifferentiation of glioblastoma cells into vascular endothelial cells. *Proc Natl Acad Sci U S A* **108**, 4274–4280 (2011).

100. Cheng, L. *et al.* Glioblastoma Stem Cells Generate Vascular Pericytes to Support Vessel Function and Tumor Growth. *Cell* **153**, 139–152 (2013).

101. Kucharzewska, P. *et al.* Exosomes reflect the hypoxic status of glioma cells and mediate hypoxia-dependent activation of vascular cells during tumor development. *Proc Natl Acad Sci U S A* **110**, 7312–7317 (2013).

102. Kim, P. M. *et al.* Serine racemase: Activation by glutamate neurotransmission via glutamate receptor interacting protein and mediation of neuronal migration. *Proceedings of the National Academy of Sciences* **102**, 2105–2110 (2005).

103. Hagiwara, H., Iyo, M. & Hashimoto, K. Neonatal disruption of serine racemase causes schizophrenia-like behavioral abnormalities in adulthood: clinical rescue by d-serine. *PLoS One* **8**, e62438 (2013).

104. Lu, L. *et al.* Astrocytes drive cortical vasodilatory signaling by activating endothelial NMDA receptors. *J Cereb Blood Flow Metab* **39**, 481–496 (2019).

105. Bejarano, L. *et al.* Single-cell atlas of endothelial and mural cells across primary and metastatic brain tumors. *Immunity* **58**, 1015-1032.e6 (2025).

106. Ohshima, K. *et al.* Serine racemase enhances growth of colorectal cancer by producing pyruvate from serine. *Nat Metab* **2**, 81–96 (2020).

107. Sun, L., Zhang, H. & Gao, P. Metabolic reprogramming and epigenetic modifications on the path to cancer. *Protein Cell* **13**, 877–919 (2022).

108. Sivanand, S. *et al.* Nuclear acetyl-CoA production by ACLY promotes homologous recombination. *Mol Cell* **67**, 252-265.e6 (2017).

109. Maddocks, O. D. K., Labuschagne, C. F., Adams, P. D. & Vousden, K. H. Serine Metabolism Supports the Methionine Cycle and DNA/RNA Methylation through De Novo ATP Synthesis in Cancer Cells. *Mol Cell* **61**, 210–221 (2016).

110. C, L. *et al.* The Prognostic Role of Serine Racemase in Patients With Pancreatic Cancer: A New Marker in Cancer Metabolism. *Pancreas* **52**, (2023).

111. Cui, Z. *et al.* Integrated Bioinformatics Analysis of Serine Racemase as an Independent Prognostic Biomarker in Endometrial Cancer. *Front Genet* **13**, 906291 (2022).

112. Pu, Y. *et al.* MiR-193a-3p and miR-193a-5p suppress the metastasis of human osteosarcoma cells by down-regulating Rab27B and SRR, respectively. *Clin Exp Metastasis* **33**, 359–372 (2016).

113. Gallo, S., Vitacolonna, A. & Crepaldi, T. NMDA Receptor and Its Emerging Role in Cancer. *Int J Mol Sci* **24**, 2540 (2023).

114. Mustafa, A. K. *et al.* Nitric oxide S-nitrosylates serine racemase, mediating feedback inhibition of D-serine formation. *Proc Natl Acad Sci U S A* **104**, 2950–2955 (2007).

115. Hua, A. B. *et al.* Repurposing the Electron Transfer Reactant Phenazine Methosulfate (PMS) for the Apoptotic Elimination of Malignant Melanoma Cells through Induction of Lethal Oxidative and Mitochondriotoxic Stress. *Cancers (Basel)* **11**, 590 (2019).

116. Wang, Y. *et al.* Esketamine/Ketamine: Dual-Action Mechanisms and Clinical Prospects beyond Anesthesia in Psychiatry, Immunology, and Oncology. *Adv Sci (Weinh)* **13**, e16024 (2025).

117. Morris, G. F. *et al.* Failure of the competitive N-methyl-D-aspartate antagonist Selfotel (CGS 19755) in the treatment of severe head injury: results of two phase III clinical trials. The Selfotel Investigators. *J Neurosurg* **91**, 737–743 (1999).

118. Albers, G. W., Goldstein, L. B., Hall, D., Lesko, L. M., & Aptiganel Acute Stroke Investigators. Aptiganel hydrochloride in acute ischemic stroke: a randomized controlled trial. *JAMA* **286**, 2673–2682 (2001).

119. Brown, P. D. *et al.* Memantine for the prevention of cognitive dysfunction in patients receiving whole-brain radiotherapy: a randomized, double-blind, placebo-controlled trial. *Neuro Oncol* **15**, 1429–1437 (2013).

120. Tsuji, S. *et al.* NMDA receptor signaling induces the chemoresistance of temozolomide via upregulation of MGMT expression in glioblastoma cells. *J Neurooncol* **160**, 375–388 (2022).